NORTHWESTERN UNIVERSITY

Investigating the Mechanisms of Acentriolar Spindle Assembly in *Caenorhabditis elegans* Oocytes

A DISSERTATION

SUBMITTED TO THE GRADUATE SCHOOL

IN PARTIAL FULFILLMENT OF THE REQUIREMENTS

for the degree

DOCTOR OF PHILOSOPHY

Field of Interdisciplinary Biological Sciences

By

Timothy J. Mullen

EVANSTON, ILLINOIS

March 2019

ABSTRACT

Investigating the Mechanisms of Acentriolar Spindle Assembly in *Caenorhabditis elegans* Oocytes

Timothy J. Mullen

When a cell divides, it must assemble a microtubule-based structure called a spindle, which provides the forces that physically segregate the chromosomes. In most cell types the microtubules that comprise the spindle are nucleated and organized by centriole-containing centrosomes. In many species, however, oocyte meiosis is carried out in the absence of centrioles. As a result, microtubule organization, spindle assembly, and chromosome segregation proceed by unique mechanisms. In this dissertation, I report insights into the principles underlying this specialized form of cell division using *C. elegans* oocyte meiosis as a model system. First, I identify two microtubule motor proteins, KLP-15 and KLP-16, which are two highly homologous members of the kinesin-14 family of minus-end-directed kinesins. These proteins localize to the acentriolar oocyte spindle and promote microtubule bundling during spindle assembly; following KLP-15/16 depletion, microtubule bundles form but then collapse into a disorganized array. Surprisingly, despite this defect I found that during anaphase, microtubules are able to reorganize into a bundled array that facilitates chromosome segregation. This phenotype therefore enabled me to identify factors promoting

microtubule organization during anaphase, whose contributions are normally undetectable in wild-type worms; I found that SPD-1 (PRC1) bundles microtubules and KLP-18 (kinesin-12) likely sorts those bundles into a functional orientation capable of mediating chromosome segregation. In the second part of this dissertation, I investigate the role of the microtubule stabilizing protein, ZYG-9 (XMAP215) during oocyte meiosis, and found that it functions to maintain the integrity of the acentriolar spindle poles. When I acutely depleted this protein from the bipolar spindle, the spindle poles lose stability and begin to fragment. The discoveries described here therefore deepen our understanding of the molecular mechanisms of acentriolar spindle assembly, spindle stability, and chromosome segregation in oocytes.

Acknowledgements

First, I have to thank Sadie Wignall. Sadie, you go above and beyond to make sure those who are lucky enough to call you their mentor are successful. Thank you for your guidance, enthusiasm for cell biology, and for creating an environment that makes doing science fun. I could not have asked for a better mentor.

A huge thank you to all of the Wignall Lab members, past and present, for all of the support and for making coming to work every day something I truly look forward to. Carissa and Amanda, it's been a pleasure going through the ups and downs of graduate school alongside you both. You're both incredible scientists and people, and I know you will both go on to do great things. Ian, thank you for always challenging me scientifically. I cannot tell you how much I have learned from our conversations (or bickering, but who's to say). Just remember, nothing matters. Nikita, Gabe, and Hannah, you are all amazing people and scientists, and it is wonderful to know the lab is in good hands for years to come. Chrissy and Mike, thank you for teaching me how to worm, and being patient with me as I started my time in the lab. Jeremy, thank you for making sure the ship doesn't sink and for your thoughtful insights. And lastly, I want to thank Zach, my first and only undergraduate mentee. I hope you learned as much about doing science as I learned about being a mentor from your time in the lab.

I cannot put into words the gratitude I owe to my parents, Mark and Karen, for everything they have done to get me here. Thank you both for shaping me into the person I am today and for your unwavering support.

I want to thank past and present members of my committee for valuable guidance and feedback over the years: Rick Morimoto, Vladimir Gelfand, Laura Lackner, and Eric Weiss. I always came away from our conversations with valuable new insights.

Finally, thank you to Jessica Hornick and the BIF facility for keeping the microscopes in working order and allowing me to focus on the research. Thank you to all of the labs that provided reagents that were used in these projects. I was supported by an National Institutes of Health/National Cancer Institute Training Grant - T32CA009560.

Abbreviations

meiosis I (MI)

meiosis II (MII)

Microtubule associated proteins (MAPs)

Microtubule organizing center (MTOC)

RNA interference (RNAi)

Kinesin-like protein (KLP)

mitotic centromere-associated kinesin (MCAK)

Pericentriolar material (PCM)

Kinetochore fiber (K-fiber)

Chromosomal passenger complex (CPC)

Ring Complex (RC)

Small ubiquitin-like modifier (SUMO)

Nuclear envelope breakdown (NEBD)

Electron microscopy (EM)

Anaphase promoting complex (APC)

Auxin-inducible-degron (AID)

Fluorescence recovery after photobleaching (FRAP)

Spindle assembly factors (SAFs)

Dedication

This dissertation is dedicated to my parents. Without their love and support, none of the work described in the following pages would have been possible.

Table of Contents

ABSTRACT 3

Acknowledgements 5

Abbreviations 7

Dedication 8

List of Tables 12

List of Figures 13

Chapter 1. Introduction 16

1.1. An overview of cell division 17

1.2. Meiosis 19

1.3. *C. elegans* as a model organism to study cell division 22

1.4. Microtubule motors and MAPs 25

1.5. Spindle assembly and chromosome segregation in *C. elegans* 28

Chapter 2. Interplay between microtubule bundling and sorting factors ensures acentriolar spindle stability during *C. elegans* oocyte meiosis 41

2.1. Introduction 42

2.2. KLP-15 and KLP-16 are required for acentriolar spindle assembly in oocytes 44

2.3. KLP-15/16 localize to spindle microtubules throughout oocyte meiosis 55

2.4. Microtubules bundle and chromosomes segregate in anaphase following KLP-15/16 depletion 61

2.5. KLP-15/16-independent anaphase microtubule bundling is mediated by SPD-1 (PRC1) 64

2.6. KLP-18 potentially facilitates the reorganization of microtubule bundles during KLP-15/16-independent anaphase 73

2.7. Lateral microtubule-chromosome contacts can be established during KLP-15/16-independent anaphase 75

2.8. Expanded studies of lateral microtubule bundles during anaphase in wild-type *C. elegans* oocytes 79

2.9. Discussion 84

Chapter 3. ZYG-9^{XMAP215} is essential for acentriolar spindle formation and spindle pole integrity during *C. elegans* oocyte meiosis 92

3.1. Introduction 93

3.2. ZYG-9 is required for acentriolar spindle assembly in oocytes 95

3.3. ZYG-9 is enriched at the acentriolar meiotic spindle poles and this localization is dependent on TAC-1 101

3.4. ZYG-9 is required for acentriolar spindle pole integrity 104

3.5. ZYG-9 dynamics at the spindle pole are cell-type specific 109

3.6. ZYG-9 depletion causes ectopic aster formation in oocytes 114

3.7. Discussion 115

Chapter 4. Summary of findings and future directions 121

4.1. Summary of findings 122

4.2. Future directions 123

4.3. Final remarks 132

Chapter 5. Materials and methods 134

References 156

Appendix A. 171

Appendix B. 173

Appendix C. 174

List of Tables

2.1	Embryonic lethality assays	49
5.1	Worm strains used in Chapter 2	135
5.2	Worm strains used in Chapter 3	136
5.3	Primer and CRISPR sequences used for KLP-16::GFP strain (SMW16) generation	137
5.4	CRISPR sequences used for *klp-16(wig)* strain (SMW15) generation	138
5.5	Primer and CRISPR sequences used for degron::EmGFP::ZYG-9 strain (SMW24) generation	140
5.6	Primer and CRISPR sequences used for mMaple3::TBA-1 strain (SMW28) generation	142

List of Figures

1.1	Overview of mitosis and meiosis	20
1.2	The mitotic and oocyte meiotic spindles in *C. elegans*	21
1.3	*C. elegans* germline organization	24
1.4	Microtubule associated proteins and microtubule motors	28
1.5	Chromosome organization during *C. elegans* oocyte meiosis	31
1.6	The stages of acentriolar spindle assembly in *C. elegans* oocytes	33
1.7	Model for chromosome segregation in *C. elegans* oocytes	39
2.1	Depletion of KLP-15/16 results in disorganized oocyte spindles	46
2.2	Amino acid sequence alignment of KLP-15 and KLP-16	48
2.3	Spindle assembly during meiosis II	51
2.4	Additional quantification of phenotypes in mutants and following *klp-15/16(RNAi)*	52
2.5	Additional analysis of spindle defects in mutants and following *klp-15/16(RNAi)*	53
2.6	KLP-15/16 localize to spindle microtubules during oocyte meiosis	57
2.7	Additional analysis of KLP-16::GFP localization	59

2.8	Microtubules bundle and chromosomes segregate in anaphase in *klp-15/16(RNAi)* oocytes	62
2.9	SPD-1 and centralspindlin localize to anaphase spindle microtubules	66
2.10	SPD-1 and KLP-18 are required for KLP-15/16-independent spindle reorganization during anaphase	68
2.11	Consequences of the anaphase defects observed in *klp-15/16(RNAi)* oocytes	71
2.12	Early anaphase in *klp-18(tm2841)*	75
2.13	Anaphase spindle organization in *klp-15/16(RNAi)* oocytes	77
2.14	Live imaging of anaphase spindles in *C. elegans* oocytes	83
2.15	Anaphase spindle organization and SPD-1 localization following cold-treatment	84
2.16	Model: Interplay between microtubule-associated factors contributes to acentriolar spindle assembly and maintenance	90
3.1	ZYG-9 is required for spindle assembly in oocytes	98
3.2	Quantification of *zyg-9(RNAi)* phenotypes	99
3.3	ZYG-9 localization during acentriolar spindle assembly	102
3.4	TAC-1 is required for enrichment of ZYG-9 to the acentriolar spindle poles	103
3.5	Long-term auxin induced depletion of degron::ZYG-9 in oocytes	105
3.6	Acute ZYG-9 depletion causes acentriolar spindle pole disruption	107
3.7	FRAP analysis of spindle pole components	111

3.8	FRAP analysis with fit curves	113
3.9	ZYG-9 depletion causes ectopic microtubule aster formation	114
4.1	Microtubule flux in *C. elegans* acentriolar spindles	129
B.1	*klp-15/16(RNAi)* and metaphase arrest	173
C.1	Oocyte expressing mMaple::TBA-1	174

CHAPTER 1

Introduction

1.1. An overview of cell division

The cell is the basic unit of life, and all cells arise from pre-existing cells. Cell division is the process by which a single parent cell divides in order to produce two new, identical daughter cells. Most eukaryotic cells divide by a process called mitosis, which results in two daughter cells that have the same number of chromosomes as the parent cell. In eukaryotes that reproduce sexually, a subset of cells undergo a specialized form of cell division called meiosis, which reduces the chromosome number by half to produce the gametes - eggs and sperm.

When a cell makes the decision to divide, it first makes a copy of each of its chromosomes during S-phase of the cell cycle. During prophase, chromosome pairs (called sister chromatids) condense into thread-like structures that remain tightly associated[1,2]. Then, the nuclear envelope breaks down, and the condensed chromatids are released into the cytoplasm. During prometaphase, the chromosome pairs make attachments to a structure called the spindle, which moves and arranges the chromosomes. At metaphase, the chromatids are aligned in the center of the cell and become bioriented, with the two chromatids attached to opposite spindle poles. During anaphase, the sister chromatids separate and are pulled to opposite poles. At telophase, once the separated chromosomes have moved far enough apart, they begin to decondense, and the nuclear envelope reforms around each set of chromosomes. The cell then splits into two daughter cells, each containing one set of the segregated chromosomes, during a process called cytokinesis. In diploid organisms, most cells contain two copies of each chromosome - one maternal and one paternal. During mitosis, the cell will replicate each chromosome once and divide once, producing two daughter cells with the same amount of genetic information as the original parent cell. In other words, each daughter cell receives both maternal and paternal sets of chromosomes to remain diploid. During meiosis,

the goal is to generate haploid gametes (egg and sperm) with half the number of chromosomes as the parent cell. This is accomplished by one round of DNA replication, followed by two rounds of cell division (meiosis I (MI) and meiosis II (MII)) - each division reducing the chromosome number by half. During MI paired homologous chromosomes, known as homologs, segregate. During MII, sister chromatids segregate to generate a cell with one copy of each chromosome. Upon fertilization of the egg by the sperm, the zygote inherits one maternal and one paternal copy of each chromosome and becomes diploid (Fig. 1.1).

In order to physically partition the chromosomes, the cell must build a structure called the spindle. The spindle is a complex, self-assembling cellular machine that performs work to align the chromosomes at metaphase and segregate them into two daughter cells during anaphase. The basic building blocks of the spindle are the microtubules. Microtubules are proteinacious filaments made up of α- and β-tubulin heterodimers. These heterodimers align in an end-to-end fashion to assemble into a protofilament. The protofilament then associates laterally with other protofilaments to form a hollow microtubule. Because of the inherent asymmetry in the α- and β-tubulin heterodimers, microtubules are polarized and have a "slow" growing minus-end and a "fast" growing plus-end[3]. Microtubules also exhibit a phenomenon called dynamic instability where a microtubule switches between periods of growth and rapid shrinkage, known as catastrophe[4]. The microtubules of the spindle are acted upon by microtubule associated proteins (MAPs) and microtubule motor proteins. MAPs and motor proteins can alter different parameters of microtubule dynamics and assembly, and are therefore necessary to construct a functional spindle of the correct size and shape and to generate the forces that ultimately segregate the chromosomes[5,6].

The metaphase spindle is a bipolar, tapered structure that aligns the chromosomes prior to partitioning them into two new cells. Disruptions in spindle architecture or bipolarity

can result in chromosome segregation errors and aneuploidy (the term for when a cell has an abnormal number of chromosomes). Aneuploidy resulting from errors in mitosis can be detrimental to the cell and is a hallmark of cancer[7]. Aneuploidy resulting from errors in the meiotic divisions can have a catastrophic impact on the development of the entire organism[8]. Therefore, understanding how cells assemble a functional bipolar spindle to ensure faithful chromosome segregation is of great importance.

During mitosis and male meiosis, microtubule assembly and spindle formation is driven primarily by two structures called centrosomes, which contain centrioles, nucleate microtubules, and act as the major microtubule organizing centers (MTOCs) that define the two poles of the spindle. During female oocyte meiosis in most organisms, spindle assembly is carried out in the absence of centriole-containing centrosomes (they are acentriolar). As a result oocytes assemble and organize the microtubules into a functional, bipolar spindle through unique, poorly understood mechanisms. Much of the work detailed in the following chapters aims to understand the basic molecular mechanisms of how oocytes assemble a bipolar spindle and segregate chromosomes in the absence of centriole-containing centrosomes.

1.2. Meiosis

Meiosis is a specialized reductional form of cell division that produces the germ cells necessary for sexual reproduction. In a diploid animal, the products of meiosis are the haploid gametes, the egg and sperm, which each contain half the number of chromosomes necessary to produce a viable embryo. That way, when an egg is fertilized by the sperm, the zygote regains the diploid state of the genome. The reduction in chromosome number during meiosis is accomplished through one round of DNA replication followed by two consecutive rounds of cell division - MI and MII. In MI each chromosome pairs with its homolog, which are held together so that they can be segregated to opposite spindle poles in the first meiotic

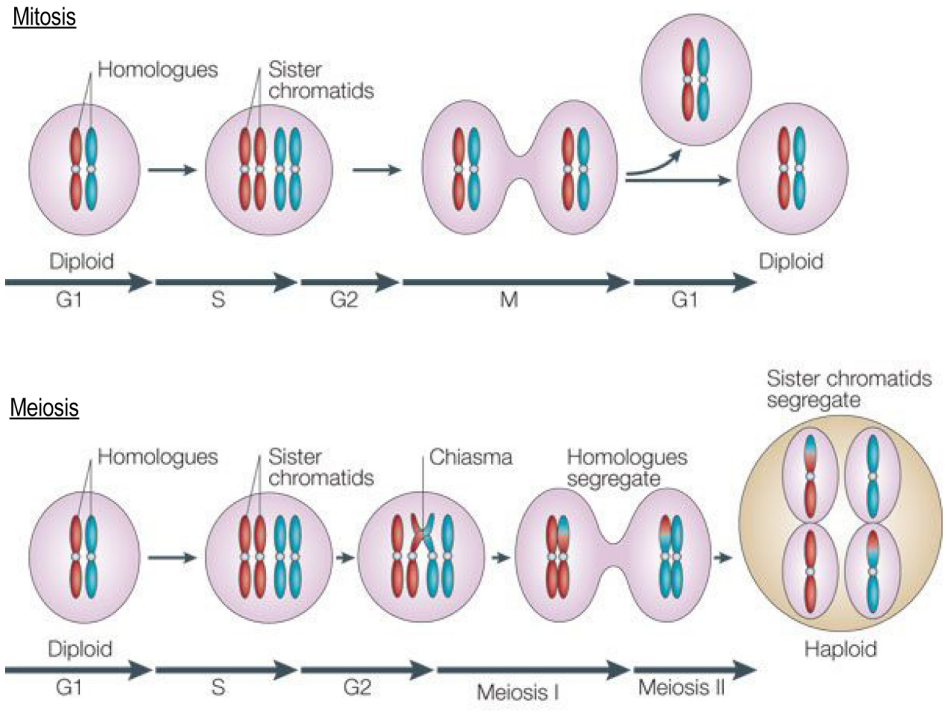

Figure 1.1. **Overview of mitosis and meiosis.** In mitosis, homologous chromosomes replicate during S phase to create sister chromatids, which are then segregated equally during a single division. During S phase of meiosis, homologous chromosomes are replicated to create sister chromatids. The paired homologs can swap DNA during a process called recombination. During meiosis I, the paired homologs segregate, and in meiosis II, the sister chromatids segregate without an intervening DNA replication step. Adapted from Marston and Amon, 2005, *Nature Reviews Molecular Cell Biology*[9].

division. Then, in MII, sister chromatids separate. MI is the most unique step in the meiotic divisions because it is at this stage that paired homologs are segregated as opposed to sister chromatids (Fig. 1.1). During spermatocyte meiosis, the end result is four haploid sperm cells - all equally viable. In most organisms, during each division of oocyte meiosis, half of the genetic material is retained inside the cell and the other half is extruded into a small polar body. As a result, the final product of female meiosis is one viable haploid egg cell.

Unlike mitosis and spermatocyte meiosis, oocyte meiosis is accomplished in the absence of centriole-containing centrosomes[10] (Fig. 1.2). The centrosomes are eliminated prior to the meiotic divisions, and therefore, oocytes assemble and organize the spindle microtubules

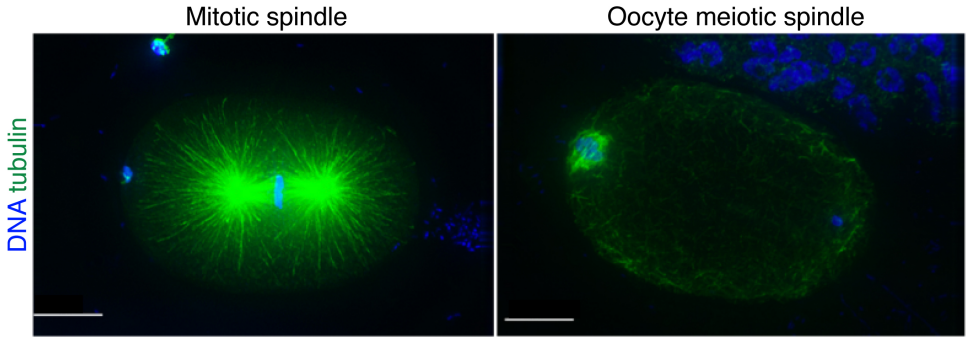

Figure 1.2. **The mitotic and oocyte meiotic spindles in *C. elegans*.** Mitotic (left) and oocyte meiotic (right) spindles stained for DNA (blue) and tubulin (green). The bipolar mitotic spindle in the embryo is organized by two centriole-containing centrosomes that nucleate a large array of microtubules. The oocyte meiotic spindle lacks centrosomes and takes on a much different morphology. Bars = 10 μm.

through unique mechanisms. The elimination of the centrosome from the oocyte may be an advantage to the organism for a few reasons. 1) Elimination of the centrosomes from the oocyte ensures that the zygote inherits only one centrosome from the sperm - extra centrosomes can be detrimental to the cell and the development of the embryo[11,12]. 2) Elimination of the centrioles reduces the size of the oocyte spindle, which may be necessary to facilitate the highly asymmetric oocyte divisions and to retain the majority of the oocyte cytoplasm. The oocyte cytoplasm is packed with the maternal load of proteins and gene products necessary to enable the rapid early embryonic divisions. 3) In *C. elegans*, the sperm centrosome provides a signal that establishes cell polarity, and therefore, elimination of the centrosome from the oocyte may prevent conflicting signals for this polarity establishment[13].

Errors during the meiotic divisions, can result in gametes with an incorrect number of chromosomes, a condition known as aneuploidy. Aneuploidy in a somatic cell is typically only detrimental to that one cell, and does not affect the organism as whole. Aneuploidy in a germ cell, however, can be lethal to the organism as all of the cells in the animal would be derived from the aneuploid zygote. In human development, the problem of aneuploidy resulting from errors in meiosis is of particular significance. It is estimated that 20-40% of

all human conceptions are aneuploid[14]. Furthermore, the vast majority of the aneuploidies in human pregnancies can be traced back to errors in oocyte meiosis as opposed to errors in spermatogenesis[15].

One potential cause of chromosome segregation errors in human oocytes was described in a recent study[16]. In this study, the authors observed acentriolar meiotic spindle assembly and chromosome segregation in live human oocytes and found that the spindles are remarkably unstable - the bipolar spindle forms, collapses, and reforms. Furthermore, the authors found that the instances of chromosome segregation errors correlated with the amount of spindle instability (i.e. the more unstable a spindle appeared to be, the more likely that spindle was to exhibit chromosome segregation errors). These findings highlight the importance of understanding the basic molecular mechanisms of acentriolar spindle assembly, spindle maintenance, and chromosome segregation in oocytes. In order to study these processes, I use the small nematode *Caenorhabditis elegans* as a model organism to generate and test hypotheses.

1.3. *C. elegans* as a model organism to study cell division

C. elegans is a powerful model system for studying the basic molecular mechanisms of both mitotic and oocyte meiotic cell division. Because many of the proteins necessary for cell division are conserved, the discoveries we make in *C. elegans* will be applicable to most organisms. Furthermore, the meiotic oocyte divisions are carried out in the absence of centriole-containing centrosomes, as is the case with most other model organisms and humans[10,16].

The gonad of a hermaphrodite *C. elegans* is a bilobed structure in which the nuclei are organized in space and time, and the meiotic stages occur in an assembly line-like fashion (Fig. 1.3). Much of the germline is a syncytium, and the nuclei share a common cytoplasm. At the

distal tip, mitotically dividing stem cells give rise to the nuclei that will undergo meiosis[17]. As these nuclei move through the germline, the chromosomes are replicated, and proceed through the early stages of prophase of meiosis I, leptotene and zygotene. It is around this stage that the chromosomes begin to pair, initiate recombination, and synapse[18]. When the nuclei enter pachytene, synapsis is completed followed by the completion of recombination. These random recombination events will produce new combinations of alleles which will then be segregated randomly during the meiotic divisions. These crossover and recombination events are necessary to produce genetic diversity within the species. At diplotene, the homologous chromosomes begin to come apart, but are held together at the site where the crossover occurred, called a chiasma. It is also around the stage of diplotene that oocyte cellularization and diakinesis occur. During diakinesis, the paired homologs (called bivalents) condense into a bilobed structure that will be divided during MI. Oocytes arrested in late prophase of MI are ovulated and proceed through the meiotic divisions every 23 minutes[19], which allows for plenty of material for experiments. After anaphase of MII, the mitotic divisions begin in the one-cell embryo. At this stage, the single cell embryo assembles a large mitotic spindle that takes up the entire volume of the cell. Because of the one-cell embryo's spindle size and proximity to the oocyte, one can easily compare these two types of cell division as they take place only one cell-cycle apart.

C. elegans is a great genetic model as well. Efficient degradation of mRNA via RNA interference (RNAi) is a simple protocol and can be done by feeding the worms bacteria transformed with a plasmid that produces dsRNA that targets a gene of interest[20]. Furthermore, there is a library of RNAi clones targeting most *C. elegans* genes, making reverse genetic screens possible[21]. Because the body of *C. elegans* is transparent, I can make fluorescently tagged proteins and view the meiotic and mitotic divisions within the live animal.

Recent advancements in CRISPR genomic editing approaches have made endogenously tagging proteins of interest relatively straightforward[22,23]. It is also possible to use CRISPR to make specific mutations or deletions in genes to test their function *in vivo*. Lastly, I can dissect out oocytes and mitotic embryos, fix and stain them with antibodies, and analyze these samples using high-resolution microscopy[24].

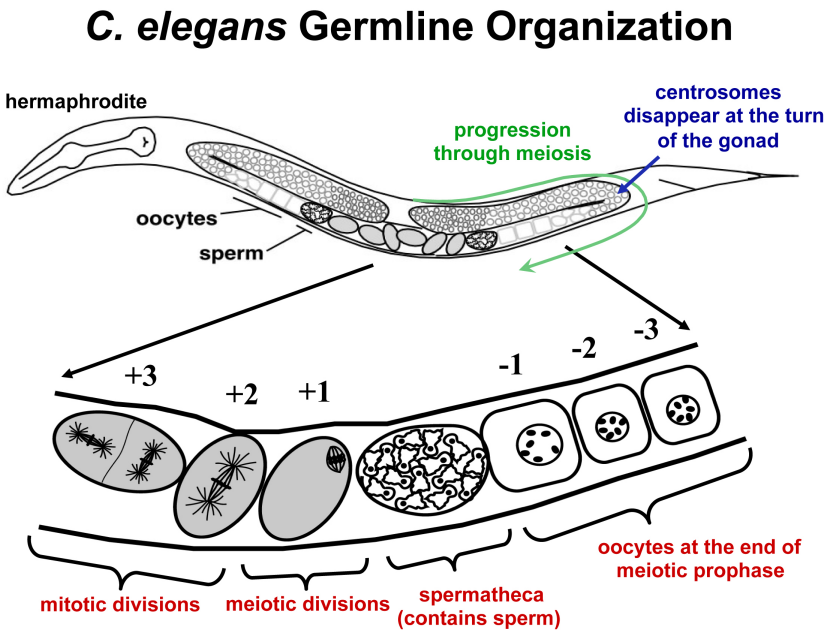

Figure 1.3. ***C. elegans* germline organization** Mitotically dividing cells at the distal end of the gonad progress through meiosis in an assembly-line fashion. Oocytes at the end of meiotic prophase I (-1 position) are ovulated into the spermatheca and begin the meiotic divisions.

1.4. Microtubule motors and MAPs

Efficient organization of the microtubules into a stable, bipolar spindle is accomplished by the actions of microtubule motor proteins and MAPs. Microtubule motor proteins convert the energy from ATP hydrolysis into mechanical work to "walk" along a microtubule substrate. MAPs function to alter microtubule dynamics and behavior to allow for efficient and correct spindle assembly. In this section I will highlight *some* of the motor proteins and MAPs that are relevant to spindle assembly with an emphasis on the *C. elegans* gene names.

Microtubule motors can exploit the inherent asymmetry in the microtubule filament, which allows the motors to be either plus-end directed or minus-end directed. The plus-end directed motors are typically members of the kinesin family of motors[25], and the major minus-end directed motor is cytoplasmic dynein[26].

Kinesins typically consist of an N-terminal globular motor domain, connected to a coiled-coil domain of α-helices at the C-terminus. The α-helical coiled-coil domains allow for the dimerization of the kinesin motor. Most kinesins are homodimers, but there are examples of kinesin heterodimers and tetramers as well. By connecting two motor domains together, each motor head can alternate through cycles of microtubule binding, ATP-hydrolysis, and unbinding to walk along a microtubule and generate force. The ability for a kinesin to move along the same microtubule without fully dissociating is called processivity, and this property varies among kinesin families[25]. The tail domain contains sites for binding partners (activators and inhibitors), kinases, and cargo[27]. These cargo can be vesicles, organelles, or another microtubule. Kinesin-5 (Eg5 in humans, BMK-1 in *C. elegans*) is an example of homotetrameric kinesin consisting of two homodimers organized in a head to tail configuration such that the two pairs of motor domains are located on opposite sides of the complex resulting in a dumbbell shape[28]. This head to tail configuration allows kinesin-5 to bind

to and walk along two microtubules at the same time, and because this motor is plus-end directed, its activity will force the minus-ends of antiparallel microtubules apart[29,30]. This type of microtubule sliding within the context of a spindle is essential to generate bipolarity by moving the poles apart. Kinesin-12 family members (KLP-18 (kinesin-like protein) in *C. elegans*) are similar to kinesin-5 and can help promote spindle bipolarity in the absence of kinesin-5[31,32]. It is currently debated whether kinesin-12 family members function as dimers or tetramers[33–36], and therefore how exactly these motors function is an open area of research. Chromokinesins of the kinesin-4 family (KLP-19 in *C. elegans*) can drive chromosome movement along microtubules and facilitate their alignment to the metaphase plate[37]. This class of kinesin can also promote anaphase midzone integrity by targeting MAPs that function to stabilize the antiparallel midzone microtubules[38].

Another family of kinesins that is important for organizing spindle microtubules is the kinesin-14 family. Kinesins that belong to the kinesin-14 family are a unique class of minus-end directed kinesins. Furthermore, these kinesins typically have their motor domain at the C-terminus of the protein and an N-terminal microtubule binding site[39]. Kinesin-14s have been shown to be important for sliding of antiparallel microtubules, bundling of parallel microtubules, and focusing the minus-ends of microtubules at the spindle poles in a variety of systems[40–43]. Investigating this class of kinesin during *C. elegans* oocyte meiotic spindle assembly will be a major focus of Chapter 2. Additionally, during cell division the kinesin-6 family member MKLP-1 (ZEN-4 in *C. elegans*) is necessary to bundle antiparallel mid-zone microtubules between the sets of segregating chromosomes during anaphase[44].

Finally, kinesins can also promote the disassembly of microtubules. The kinesin-13 family member MCAK (mitotic centromere-associated kinesin; KLP-7 in *C. elegans*) stabilizes the

curling of protofilaments and the removal of tubulin dimers at the microtubule ends to promote catastrophe[45,46]. This activity is necessary to ensure proper kinetochore-microtubule attachments by destabilizing incorrect attachments[47].

Cytoplasmic dynein is the premier minus-end directed motor inside the cell. Dynein's structure differs considerably from that of kinesin motors. Dynein functions as a dimer with each monomer consisting of a large (∼500kDa) heavy chain that contains a microtubule binding domain at the C-terminus, a AAA+ ATPase motor domain, and an N-terminal tail where different adapters, which specify the type of cargo[48], can bind. During spindle assembly, dynein functions to slide parallel microtubules to focus their minus-ends at the spindle poles[49].

In addition to microtubule motors, MAPs have important roles during spindle assembly and anaphase to ensure correct partitioning of the chromosomes. Microtubule stabilizers such as XMAP215 family members (ZYG-9 in *C. elegans)* promote microtubule assembly the formation of long microtubules[50]. Opposing the activity of microtubule stabilizers are microtubule severing proteins such as katanin (MEI-1/2 in *C. elegans*), which ensures correct spindle microtubule number and length[51]. MAPs such as Asp (ASPM-1 in *C. elegans*) can bind to microtubule minus-ends to slow their growth and also promote focusing of the spindle poles[52–54]. Finally, PRC1 (SPD-1 in *C. elegans*) selectively binds to and bundles antiparallel microtubules, which is essential for promoting anaphase spindle stability[44,55,56]. The collective actions of these molecular motors and MAPs are essential to coordinate the assembly of both centriolar mitotic and acentriolar meiotic spindles (Fig. 1.4).

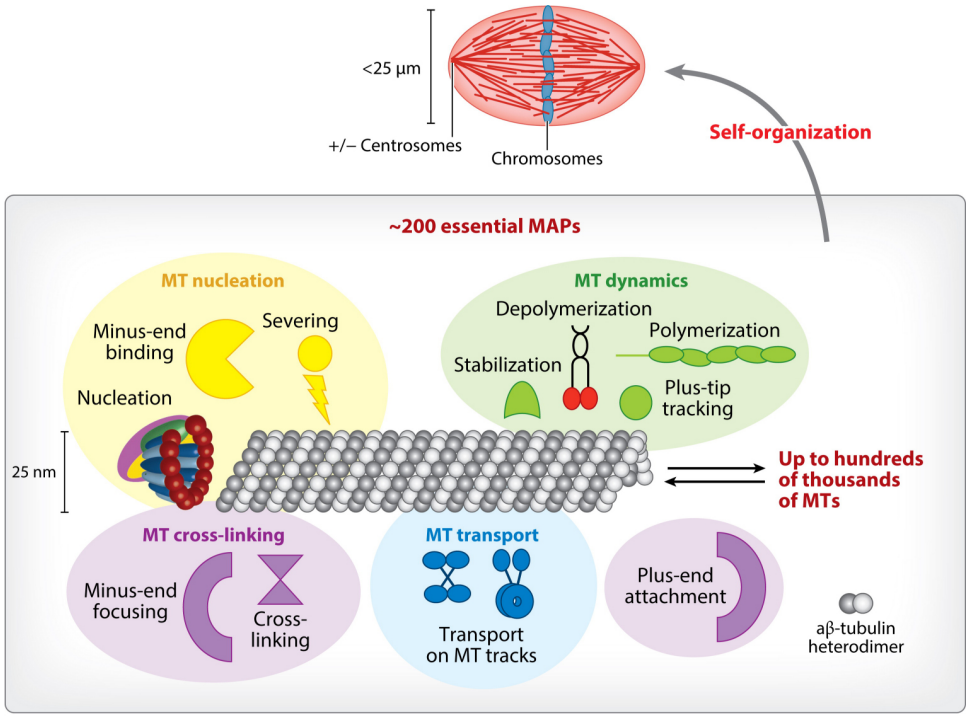

Figure 1.4. **Microtubule associated proteins and microtubule motors.** Examples of different classes of MAPs and microtubule motors and how they can alter microtubule behavior and organization within the spindle. Adapted from Petry, S. *Ann. Rev. Biochemistry* (2016)[57].

1.5. Spindle assembly and chromosome segregation in *C. elegans*

In this section I will highlight the major elements of mitotic spindle assembly and chromosome segregation, and then provide a detailed overview of oocyte meiotic spindle assembly and chromosome segregation. In both of these sections, I will place an emphasis on the *C. elegans* gene names and proteins involved in these processes.

1.5.1. Mitotic spindle assembly and chromosome segregation

During mitosis, assembly of the bipolar spindle is driven by two centriole-containing centrosomes. The centrosomes serve as the major microtubule organizing centers and define the

poles of the spindle. A cell begins each cell cycle with one centrosome that is then duplicated concurrently with the genome. That way each pole of the bipolar spindle contains one centrosome and each daughter cell will inherit only one centriole-containing structure. The centrosome is a membraneless organelle comprised of two microtubule-based centrioles surrounded by an assembly of proteins called the pericentriolar material (PCM). The main function of the PCM is to serve as a scaffold that promotes microtubule nucleation and to provide an anchor for the minus-ends of microtubules[58]. In most systems, the centrosome accomplishes this nucleation activity by concentrating γ-tubulin, which serves as a template to promote microtubule assembly[59]. Interestingly, in *C. elegans*, γ-tubulin is not absolutely required for the assembly of microtubules from mitotic centrosomes[60,61], suggesting that there are redundant or alternative pathways for microtubule nucleation during mitosis. Once the microtubules are nucleated, they are further organized by MAPs and microtubule motor proteins. One such MAP is the XMAP215 microtubule polymerase family member ZYG-9, which functions to stabilize the microtubules and promote their efficient assembly[50]. In most systems, the kinesin Eg5 acts on overlapping interpolar microtubules emanating from each pole to drive the poles apart[29,30]. The outward force generated by Eg5 is opposed by the action of dynein. Inhibition of Eg5's activity results in a loss of bipolarity, and a collapse of the two poles into a single monopole[62,63]. Interestingly, depletion of *C. elegans* Eg5 (BMK-1) has no effect on mitotic spindle assembly and results in only a subtle spindle elongation defect during anaphase[64,65], suggesting that there are other, Eg5 independent mechanisms to promote centrosome separation and spindle bipolarity.

The microtubule plus-ends emanating from the centrosome reach into and search the cytoplasm until they capture kinetochores[66]. Once enough microtubules make end-on attachments to the kinetochore, these microtubules are stabilized in the form of a kinetochore

fiber (K-fiber)[67,68]. Once each sister chromatid makes a K-fiber attachment emanating from each pole, the chromatid becomes bioriented and aligns at the metaphase plate. When all of the sister chromatids become attached to the spindle and bioriented, the spindle assembly checkpoint is satisfied and the chromosomes segregate to the poles during anaphase[69].

Anaphase during mitosis proceeds in two distinct stages, anaphase A and anaphase B. During anaphase A in most cell types, the chromosomes are moved towards the poles through shortening of the K-fibers, and this depolymerization of K-fibers is driven by MCAK[70]. In *C. elegans*, however, K-fibers do not play a role in anaphase A as there is no K-fiber shortening[71]. Instead, the current model for segregation during *C. elegans* mitosis is that chromosomes are pushed apart through polymerization of inter-chromosomal microtubules in the midzone in a CLASP and Ran dependent manner[64]. These midzone microtubules are stabilized by the centralspindlin complex, which consists of CYK-4 (RhoGAP) and the kinesin-6 family member ZEN-4 (MKLP1)[44]. These midzone microtubules are also stabilized by the antiparallel microtubule bundler SPD-1 (PRC1)[55,56,64,72,73]. During anaphase B, the astral microtubules of the centrosomes are pulled on by cortically anchored dynein which forces the centrosomes and the attached chromosomes farther apart[74]. This dynein derived force acting on the astral microtubules is also important for spindle positioning prior to anaphase[74]. Finally, the cell is divided in two during cytokinesis.

1.5.2. Oocyte meiotic spindle assembly and chromosome segregation

Prior to spindle assembly and the meiotic divisions, the bivalents must load the necessary kinetochore and chromosomal passenger complex (CPC) components (Fig. 1.5). By the time the meiotic bivalents have complete diakinesis and have condensed, kinetochore components load onto the holocentric chromosomes, which appear to cup the ends of the bivalents[75]. Also during late diakinesis, the bivalents begin to load the CPC components including the Aurora

B kinase AIR-2, which forms a ring-like structure (the ring complex or RC) at the center of each bivalent[76–78]. During MII, the RC is loaded onto the sister chromatid interface. In addition to the CPC, the RC contains many proteins necessary for the faithful execution of the meiotic divisions[78,79], including the chromokinesin KLP-19 (kinesin-4), which provides the plus-end directed force to align the chromosomes at the metaphase plate[37]. Moreover, the RC is a dynamic structure whose assembly and regulated disassembly rely on a balance of addition and removal of the small ubiquitin-like modifier, SUMO[80,81].

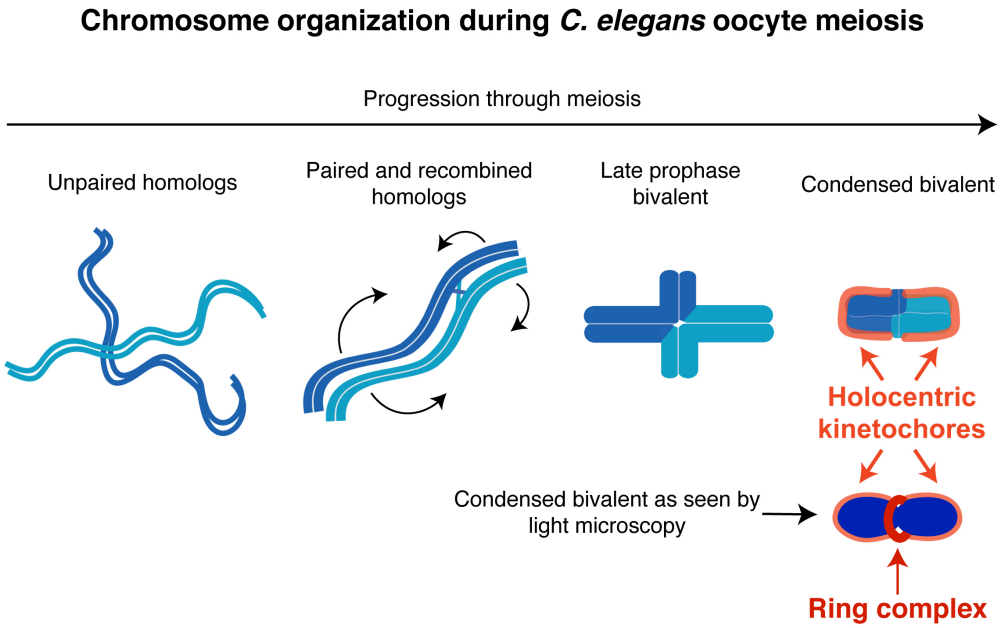

Figure 1.5. **Chromosome organization during *C. elegans* oocyte meiosis.** As meiosis progresses, paired homologs recombine and then reorganize into a cruciform bivalent by late prophase. The bivalent further condenses and the short arms of the chromosomes are tucked into the structure. Holocentric kinetochores form cup-like structures around each bivalent. The ring complex (RC) containing the CPC is assembled at the midbivalent region. By light microscopy, the bivalents (MI) and paired sister chromatids (MII) appear as bilobed structures.

As discussed above, oocytes in many organisms assemble their spindles in the absence of centriole-containing centrosomes. In *C. elegans*, the centrioles are eliminated at the diplotene

stage of meiotic prophase I through poorly understood mechanisms[82]. Then, oocytes arrested at the end of prophase I, located proximal to the spermatheca, are activated by a sperm secreted hormone[83] and begin the meiotic divisions. After nuclear envelope breakdown (NEBD), bipolar spindle assembly then proceeds by: 1) microtubule nucleation and assembly of the microtubules into a cage-like structure that is closely associated with the disassembling nuclear envelope, 2) sliding and reorganizing of the microtubules such that the minus-ends of the microtubules are forced to the periphery of the structure where they are gathered into multiple nascent poles, and finally 3) the multiple nascent poles coalesce into a bipolar structure[84] (Fig. 1.6). Early on in this process, microtubule bundles make lateral associations with the chromosomes, and these interactions are maintained through anaphase. In this system, there are no end-on kinetochore-microtubule attachments. Instead, the lateral associations are necessary for chromosome movement to the metaphase plate[37] and chromosome segregation during anaphase[85]. Many factors are responsible for the completion and proper assembly of a bipolar acentriolar spindle. In the following paragraphs, I will provide an overview of the current state of knowledge regarding *C. elegans* acentriolar spindle assembly.

Currently, it is not known how the microtubules are initially nucleated and assembled at the cage-stage. γ-tubulin is present around the disassembling nuclear envelope, but depletion of γ-tubulin does not appear to cause any defects in spindle assembly[86,87]. Additionally, γ-tubulin does not localize to the bipolar metaphase spindle[60,87,88]. Another microtubule nucleation modality that could be contributing to microtubule assembly at the cage stage is the Ran pathway. Active Ran has been shown to be important for spindle assembly in *Xenopus* egg extract, mouse, *Drosophila*, and human oocytes[16,89–91]. In *C. elegans*, Ran has been reported to be dispensable for accurate chromosome segregation in oocytes, but has

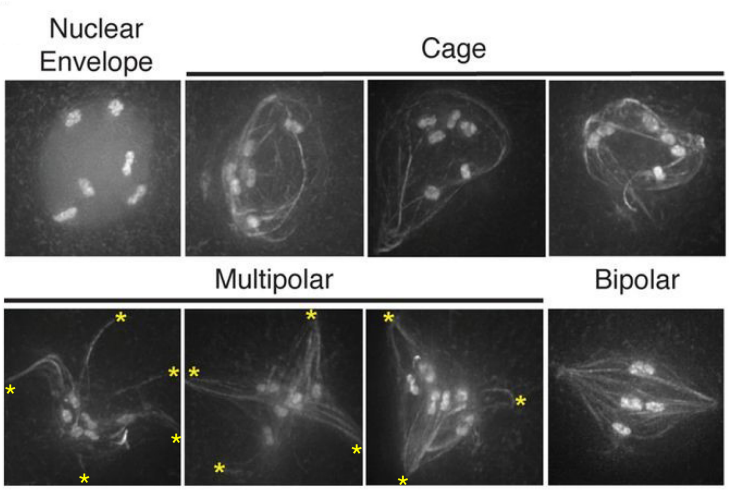

Figure 1.6. **The stages of acentriolar spindle assembly in *C. elegans* oocytes.** The stages of acentriolar spindle assembly in a worm strain expressing GFP::tubulin and GFP::histone to mark the microtubules and the chromosomes, respectively. After nuclear envelope breakdown, the microtubules are nucleated and assembled into a cage-like structure. The microtubules are then sorted, and the minus-ends of the microtubules are moved to the periphery of the array where they are organized into multiple nascent poles (denoted by yellow asterisks). The nascent poles coalesce and a bipolar spindle is formed. Adapted from Wolff, et al., *Mol. Bio. Cell* (2016)[84].

not been studied in any careful detail[92]. The cage-like configuration of microtubules has only to date been observed in *C. elegans* oocytes, and therefore may be mediated through unique mechanisms. Furthermore, there is no cage-stage in MII as there is no disassembling nuclear envelope. During MII, the microtubules appear to nucleate in the vicinity of the chromosomes[84], suggesting that there are different modes of microtubule nucleation during MI and MII. This is an interesting problem that warrants further studies.

Following the cage-stage, the microtubules are sorted and the minus-ends of the microtubules are forced to the periphery of the structure where they are organized into multiple "nascent" poles. Fixed and live imaging of these nascent poles revealed that they are enriched with the microtubule minus-end binding protein ASPM-1[53,84]. This microtubule sorting is driven by the activity of KLP-18 and MESP-1[53,84,93]. KLP-18 is a plus-end directed motor

of the kinesin-12 family, and MESP-1 is an auxiliary protein that likely forms a complex with KLP-18, which allows the motor to function and promote microtubule sorting by generating an outward sliding force on the microtubules[37,84]. In support of this outward-force generation function of KLP-18, depletion of KLP-18 or MESP-1 results in a monopolar spindle phenotype with all of the microtubule minus-ends concentrated in a single pole[37,84,93]. Interestingly, depletion of the Eg5 homolog in *C. elegans*, BMK-1 has been shown to have no effect on acentriolar spindle bipolarity, suggesting that KLP-18 is the major outward force generator in this system[65].

Several other factors have been implicated in the focusing of the nascent poles into a bipolar spindle. The activity of the MEI-1/2 (katanin) microtubule severing complex is necessary for maintaining spindle bipolarity, and experiments using a fast acting temperature sensitive allele of *mei-1* showed a loss of spindle bipolarity when spindles arrested at metaphase were shifted to the restrictive temperature[94]. ASPM-1 is also important for the early stages of pole focusing, and inhibition of ASPM-1 activity results in spindles that have unfocused poles early during spindle assembly, however, bipolarity is eventually achieved[53]. More recently, it was shown that katanin and ASPM-1 can form a complex *in vivo*[52], and therefore may function in the same pathway to promote bipolarity. Dynein has also been implicated in spindle pole focusing. Dynein localizes diffusely to the acentriolar spindle during metaphase before becoming enriched at the spindle poles at the metaphase-to-anaphase transition[95–97]. Experiments using the dynein inhibitor ciliobrevin and partial RNAi depletions of the dynein heavy chain (*dhc-1*) caused spindle assembly defects suggesting that the minus-end directed activity of dynein is important for organizing the spindle poles[85]. Finally, the kinesin-13 family member MCAK (KLP-7) is required for pole coalescence and

bipolarity by balancing the forces generated by the microtubules that attach to the kinetochores[53]. In this study, the authors proposed that MCAK acts to destabilize improper kinetochore-microtubule attachments, and in the absence of MCAK, there are too many attachments leading to an imbalance of forces and a failure of pole coalescence. In mitosis, MCAK functions to destabilize improper end-on kinetochore-microtubule attachments[47]. It is unclear exactly how such a mechanism would work in *C. elegans* oocyte meiosis as there are no end-on kinetochore-microtubule attachments in the acentriolar spindles in this system[37]; however, there may still be an optimal number of lateral kinetochore-microtubule attachments. Indeed, when the authors co-depleted the kinetochore component responsible for making kinetochore-microtubule attachments during mitosis[98], bipolarity was restored presumably because the balance of forces had been equalized.

A common feature of acentriolar meiotic spindles is that they lack long microtubules that extend from the poles to the chromosomes. In *Xenopus* and *Drosophila*, the meiotic spindles are comprised of many short microtubules organized into a tiled array with microtubule minus-ends throughout[99–103]. This is also true for the acentriolar *C. elegans* spindle. A partial electron microscopy (EM) reconstruction of a *C. elegans* acentriolar metaphase spindle revealed the presence of many short microtubules[51]. The authors then go on to do an EM reconstruction of a spindle from an oocyte depleted of MEI-1/2 (katanin), and found that the spindle was comprised of fewer, longer microtubules. This lead to a model in which the severing activity of katanin produces many short microtubules that can be arranged by other spindle assembly factors into a functional bipolar spindle of the correct length. How these short microtubules might be bundled and organized within the spindle is discussed in Chapter 2.

The acentriolar poles of the *C. elegans* oocyte spindle lack the core PCM components SPD-2 and SPD-5[104–106], however some factors that localize to the centrosome are also found at the acentriolar spindle poles including ASPM-1, ZYG-9, the transforming acid coiled-coil protein TAC-1, MESP-1, and KLP-18[53,84,95,107–109]. Additionally, the Aurora A kinase AIR-1 is found at the mitotic spindle poles, and localizes diffusely to oocyte spindles. In mitosis, AIR-1 is required for centrosome maturation[110], and during oocyte meiosis, it is required for the formation and maintenance of microtubules that get incorporated into the spindle[111]. KLP-18 does not have any phenotype when depleted from mitotic embryos, but depletion from oocytes results in monopolar spindles[37,53,84,93]. Furthermore, it is interesting that the proposed function of KLP-18 is to generate bipolarity in the acentriolar spindle by sliding antiparallel microtubules apart in the midspindle region where there would be an overlap zone of microtubules, yet KLP-18 is enriched at the spindle poles. It is possible that KLP-18 and/or KLP-18's binding partner MESP-1[84] have other functions at the acentriolar spindle poles, but that is an open question. ZYG-9 and TAC-1 typically form a complex and promote microtubule formation and spindle assembly during mitosis, and have both been implicated in acentriolar spindle assembly. However, the conclusions that ZYG-9 and TAC-1 are necessary for acentriolar spindle assembly were based on observations of chromosome segregation defects alone, and a detailed characterization of these factors has not been done[107–109,112]. Moreover, a detailed analysis comparing the overall composition and behavior of the acentriolar and centrosomal poles has not been carried out either. Initial studies into the role of ZYG-9 and spindle pole composition are the subjects of Chapter 3.

Anaphase is initiated by the activation of the anaphase promoting complex (APC). APC activation triggers a number of events that culminate in the segregation and expulsion of

half of the genetic material into a small polar body. First, APC activation degrades cyclin-B/CDK-1, which promotes dynein accumulation at the spindle poles and on the cortex near the spindle[113]. This dynein accumulation is necessary to rotate the spindle 90^o so that the long axis is perpendicular to the cortex[95,97,113]. The APC-mediated degradation of securin activates separase (SEP-1), and active SEP-1 promotes homologous chromosome (in MI) or sister chromatid (in MII) separation by cleaving cohesin[114]. The spindle also shrinks and becomes more rounded in shape at the time of rotation[99,115,116].

The anaphase movements of the chromosomes in *C. elegans* oocytes are kinetochore-independent as the kinetochores are normally removed from the chromosomes prior to anaphase, and experimental depletion of kinetochore components does not alter the chromosome segregation rates[78]. Chromosome movement is dependent on the RC, which is left behind in the center of the spindle as the chromosomes are segregated[76,77] (Fig. 1.7). Therefore, how the chromosomes are segregated in this system is not completely understood. There are competing models for how the forces are generated that segregate the chromosomes on the acentriolar spindles in *C. elegans* oocytes. In the model initially put forth by our lab, during anaphase, the spindle poles broaden, and the lateral microtubule bundles are arranged in a parallel array, which allows for microtubule-free channels. The chromosomes then move pole-ward through these channels via a dynein-mediated mechanism[85]. The RCs remain in the channels to keep them open and allow for the movement of the chromosomes through the channels; then, the spindle elongates in a mechanism analogous to anaphase B, driving the chromosomes further apart[85] (Fig. 1.7). Since then, it has become appreciated that much of the chromosome separation in this system occurs after the chromosomes have reached the poles at the end of anaphase A, suggesting that anaphase B drives the majority of segregation. Furthermore, the chromosome movement to the poles (anaphase

A) and spindle elongation (anaphase B) appear to occur in a sequential manner (Fig. 1.7). One model proposed that the spindle shrinkage brings the chromosomes into close proximity to the spindle poles, the chromosomes move slightly towards those now closer poles, and a physical chromosome-pole tether is formed. Then, spindle elongation in anaphase B, driven by microtubule polymerization stimulated by the doublecortin family protein ZYG-8, is responsible for most of the chromosome movement[88]. Additionally, two recent studies used 3D reconstruction of *C. elegans* oocyte anaphase spindles generated by electron tomography to assess the microtubule architecture of these spindles. Both studies found that microtubules appear to make end-on associations with the chromosomes and suggested that microtubule pushing on the inside surfaces of chromosomes either by polymerization or motor-driven sliding could be responsible for spindle elongation during anaphase B[96,117]. These reconstructions, however, were unable to detect the presence of lateral microtubule-chromosome bundles during anaphase B, which brings into question the contribution of these type of associations during spindle elongation. It is likely that there is some contribution from all of these mechanisms promoting chromosome segregation on *C. elegans* acentriolar spindles. In Chapter 2, I present evidence for the presence of lateral microtubule-chromosome associations during anaphase B, in an attempt to reconcile and unify these different models of segregation.

Once the chromosomes have been segregated, the set closest to the cortex is extruded into a small polar body. This is dependent on the activity of the centralspindlin complex of ZEN-4(MKLP1) and CYK-4(RhoGAP), which binds to microtubules in the spindle midzone during anaphase and helps correctly position the ingressing contractile ring[118,119]. A spindle is then assembled around the chromosomes that are retained in the oocyte, which facilitates the portioning of sister chromatids in MII.

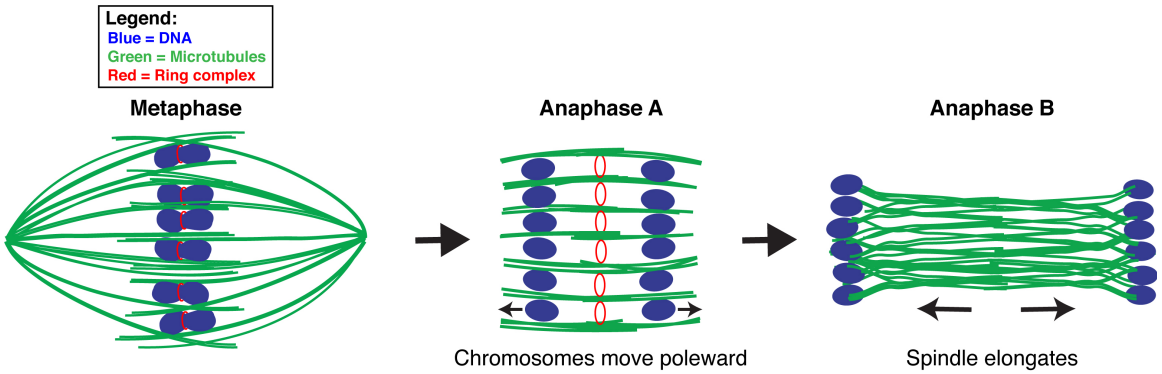

Figure 1.7. **Model for chromosome segregation in *C. elegans* oocytes.** At metaphase, the bivalents are aligned between overlapping microtubule bundles. At anaphase onset, the lateral chromosome-microtubule associations are maintained, the spindle shrinks, and the poles broaden creating microtubule-free channels. During anaphase A, the RC remains in the middle of the spindle and the chromosomes move to the poles through the microtubule-free channels. In anaphase B, the spindle elongates to drive the chromosomes further apart.

The goal of this dissertation is to deepen our understanding of the molecular mechanisms underlying the oocyte meiotic divisions. In Chapter 2, I describe the characterization of two kinesin-14 motor proteins, KLP-15 and KLP-16. I found that these motors are essential for bundling acentriolar spindle microtubules, and in the absence of these proteins, the oocyte spindles are highly disorganized. Interestingly, despite the aberrant spindle phenotype following KLP-15/16 depletion, oocytes progress through anaphase, and the spindle microtubules are bundled and reorganized into a structure capable of segregating chromosomes. I found that the microtubule bundling protein, SPD-1, is responsible for this secondary microtubule bundling activity during anaphase in the absence of KLP-15/16. Furthermore, I found that KLP-18, a kinesin-12, likely sorts the bundles formed by SPD-1 and arranges them along a common axis to allow for chromosome segregation. These discoveries highlight how the oocyte coordinates the activity of multiple microtubule motors and MAPs to promote proper spindle architecture and underscores nature's use of redundant mechanisms to impart robustness into complex cellular processes such as the meiotic divisions. In Chapter 3, I describe

studies aimed at elucidating how the acentriolar spindle maintains structural stability once bipolarity is achieved. This work focuses on the XMAP215 family member ZYG-9, which I show to be essential for acentriolar spindle pole integrity. Acute depletion of ZYG-9 from bipolar acentriolar spindles causes spindle pole instability and fragmentation of the poles. Collectively, the work described in this dissertation advances our understanding of how the acentriolar oocyte spindle is assembled and stabilized to ensure the accurate partitioning of the chromosomes.

CHAPTER 2

Interplay between microtubule bundling and sorting factors ensures acentriolar spindle stability during *C. elegans* oocyte meiosis

The majority of the data presented in this chapter is published in *PLOS Genetics*[120]. The movie of MII spindle assembly (Fig. 2.3A) is published in *Molecular Biology of the Cell*[84]. The live imaging of anaphase spindles and the cold-stable SPD-1 localization experiment are part of a forthcoming manuscript in preparation on which I am a co-author.

2.1. Introduction

During mitosis, centriole-containing centrosomes duplicate and then move to opposite ends of the cell where they nucleate microtubules and form the spindle poles. However, oocytes of many species lack centrioles, and as a result, spindles in these cells assemble using a different pathway[121]. I am interested in understanding the molecular mechanisms underlying this unique, acentriolar pathway of spindle assembly.

Using *C. elegans* oocyte meiosis as a model, we recently found that acentriolar spindle assembly in this system proceeds by: 1) formation of a cage-like structure comprised of prominent bundles of microtubules that are constrained by the disassembling nuclear envelope, 2) reorganization of this structure such that the microtubule minus-ends are sorted away from the chromosomes to the periphery of the array where they are focused into multiple nascent poles, and then 3) coalescence of these poles until bipolarity is achieved[84]. During this process, the microtubule bundles project into the space near the homologous chromosome pairs (bivalents) and then begin to form lateral associations with them, an interaction that is maintained through anaphase. These lateral associations contribute to the alignment of bivalents at metaphase[37]. Subsequently, during anaphase, spindle morphology changes: the spindle shrinks and rotates 90 degrees such that it is perpendicular to the cell cortex, the spindle poles broaden, and the microtubule bundles reorganize into a parallel array, creating open channels[85,99,115]. Anaphase then proceeds through two phases, with chromosome-to-pole movement through the open channels in Anaphase A, and spindle elongation driving chromosomes further apart in Anaphase B[88,96]. This unique mode of chromosome segregation is kinetochore-independent[78], and instead relies on a complex of proteins containing AIR-2 (Aurora B kinase) that concentrates at the center of each bivalent[76,77], forming a ring-like structure (the "midbivalent ring" or RC). These rings localize to chromosomes during

spindle formation[37] and then are removed from chromosomes in anaphase, remaining in the channels in the center of the spindle[78,79].

In this system, numerous factors have been shown to contribute to different aspects of acentriolar spindle assembly (e.g., microtubule length regulation and spindle pole formation), including MEI-1/2 (katanin), KLP-7 (MCAK), ASPM-1, dynein, and others (reviewed in Severson et. al.[122]). Additionally, the kinesin-12 family member KLP-18 promotes spindle bipolarity[37,53,93] by sorting microtubule bundles and forcing the minus-ends outward where they can be organized into the spindle poles[84]. However, the factors that are required for bundling microtubules and stabilizing these bundles in the absence of centrioles and canonical centrosomes are unknown. Furthermore, little is known about how the acentriolar anaphase spindle is organized and stabilized. During mitosis in *C. elegans*, the centralspindlin complex of CYK-4 (RhoGAP) and the kinesin-6 family member ZEN-4 (MKLP1) binds to and bundles antiparallel microtubules in the midzone of the anaphase spindle, providing stability to the structure[44]. The centralspindlin complex also localizes to the meiotic anaphase spindle in oocytes, and although this complex is required for the completion of cytokinesis and polar body formation[118], depletion has no effect on anaphase spindle morphology[78]. Another component important for anaphase spindle organization during *C. elegans* mitosis is the microtubule bundling protein SPD-1 (PRC1), which is required for proper central spindle structure[56,72,73], and localizes to the spindle midzone during mitosis[56] and meiosis[123,124]. However, depletion of SPD-1 from *C. elegans* oocytes does not produce an obvious phenotype[78], making it unclear if this protein functions during oocyte meiosis.

Now, I have identified KLP-15 and KLP-16, members of the conserved kinesin-14 family of minus-end-directed kinesins[125], as factors required for microtubule bundling and organization during acentriolar spindle assembly in *C. elegans* oocytes; in the absence of these proteins, spindles are unable to maintain stable microtubule bundles and as a result are severely aberrant at metaphase and early anaphase. However, despite these defects, microtubules are then able to reorganize into a spindle capable of mediating chromosome segregation during anaphase. Importantly, this unexpected spindle reorganization phenotype enabled me to gain new insights into the mechanisms underlying anaphase spindle organization and chromosome segregation during acentriolar meiosis, uncovering previously unidentified roles for SPD-1 and KLP-18 in anaphase. These studies have revealed a role for minus-end kinesins in acentriolar spindle assembly in *C. elegans* oocytes and highlight how the interplay of multiple mechanisms functions to promote the formation of a bipolar spindle that is capable of faithfully segregating chromosomes in this specialized type of cell division.

2.2. KLP-15 and KLP-16 are required for acentriolar spindle assembly in oocytes

To identify proteins required for acentriolar spindle assembly in *C. elegans* oocytes, I and others in the lab performed a targeted RNAi screen of genes previously reported to be embryonic lethal, visually screening for spindle defects in a strain expressing GFP::tubulin and GFP::histone[37]. This screen identified KLP-15 and KLP-16, two highly homologous minus-end-directed kinesins (91.1% identical in amino acid sequence and 93% identical in mRNA sequence) of the kinesin-14 family[126]. I observed the same spindle defects when I used the RNAi library clone annotated as targeting *klp-15* as I did when I used the *klp-16* clone, likely because both RNAi constructs target both transcripts due to the high sequence similarity

between them (Fig. 2.1A and 2.2). Consistent with this interpretation, my RNAi conditions caused high embryonic lethality (95.6%; Table 2.1), whereas single deletion mutants of either motor were largely viable; *klp-15(ok1958)* had 14% embryonic lethality and a new deletion mutant I generated, *klp-16(wig1)*, had 2.6% embryonic lethality. Treatment of *klp-15(ok1958)* with the RNAi clone annotated as targeting *klp-15* and treatment of *klp-16(wig1)* with the clone annotated as targeting *klp-16* caused high embryonic lethality (89.8% and 94.6%, respectively; Table 2.1), consistent with the interpretation that both proteins are expressed, and that each RNAi library clone can target both proteins. These results suggest that KLP-15 and KLP-16 are redundant, and therefore, I refer to these proteins collectively as KLP-15/16 (in describing assays and results where I cannot distinguish between them).

Previous work from other groups had suggested a role for KLP-15/16 in the segregation of meiotic chromosomes. In addition to embryonic lethality, inhibition of these proteins resulted in phenotypes such as polar body defects, a high incidence of male progeny (which results from non-disjunction of the X chromosome in the oocyte) and multiple female pronuclei in the one-cell stage embryo[18,21,125,127–130]. However, a careful analysis to determine the causes of these segregation errors had not been reported. Therefore, I performed detailed live and fixed imaging of oocytes following *klp-15/16(RNAi)*. During MI in control oocytes, after nuclear envelope breakdown (NEBD) is initiated, microtubules form prominent bundles that organize into a cage-like structure (Figs. 2.1B and 2.1C, arrows; Movie 2-1). The microtubules are then sorted such that the minus-ends of the microtubule bundles, visualized by ASPM-1[52,54,95], are on the periphery of the array, where they are organized into multiple nascent poles that coalesce until bipolarity is achieved (Figs. 2.1B, 2.1C, 2.1D, 2.4A, and 2.4B, top; Movie 2-1 and 2-3). During meiosis I in *klp-15/16(RNAi)* oocytes, although the microtubule cage appears form normally (Figs. 2.1C, bottom, arrows; 2.4B, bottom), the microtubule

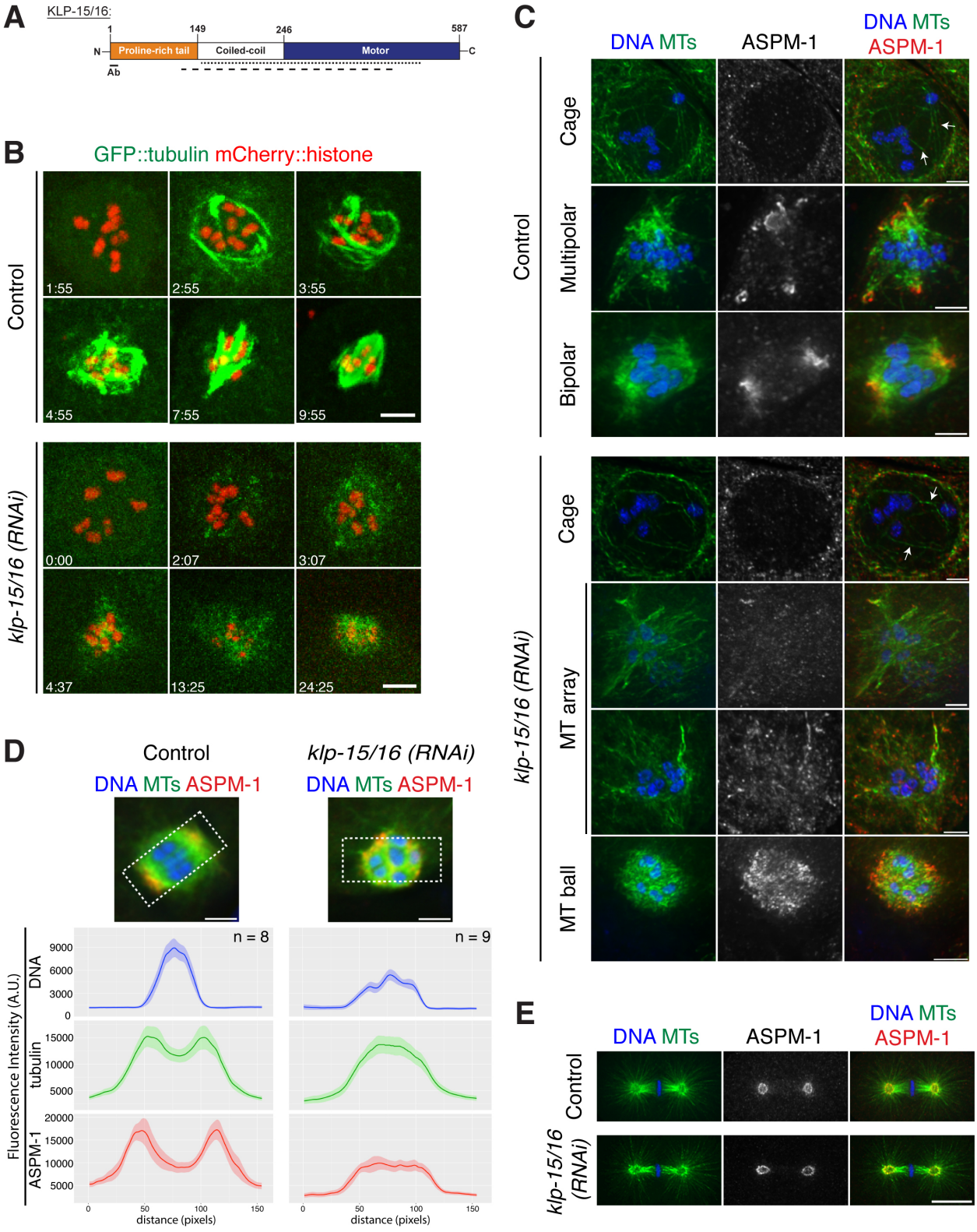
A
KLP-15/16:
1
149
246
587
N
Proline-rich tail
Coiled-coil
Motor
C
Ab
B
GFP::tubulin mCherry::histone
Control
1:55
2:55
3:55
4:55
7:55
9:55
klp-15/16 (RNAi)
0:00
2:07
3:07
4:37
13:25
24:25
C
DNA MTs
ASPM-1
DNA MTs ASPM-1
Control
Cage
Multipolar
Bipolar
klp-15/16 (RNAi)
Cage
MT array
MT ball
D
Control
klp-15/16 (RNAi)
DNA MTs ASPM-1
DNA MTs ASPM-1
n = 8
n = 9
Fluorescence Intensity (A.U.)
DNA
tubulin
ASPM-1
9000
6000
3000
0
15000
10000
5000
20000
15000
10000
5000
0
50
100
150
distance (pixels)
E
DNA MTs
ASPM-1
DNA MTs ASPM-1
Control
klp-15/16 (RNAi)

Figure 2.1

Figure 2.1. **Depletion of KLP-15/16 results in disorganized oocyte spindles.** (A) Schematic of KLP-15/16 with the proline-rich tail in orange, coiled-coil domain in white, and the motor domain in blue. The dotted line represents where *klp-15(RNAi)* targets, and the dashed line represents where *klp-16(RNAi)* targets. The underlined region labeled "Ab" is the region of the protein my antibody was made against. (B) Movie stills from *in utero* control and *klp-15/16(RNAi)* oocytes expressing GFP::tubulin and mCherry::histone. In the control, after NEBD, diffuse tubulin can be seen inside the nucleus[124] . Then microtubules are nucleated and bundled to form a cage-like structure before reorganizing into a multipolar spindle and achieving bipolarity (in 5/5 control movies examined, spindles achieved bipolarity prior to anaphase onset). Following *klp-15/16(RNAi)*, microtubules form a transient cage that then forms a disorganized array that fails to achieve bipolarity and collapses into a microtubule ball (in 6/6 *klp-15/16 (RNAi)* movies examined, spindles entered anaphase without achieving bipolarity); although strong cage bundles are not evident in this particular example, fixed imaging has confirmed that they are able to form. (C, D, and E) Meiotic (C and D) and mitotic (E) spindles stained for DNA (blue), tubulin (green) and ASPM-1 (red). (C) In the control, ASPM-1 marks spindle poles at the multipolar and bipolar stages. In *klp-15/16(RNAi)* oocytes, the microtubule cage forms, but then aberrant structures form with diffuse ASPM-1 staining. (D) Line scans of metaphase spindles in control and *klp-15/16(RNAi)* oocytes. 6 z-slice sum projections of spindles were used for the analysis and the average fluorescence intensities are graphed (solid line) with the SEM (shaded area). The y-axes of the graphs are the same for the control and experimental conditions for a given channel. (E) Mitotic spindles are normal in *klp-15/16(RNAi)* embryos (12/12 *klp-15/16(RNAi)* spindles analyzed were bipolar and indistinguishable from control spindles). Bars = (B) 5 μm; (C and D) 2.5 μm; (E) 10 μm.

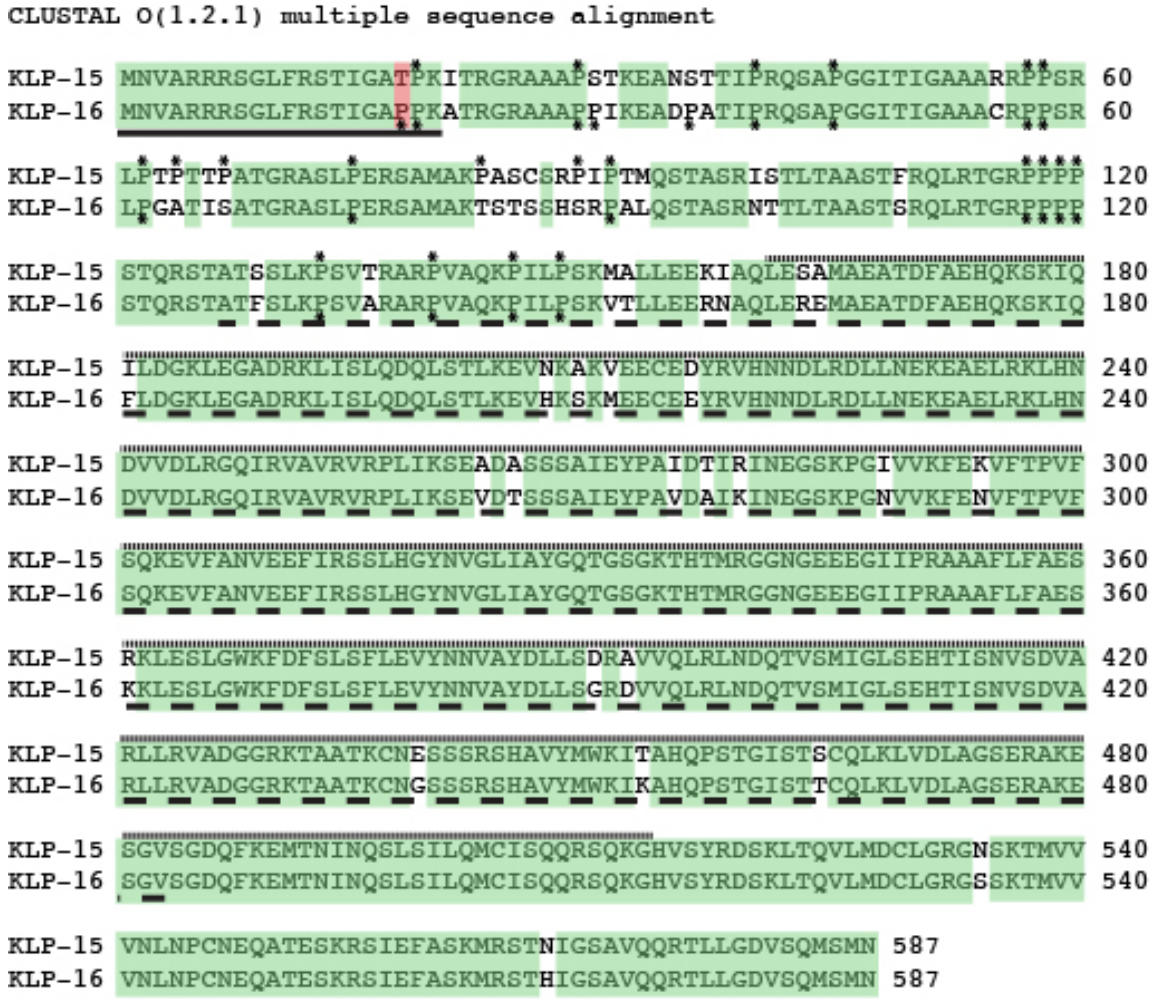

Figure 2.2. **Amino acid sequence alignment of KLP-15 and KLP-16.** Residues shaded in green are identical between the two proteins. Prolines in the proline-rich tail (1–149 aa) are denoted with asterisks. The dotted line denotes the region of complementarity to *klp-15(RNAi)* and the dashed line denotes the region of complementarity to *klp-16(RNAi)*. The solid line under the N-terminal 20 amino acids marks the peptide sequence that was used to make my KLP-15/16 antibody; the red shaded residue is the single amino acid difference between KLP-15 and KLP-16 in the sequence used to make my antibody.

Allele	Condition	Embryonic Lethality
Wild-type	Control	3.56% n = 2109
	klp-16(RNAi)	95.6% n = 2032
klp-15(ok1958)	Control	14% n = 946
	klp-15(RNAi)	89.8% n = 1236
klp-16(wig1)	Control	2.6% n = 1104
	klp-16(RNAi)	94.6% n = 808

Table 2.1. **Embryonic lethality assays.** Results of embryonic lethality assays from wild-type, *klp-15(ok1958)*, and *klp-16(wig1)* worms. The wild-type and *klp-16(wig1)* worms were fed bacteria expressing the RNAi clone annotated as targeting KLP-16, and *klp-15(ok1958)* worms were fed bacteria expressing the RNAi clone annotated as targeting KLP-15.

bundles are not maintained and begin to fall apart, resulting in a disorganized array that lacks focused nascent poles. Then, the array collapses into a "microtubule ball" comprised of short microtubules surrounding the chromosomes (Figs. 2.1B, 2.1C, and 2.4B; Movies 2-1 and 2-2). ASPM-1 localization appears largely diffuse at both the microtubule "array" and "ball" stages (Figs. 2.1C, 2.1D, and 2.5A; Movie 2-4), suggesting that microtubule minus-ends are distributed throughout these structures. However, since there are examples of spindles where ASPM-1 does have areas of slight concentration within the microtubule ball structures (Fig. 2.5A, arrowheads), it is possible that these spindles have some small degree of microtubule organization. During MII in control oocytes, the microtubules are nucleated in the region surrounding the chromosomes. These microtubules are then bundled and sorted to form nascent poles marked by ASPM-1 that coalesce to form a bipolar spindle (Fig. 2.3A, 2.3B; Movie 2-5)[84]. In *klp-15/16(RNAi)* MII oocytes, the microtubules are nucleated around the chromosomes, similar to control oocytes, but these microtubules are never organized properly. As a result, I observe the microtubules assemble into a "microtubule ball" similar to MI (Fig.

2.3B). How these incredibly disorganized spindles partition chromosomes, extrude a polar body, and progress to MII is discussed later in this chapter.

My analysis therefore demonstrates that depletion of KLP-15/16 affects the early stages of spindle assembly, resulting in structures that lack prominent microtubule bundles past the cage stage in MI and after the microtubules are nucleated near the chromosomes in MII. These two kinesins likely function redundantly at this stage, since spindles appeared normal in the *klp-15(ok1958)* and the *klp-16(wig1)* single mutants (Fig. 2.5C). Interestingly, despite the severe spindle defects in oocytes following *klp-15/16(RNAi)*, I observed that mitotic spindles in the one-cell stage embryo formed normally (Fig. 2.1E; Movie 2-6), suggesting that these proteins are not essential when centriole-containing centrosomes are present.

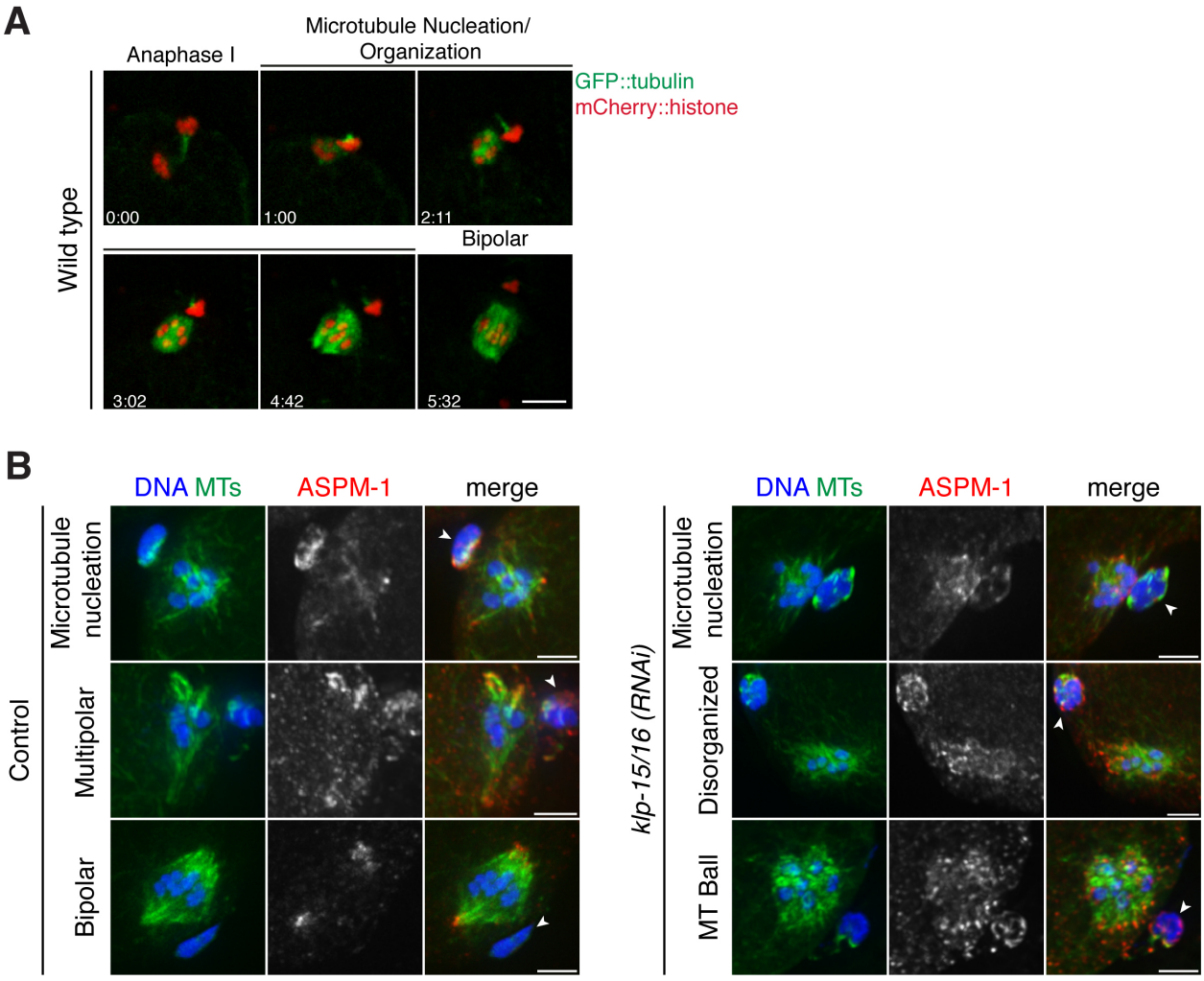

Figure 2.3. **Spindle assembly during meiosis II.** (A) Movie stills of wild-type MII spindle assembly in oocytes expressing GFP::tubulin;mCherry::histone. In wild type MII oocytes, the microtubules are nucleated in the region adjacent to the chromosomes that were retained inside the cell after anaphase I. These microtubules are then bundled and sorted to form a bipolar spindle. (B) MII spindles stained for DNA (blue), tubulin (green), and ASPM-1 (red). In control oocytes, The microtubules are nucleated in the region around the chromosomes. These microtubules are bundled and sorted to form the nascent poles (marked by ASPM-1) of the multipolar spindle, which then coalesce to form the two poles of the spindle. In *klp-15/16(RNAi)* MII oocytes, the microtubules nucleate in the region adjacent to the chromosomes but are never bundled and organized into a bipolar spindle. Arrowheads = polar bodies. Bars = (A) 5 μm; (B) 2.5 μm.

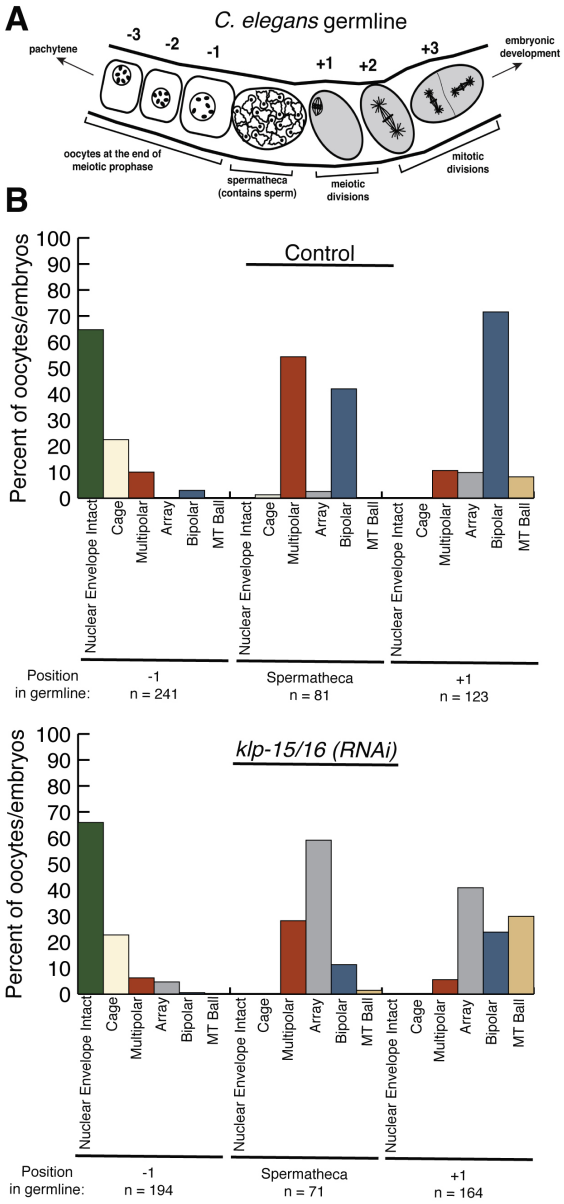

Figure 2.4. **Additional quantification of phenotypes in mutants and following *klp-15/16(RNAi).*** (A) Diagram of the *C. elegans* germline. The germline is organized in an assembly-line fashion where oocytes in prophase (-3 to -1 positions) are ovulated into the spermatheca where they are fertilized. These fertilized embryos begin the meiotic divisions and exit the spermatheca to the +1 position where they continue to progress through meiosis and subsequently mitosis. This organization enables staging of spindles based on the position of the oocyte/embryo in the germline. (B) Quantification of spindle phenotypes in control and *klp-15/16(RNAi)* worms. This analysis was done using live worms expressing GFP::tubulin, GFP::histone. n represents the number of oocytes/embryos analyzed for each condition.

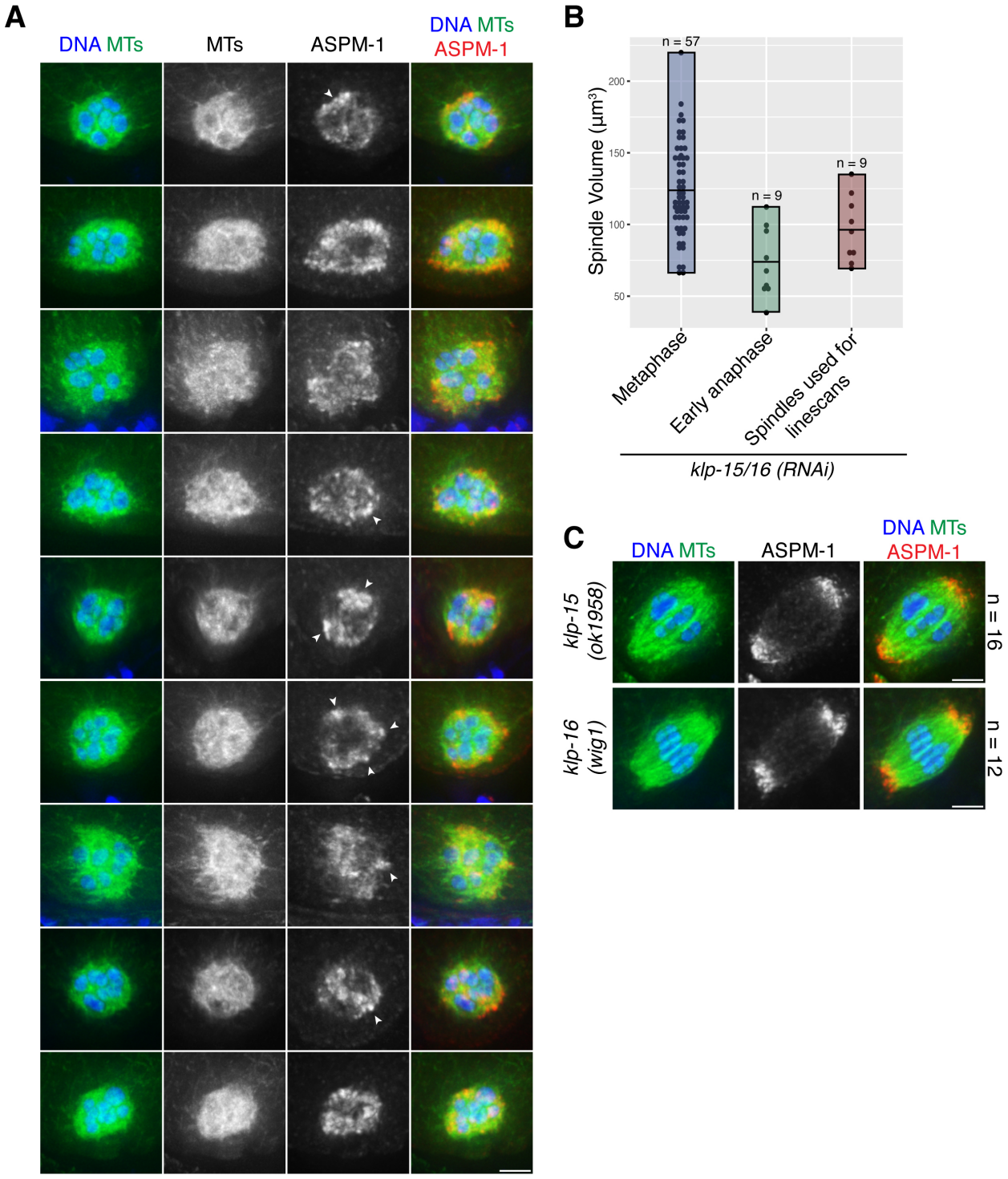
A
DNA MTs
MTs
ASPM-1
DNA MTs
ASPM-1
B
Spindle Volume (µm³)
200
150
100
50
n = 57
n = 9
n = 9
Metaphase
Early anaphase
Spindles used for linescans
klp-15/16 (RNAi)
C
DNA MTs
ASPM-1
DNA MTs
ASPM-1
klp-15 (ok1958)
klp-16 (wig1)
n = 16
n = 12

Figure 2.5

Figure 2.5. **Additional analysis of spindle defects in mutants and following *klp-15/16(RNAi)*.** (A) Shown are DNA (blue), microtubules (green), and ASPM-1 (red) for the nine *klp-15/16(RNAi)* microtubule ball images used for the linescan analysis performed in Fig. 2.1D. ASPM-1 sometimes displays areas of concentration within these structures (examples denoted with arrowheads), that could get averaged out in the graph shown in Fig. 2.1D due to the heterogeneity of the structures. However, I did not observe any clear examples where microtubules appeared to be well-organized into ASPM-1-rich poles that resembled those in wild type spindles, demonstrating that spindle organization is disrupted. (B) Boxplot of spindle volumes of metaphase, early anaphase and the spindles that were used for the linescan analysis in Fig. 2.1D. Metaphase and early anaphase spindles were staged by SEP-1 and AIR-2 localization. Shaded bars represent the range of volumes, bar within the boxes represents the mean, and n represents the number of spindles analyzed for each condition. The range of volumes of the spindles used for linescans suggest that my analysis included both metaphase and early anaphase spindles. (C) DNA (blue), microtubules (green), ASPM-1 (red). In both *klp-15(ok1598)* and *klp-16(wig1)* oocytes, spindles are indistinguishable from wild-type spindles. n represents the number of spindles observed for each condition. Bars = 2.5 μm.

2.3. KLP-15/16 localize to spindle microtubules throughout oocyte meiosis

Given the strong phenotype observed in oocytes upon KLP-15/16 depletion, I next assessed the localization of these proteins. To this end, I generated a peptide antibody against the N-terminal 20 amino acids of KLP-16; because there is only one amino acid different between KLP-15 and KLP-16 in this region, this antibody likely recognizes both proteins (Fig. 2.2). Indeed, this antibody recognizes a band corresponding to the size of both proteins in a Western blot of control worms, and this band was greatly reduced when RNAi was performed using a clone from the RNAi library that had been annotated as targeting *klp-16* (Fig. 2.6A). This band was also reduced when *klp-15(ok1958)* worms were treated with the clone annotated as targeting *klp-15*, and when *klp-16(wig1)* worms were treated with the *klp-16* clone (Fig. 2.6A), further demonstrating the specificity of the antibody and confirming that RNAi treatment using either of the RNAi library clones for *klp-15* or *klp-16* targets both proteins.

Using this antibody, I found that KLP-15/16 localize in the cytoplasm prior to NEBD and then begin to accumulate on microtubules during the multipolar stage, becoming uniform on the spindle throughout metaphase and anaphase (Fig. 2.6B). This localization is specific and likely represents both proteins, as it is abolished following RNAi depletion of KLP-15/16, but it is indistinguishable from wild-type in both the *klp-15(ok1958)* mutant and the *klp-16(wig1)* mutant (Fig. 2.6C). I observed a similar localization pattern in a worm strain expressing KLP-16::GFP from the endogenous locus, but this strain also revealed clear localization of KLP-16 to microtubule bundles at the cage stage (Figs. 2.6D and 2.7B) and to the centrosomes and mitotic spindle microtubules in one-cell stage embryos (Figs. 2.6E and 2.7C), patterns that were not apparent with the KLP-15/16 antibody (quantification in Chapter 5: Materials and methods). This discrepancy is likely due to variability with the

fixed imaging, because even for the stages where I could observe robust staining of spindle microtubules using the KLP-15/16 antibody, not all spindles were stained. Furthermore, when I stained oocytes from the KLP-16::GFP strain with an anti-GFP antibody, I saw similar variability (quantification in Chapter 5: Materials and methods) (Figs. 2.7D, 2.7E), despite the fact that when this strain was viewed live, every oocyte/embryo imaged had bright KLP-16 fluorescence that appeared to mark spindle structures (Fig. 2.7A). Therefore, I conclude that KLP-15/16 localize to spindle structures through all stages of oocyte spindle assembly, and also to microtubules in mitotic one-cell stage embryos.

Although KLP-15/16 localize to microtubule bundles at the cage stage (Figs. 2.6D and 2.7B), these motors are not necessary for the formation of these bundles (Fig. 2.1C), suggesting that they act redundantly with other microtubule associated factors at this initial stage of spindle assembly. Similarly, KLP-15/16 localize to spindle microtubules in mitotic embryos (Figs. 2.6E, 2.7C, and 2.7E), but they are not necessary for the assembly of these spindles (Fig. 2.1E), potentially because centrosomes provide the primary source of microtubule organization in these cells. Taken together, the phenotype of *klp-15/16(RNAi)* and the localization pattern of these proteins support a role for KLP-15/16 in acentriolar meiotic spindle assembly where they stabilize the microtubule bundles formed during the cage stage in MI and bundle microtubules nucleated in the vicinity of the chromosomes in MII. These stabilized microtubule bundles can then be sorted by other molecular motors such as KLP-18 to achieve bipolarity[84].

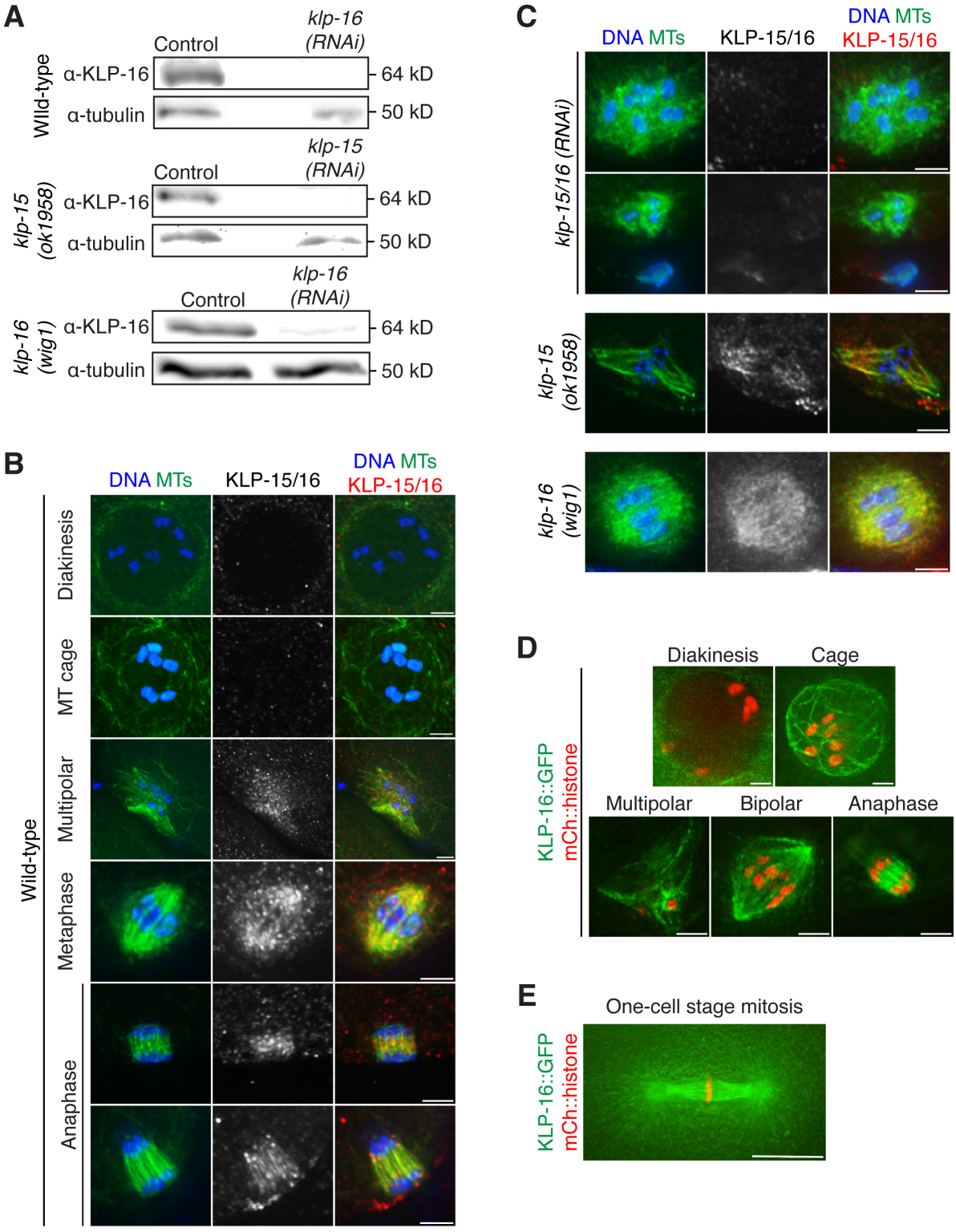
A
Control
klp-16 (RNAi)
Wild-type
α-KLP-16
α-tubulin
64 kD
50 kD
klp-15 (RNAi)
klp-15 (ok1958)
klp-16 (wig1)
B
DNA MTs
KLP-15/16
DNA MTs KLP-15/16
Wild-type
Diakinesis
MT cage
Multipolar
Metaphase
Anaphase
C
klp-15/16 (RNAi)
D
Diakinesis
Cage
Multipolar
Bipolar
Anaphase
KLP-16::GFP
mCh::histone
E
One-cell stage mitosis

Figure 2.6

Figure 2.6. **KLP-15/16 localize to spindle microtubules during oocyte meiosis.** (A) Western blot from control, *klp-15* or *klp-16(RNAi)* worms probed with the KLP-16 antibody or tubulin as a loading control. (B and C) DNA (blue), tubulin (green) and KLP-15/16 (red). (B) Wild-type meiotic spindles at all stages of spindle assembly; KLP-15/16 begin to accumulate on microtubules at the multipolar stage and remain associated through anaphase (quantification in Chapter 5: Materials and methods). (C) The KLP-15/16 signal is lost following *klp-15/16(RNAi)*, though staining of *klp-15(ok1958)* and *klp-16(wig1)* is not different from wild-type spindles (quantification in Chapter 5: Materials and methods). (D and E) *In utero* live-imaging of worms expressing KLP-16::GFP and mCherry::histone shows that KLP-16 localizes to microtubule bundles at the cage stage (which was not apparent in the KLP-16 antibody staining) and remains associated with the spindle (D). The multipolar image is a partial projection of the entire structure. Stages of spindle assembly were discerned by spindle morphology, chromosome organization, and position in the germline. (E) KLP-16 is also present on mitotic spindle microtubules and centrosomes at the one-cell stage (in 5/5 embryos analyzed). Bars = (B, C, and D) 2.5 μm; (E) 10 μm.

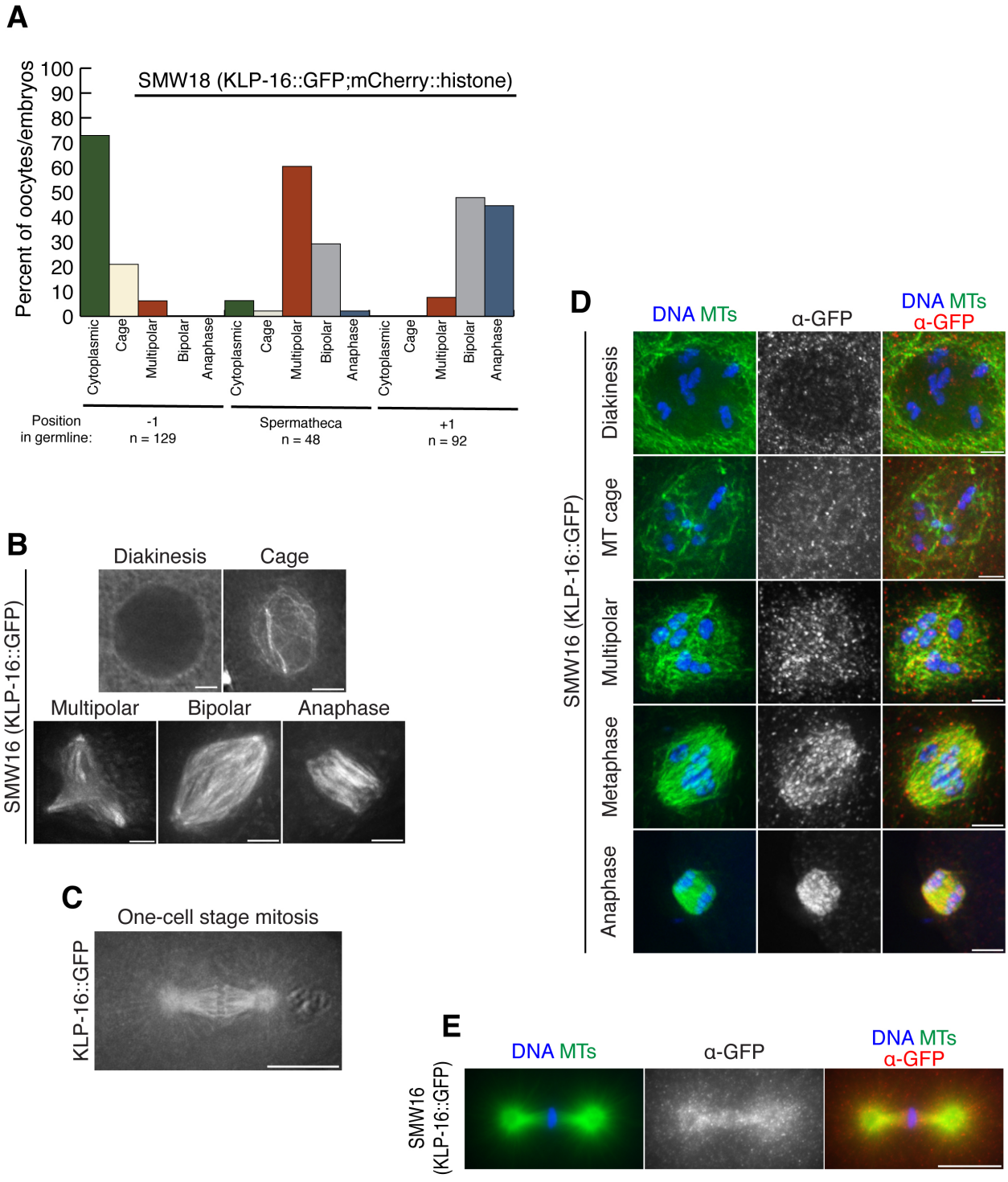
A
SMW18 (KLP-16::GFP;mCherry::histone)
Percent of oocytes/embryos
100
90
80
70
60
50
40
30
20
10
0
Cytoplasmic
Cage
Multipolar
Bipolar
Anaphase
Position in germline:
-1
n = 129
Spermatheca
n = 48
+1
n = 92
B
SMW16 (KLP-16::GFP)
Diakinesis
Cage
Multipolar
Bipolar
Anaphase
C
One-cell stage mitosis
KLP-16::GFP
D
SMW16 (KLP-16::GFP)
DNA MTs
α-GFP
DNA MTs
α-GFP
Diakinesis
MT cage
Multipolar
Metaphase
Anaphase
E
SMW16 (KLP-16::GFP)
DNA MTs
α-GFP
DNA MTs
α-GFP

Figure 2.7

Figure 2.7. **Additional analysis of KLP-16::GFP localization.** (A) Quantification of KLP-16 localization in live worms expressing KLP-16::GFP and mCherry::histone (SMW18). KLP-16 localization was scored as "cytoplasmic" if the GFP signal was absent from inside the nucleus. At all other stages, the GFP signal was enriched on the spindle near the chromosomes. n represents the number of oocytes/embryos analyzed for each condition. (B and C) Examples of KLP-16 localization in live worms expressing KLP-16::GFP (SMW16). (B) KLP-16::GFP is absent from the nucleus prior to spindle assembly. During spindle assembly, KLP-16 localizes to the spindle microtubule bundles and remains associated through anaphase; the image of the cage stage is a sum projection of the spindle structure. (C) KLP-16 localizes to mitotic spindle microtubules and centrosomes in one-cell stage embryos. (D and E) DNA (blue), microtubules (green), GFP (red). Meiotic (D) and mitotic (E) spindles from worms expressing KLP-16::GFP (SMW16) were stained with an anti-GFP antibody. The staining pattern of KLP-16::GFP on meiotic spindles (D) is identical to the staining pattern using the anti-KLP-15/16 antibody. (E) KLP-16::GFP was detected on spindle microtubules and centrosomes (quantification in Chapter 5: Materials and methods). The mitotic image was not deconvolved. Bars = (B and D) 2.5 μm; (C and E) 10 μm.

2.4. Microtubules bundle and chromosomes segregate in anaphase following KLP-15/16 depletion

While filming *klp-15/16(RNAi)* oocytes, I made the surprising observation that although spindle assembly was severely aberrant, microtubules were often able to reorganize into a bundled structure capable of segregating chromosomes, suggesting the presence of a second, KLP-15/16-independent mechanism for bundling microtubules that operates during anaphase (Movie 2-7). Therefore, I used markers of anaphase progression to carefully examine anaphase in *klp-15/16(RNAi)* oocytes, to better understand this mechanism.

During meiosis in wild-type oocytes, separase (SEP-1) relocates from the kinetochore to the midbivalent ring complex at anaphase onset and then disappears from the rings by late anaphase (Fig. 2.8A)[85]. Aurora B (AIR-2), a component of the midbivalent ring complex, is removed from the rings at anaphase onset and relocalizes to the microtubules by mid anaphase (Fig. 2.8A)[79,131]. Therefore, I used these markers to stage oocytes following *klp-15/16(RNAi)*, allowing me to distinguish pre-anaphase (AIR-2 on the ring structures, SEP-1 on kinetochore), early anaphase (both proteins in rings), and mid/late anaphase (AIR-2 on microtubules, SEP-1 gone).

Using these markers to stage *klp-15/16(RNAi)* spindles, I found that the microtubule ball configuration observed in our imaging (Fig. 2.1B, 2.1C, and 2.1D) represents a mixture of metaphase and early anaphase (Fig. 2.8A), although the structures in early anaphase tended to be smaller (Fig. 2.5B). Note that the spindles that I used for our linescan analysis in Fig. 2.1D all were within the range of volumes observed for metaphase spindles (Fig. 2.5B). This analysis suggests that the metaphase disorganized microtubule array begins to shrink in preparation for anaphase, similar to what happens in wild-type spindles[99]. Following this stage, when AIR-2 has relocalized to the microtubules and SEP-1 is gone in mid/late

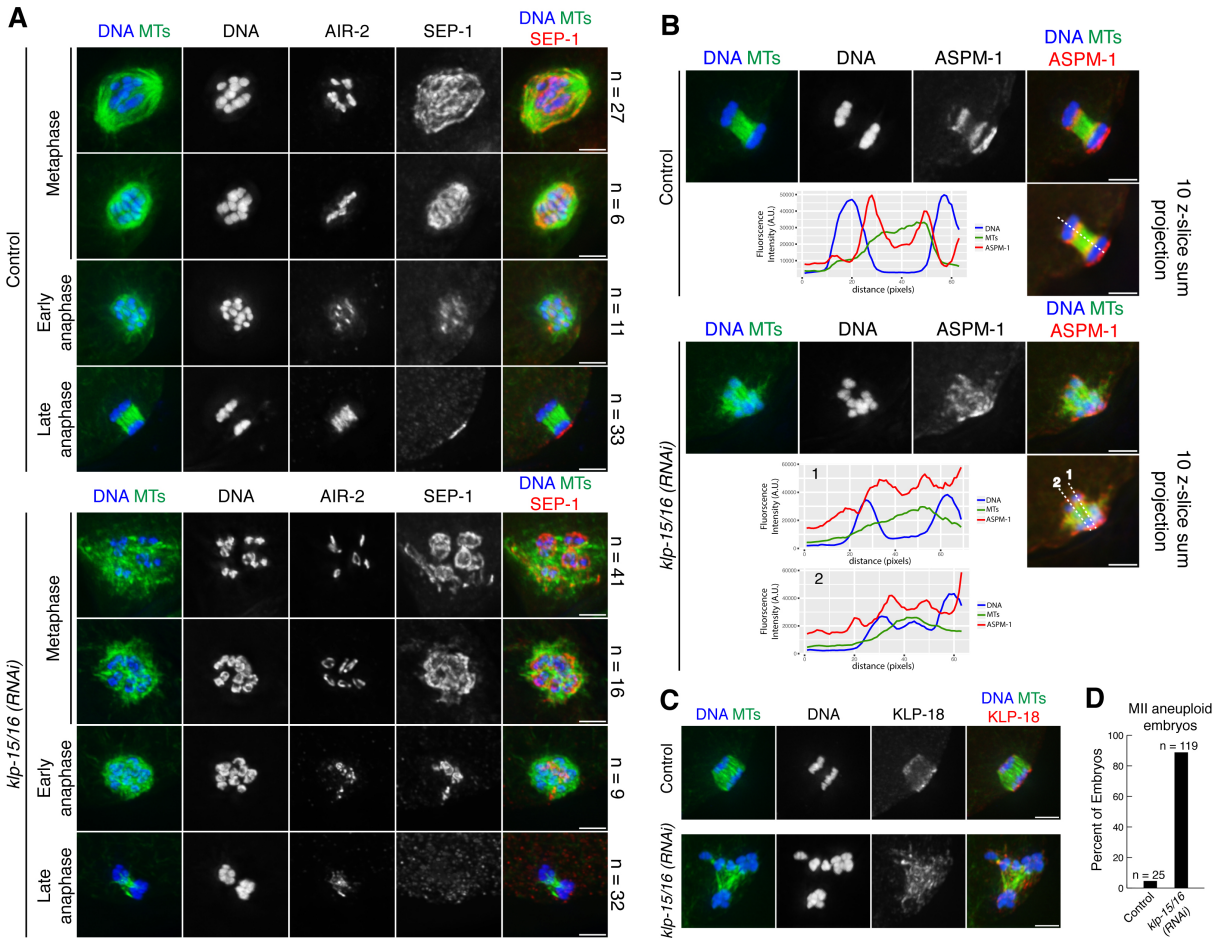
A
DNA MTs
DNA
AIR-2
SEP-1
DNA MTs SEP-1
Control
Metaphase
Early anaphase
Late anaphase
n = 27
n = 6
n = 11
n = 33
klp-15/16 (RNAi)
n = 41
n = 16
n = 9
n = 32
B
DNA MTs
DNA
ASPM-1
DNA MTs ASPM-1
Control
klp-15/16 (RNAi)
10 z-slice sum projection
Fluorescence Intensity (A.U.)
distance (pixels)
DNA
MTs
ASPM-1
1
2
C
DNA MTs
DNA
KLP-18
DNA MTs KLP-18
Control
klp-15/16 (RNAi)
D
MII aneuploid embryos
Percent of Embryos
n = 25
n = 119
Control
klp-15/16 (RNAi)

Figure 2.8

Figure 2.8. **Microtubules bundle and chromosomes segregate in anaphase in *klp-15/16(RNAi)* oocytes.** (A) DNA (blue), tubulin (green), AIR-2 (not in merge) and SEP-1 (red in merge), showing anaphase progression in control and *klp-15/16(RNAi)* oocytes. At metaphase, AIR-2 is in the midbivalent ring and SEP-1 displays a staining pattern characteristic of outer kinetochore proteins in *C. elegans* MI oocytes (cupping the bivalents and also forming filamentous linear structures within the spindle[75]). In early anaphase, SEP-1 co-localizes with AIR-2 in the rings, and in late anaphase, SEP-1 is gone and AIR-2 is relocalized onto the microtubules. In *klp-15/16(RNAi)* oocytes, microtubules are disorganized in metaphase and early anaphase, but in late anaphase microtubules are bundled and chromosomes segregate into distinct masses; note that SEP-1 also localizes to the cell cortex in late anaphase. n represents the number of spindles observed for each condition. (B and C) Anaphase spindles with DNA (blue), tubulin (green), and ASPM-1 (B) or KLP-18 (C) (red). (B) Line scans of anaphase spindles in control and *klp-15/16(RNAi)* oocytes. The top row for each condition is a max projection of the entire spindle and the image used for the line scan is a 10 z-slice sum projection. ASPM-1 is enriched at the poles in control spindles (21/24 of spindles analyzed had ASPM-1 enriched at two poles; 88%), but is diffuse along spindle microtubules in anaphase of *klp-15/16(RNAi)* oocytes (only 9/26 spindles could be classified as having any type of ASPM-1 enrichment at pole-like foci; 35%); in both cases ASPM-1 also displays cortical localization. (C) KLP-18 is enriched at spindle poles in the control (11/12 spindles analyzed; 92%), but is localized throughout the spindles in *klp-15/16(RNAi)* oocytes (6/6 spindles had diffuse KLP-18 localization). (D) Percentage of aneuploid MII embryos from control and *klp-15/16(RNAi)* worms. Chromosomes were counted in images of MII embryos, and embryos were counted as aneuploid if the number of chromosomes did not equal 6. Bars = 2.5 μm.

anaphase, microtubules reform into a bundled structure and chromosomes are able to segregate into distinct masses (Fig. 2.8A). Despite this anaphase spindle reorganization, I observed segregation errors such as lagging chromosomes and segregation of chromosomes along different axes (Fig. 2.8B and 2.8C.; Movie 2-7) that resulted in high levels of aneuploidy in MII embryos (Fig. 2.8D), likely due to the severely aberrant metaphase spindles that were unable to align chromosomes (Fig. 2.1B and 2.1C). The high rates of aneuploidy also raised the possibility that the microtubules in the *klp-15/16(RNAi)* anaphase spindles may not be organized like in wild-type spindles, where a high concentration of microtubule minus-ends are found at the spindle poles. To test this hypothesis, I assessed the localization of ASPM-1 and KLP-18 (a kinesin that is enriched at the poles of wild-type oocyte spindles[93]), and found that the microtubules of anaphase spindles in *klp-15/16(RNAi)* oocytes, although bundled, are likely not organized properly, since ASPM-1 and KLP-18 are distributed throughout the entire spindle instead of being enriched at the poles (Fig. 2.8B and 2.8C). Although it is possible that microtubules within the bundles are properly organized and that the signals to localize ASPM-1 and KLP-18 are defective, I favor the interpretation that the secondary mechanism I identified bundles microtubules without first sorting them, resulting in bundles comprised of microtubules of mixed polarity. This interpretation is also consistent with my findings discussed later in this chapter where I identify the factor responsible for the anaphase microtubule bundling activity in the absence of KLP-15/16.

2.5. KLP-15/16-independent anaphase microtubule bundling is mediated by SPD-1 (PRC1)

Next, I wanted to uncover factors that are responsible for bundling anaphase microtubules in *klp-15/16(RNAi)* oocytes. Two possible candidates are the centralspindlin complex (comprised of ZEN-4 and CYK-4) and SPD-1, since these proteins have clearly defined roles during

anaphase in *C. elegans* mitosis[44,56,73,132] and have been shown to concentrate at the midzone of the anaphase spindle in *C. elegans* oocytes[78,123,124]. Therefore, I assessed the localization of SPD-1 and ZEN-4 at high resolution on *C. elegans* oocyte spindles. As expected from previous studies, I found that neither centralspindlin (ZEN-4) nor SPD-1 localize to metaphase spindles in control oocytes (Fig. 2.9A). However, during anaphase, ZEN-4 and SPD-1 both become enriched in a short region at the center of the spindle (Fig. 2.9A), with similar though non-identical localization (Fig. 2.9C). Following *klp-15/16(RNAi)*, I observed a similar pattern, with neither ZEN-4 nor SPD-1 present on the disorganized spindle structures prior to anaphase, but then prominent localization on the bundled microtubules between the sets of segregating chromosomes during anaphase (Fig. 2.9B). This localization was clear even in spindles with multiple sets of segregating chromosomes, where the bundles were not all oriented along the same axis (Fig. 2.9B, bottom zoom). Therefore, because centralspindlin and SPD-1 both localize to microtubule bundles following *klp-15/16(RNAi)*, these factors are in a location where they could potentially contribute to the anaphase-bundling mechanism I identified.

To test this hypothesis, I assessed a potential functional role for these proteins in anaphase microtubule bundling. In previous work, single or co-depletion of ZEN-4 and SPD-1 did not affect anaphase spindle structure[78], suggesting that these proteins may not play a role in oocytes. However, my studies have revealed a mechanism that operates in parallel with KLP-15/16 (since KLP-15/16 are normally present on anaphase microtubules, Fig. 2.6B and 2.6D). Thus, I expect that single depletion of this putative anaphase bundling factor may have only a mild (or no) anaphase phenotype, but that depletion of KLP-15/16 in combination with the secondary factor would completely abolish anaphase bundling. Therefore, I tested each candidate by single depletion and also by co-depletion/inhibition with

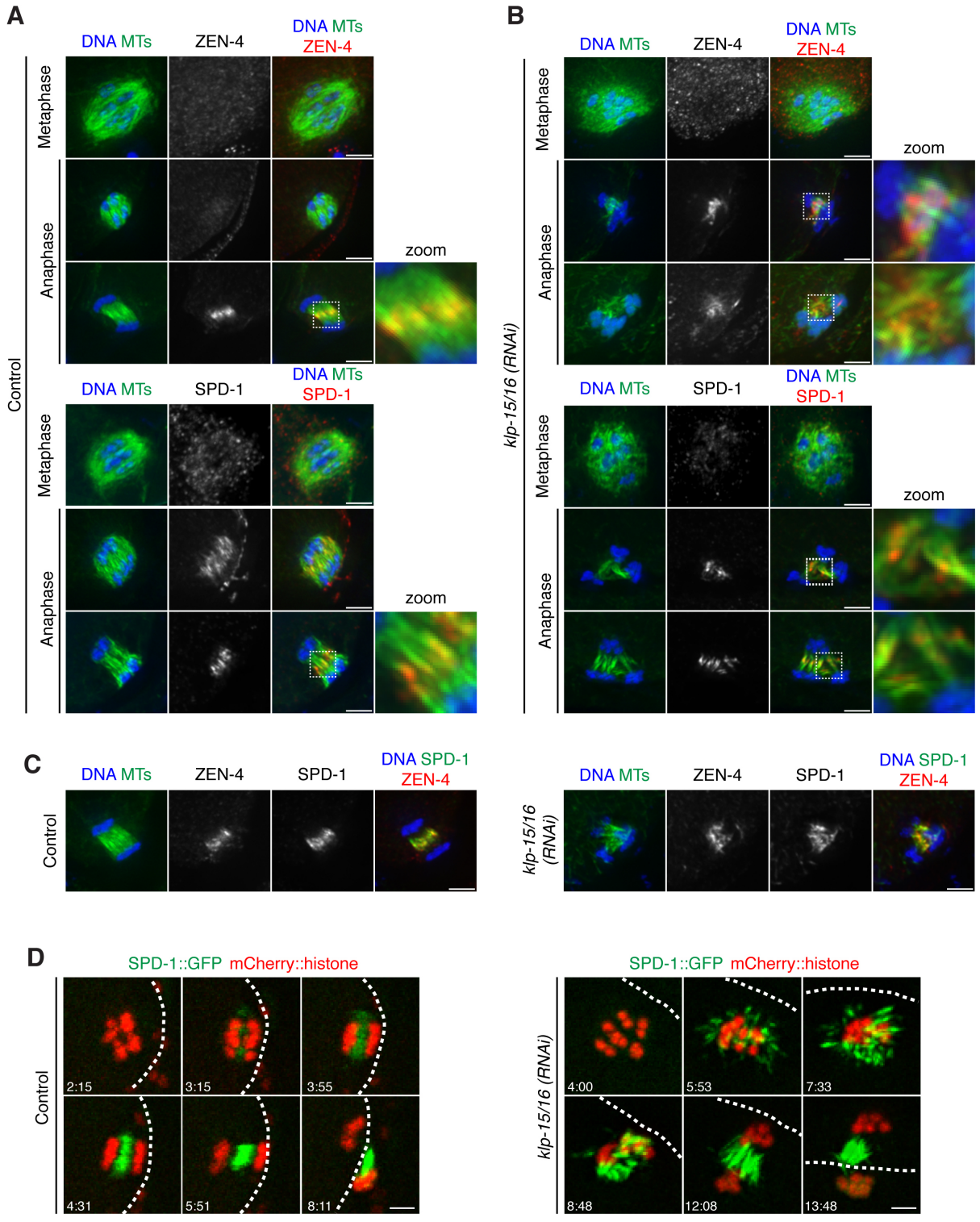
A
DNA MTs
ZEN-4
DNA MTs
ZEN-4
Metaphase
Anaphase
zoom
Control
DNA MTs
SPD-1
DNA MTs
SPD-1
B
klp-15/16 (RNAi)
C
DNA MTs
ZEN-4
SPD-1
DNA SPD-1
ZEN-4
Control
klp-15/16 (RNAi)
D
SPD-1::GFP mCherry::histone
2:15
3:15
3:55
4:31
5:51
8:11
4:00
5:53
7:33
8:48
12:08
13:48

Figure 2.9

Figure 2.9. **SPD-1 and centralspindlin localize to anaphase spindle microtubules.** (A and B) DNA (blue), tubulin (green) and ZEN-4 (top) or SPD-1 (bottom) (red) in control (A) or *klp-15/16(RNAi)* (B) oocytes. ZEN-4 does not localize to metaphase spindles in either condition. In anaphase, ZEN-4 localizes to a distinct region in the midzone of control spindles (A, top zoom), but is sometimes not seen on spindles with a short chromosome segregation distance. Following *klp-15/16(RNAi*), ZEN-4 localizes to the microtubule bundles but is not concentrated to as distinct a band as in the control (B, top zoom). In both control and *klp-15/16(RNAi)* oocytes, SPD-1 does not localize to metaphase spindles. In control oocytes, SPD-1 localizes to the microtubules between the chromosomes in early anaphase and then becomes concentrated in a band on the microtubule bundles in the center of the spindle (A, bottom zoom). Following *klp-15/16(RNAi)*, SPD-1 localizes to microtubule bundles between segregating chromosomes, even when bundles are not all oriented along the same axis (B, bottom zoom) (quantification in Chapter 5: Materials and methods). (C) DNA (blue), tubulin (green), ZEN-4 (red) and SPD-1 (green in final merge). In both control and *klp-15/16(RNAi)* oocytes, ZEN-4 and SPD-1 have similar but distinct localization patterns. (D) Movie stills of oocytes expressing mCherry::histone and SPD-1::GFP in both control and *klp-15/16(RNAi).* In control spindles, SPD-1 localizes between chromosomes as they begin to segregate and continues to accumulate as anaphase progresses, consistent with previous studies[123,124]. Following *klp-15/16(RNAi)*, SPD-1 begins to load all over the microtubules, and as SPD-1 accumulates, long bundles begin to form that then orient along the same axis and the chromosomes segregate (4/4 movies analyzed). White dashed lines = cell cortex. Bars = 2.5 μm.

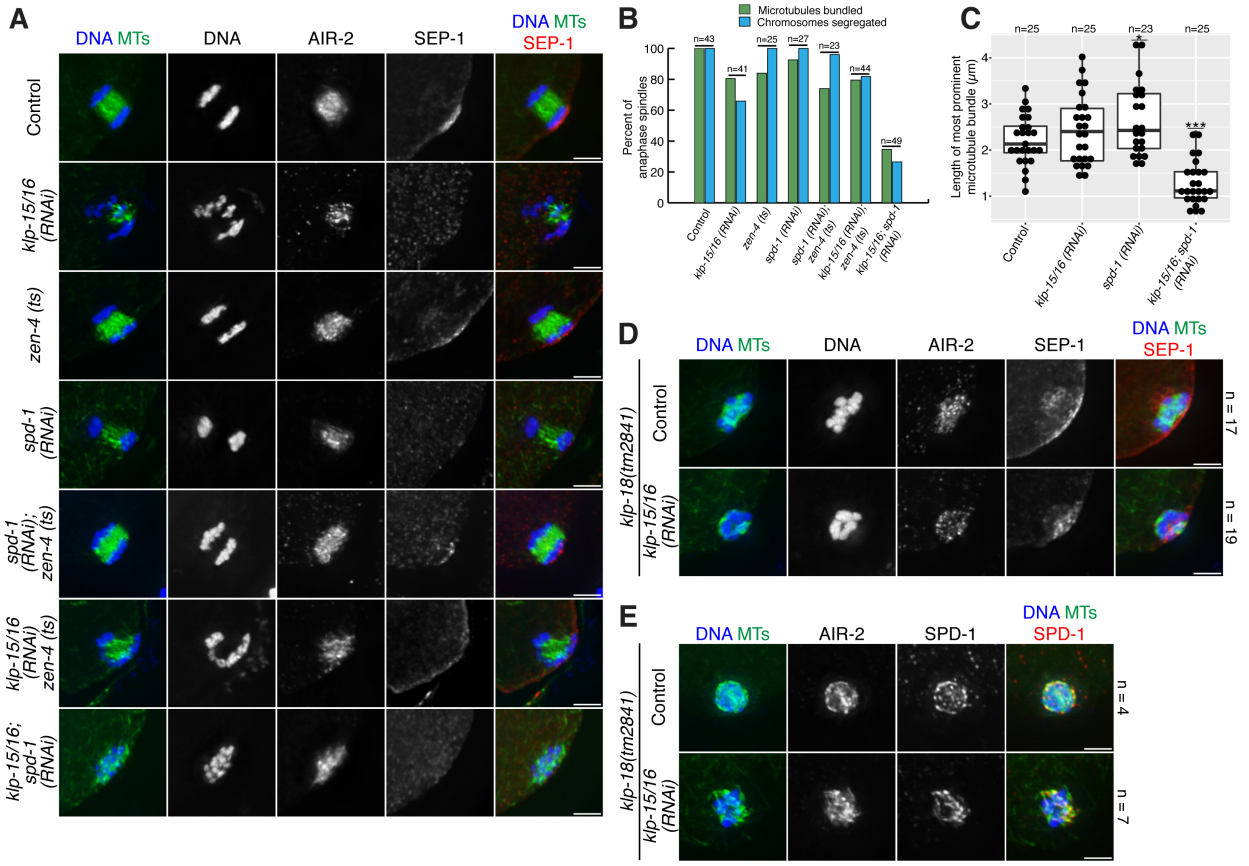
A
DNA MTs
DNA
AIR-2
SEP-1
DNA MTs SEP-1
Control
klp-15/16 (RNAi)
zen-4 (ts)
spd-1 (RNAi)
spd-1 (RNAi); zen-4 (ts)
klp-15/16 (RNAi) zen-4 (ts)
klp-15/16; spd-1 (RNAi)
B
Microtubules bundled
Chromosomes segregated
Percent of anaphase spindles
n=43
n=41
n=25
n=27
n=23
n=44
n=49
Control
klp-15/16 (RNAi)
zen-4 (ts)
spd-1 (RNAi)
spd-1 (RNAi); zen-4 (ts)
klp-15/16 (RNAi); zen-4 (ts)
klp-15/16; spd-1 (RNAi)
C
n=25
n=25
n=23
n=25
Length of most prominent microtubule bundle (μm)
***
Control
klp-15/16 (RNAi)
spd-1 (RNAi)
klp-15/16; spd-1 (RNAi)
D
DNA MTs
DNA
AIR-2
SEP-1
DNA MTs SEP-1
klp-18(tm2841) Control
klp-18(tm2841) klp-15/16 (RNAi)
n = 17
n = 19
E
DNA MTs
AIR-2
SPD-1
DNA MTs SPD-1
klp-18(tm2841) Control
klp-18(tm2841) klp-15/16 (RNAi)
n = 4
n = 7

Figure 2.10

Figure 2.10. **SPD-1 and KLP-18 are required for KLP-15/16-independent spindle reorganization during anaphase.**(A and D) DNA (blue), tubulin (green), AIR-2 (not in merge) and SEP-1 (red in merge); all spindles shown are mid/late anaphase, with SEP-1 gone and AIR-2 relocalized to the microtubules. (A) Singly depleting/inhibiting *klp-15/16*, *spd-1*, or *zen-4* or doubly depleting/inhibiting *klp-15/16;zen-4* and *spd-1;zen-4* all resulted in anaphase spindles that were able to bundle microtubules and segregate chromosomes, while double depletion of *klp-15/16;spd-1* abolished microtubule bundling and chromosome segregation. (B) Quantification of the experiment shown in (A). The simple matching coefficient for microtubule bundling and chromosome segregation = 0.82 (n = 251); in other words, 82% of the spindles either showed chromosome segregation when microtubules were bundled or did not show chromosome segregation when microtubules were not bundled. (C) Box plots showing anaphase microtubule length measurements; for a given image, the most prominent and longest microtubule bundle in the spindle was measured. Box represents first quartile, median, and third quartile. Lines extend to data points within 1.5 interquartile range. Asterisks (***) represent significant difference ($p < 0.001$, two tailed t-test) compared to the other three conditions; (*) represents significant difference ($p < 0.05$, two tailed t-test) compared to control conditions. (D) Anaphase spindle reorganization and chromosome segregation are not observed in *klp-18(tm2841)* following either control or *klp-15/16(RNAi)*; in both conditions microtubules are disorganized and segregation fails, suggesting that KLP-18 could potentially mediate the anaphase spindle reorganization observed in KLP-15/16-depleted oocytes. n represents the number of spindles observed for each condition. (E) DNA (blue), tubulin (green), AIR-2 (not in merge) and SPD-1 (red in merge); SPD-1 localizes to spindle microtubule bundles in *klp-18(tm2841)* and *klp-18(tm2841);klp-15/16(RNAi)* oocytes. n represents the number of spindles observed for each condition. Bars = 2.5 μm.

KLP-15/16 (Fig. 2.10A), and then scored microtubule bundling in mid/late anaphase (using SEP-1 and AIR-2 as markers to stage anaphase, as before; Fig. 2.10B). In addition to microtubule bundling, I also assessed chromosome segregation as a functional readout for anaphase spindle organization, by scoring whether chromosomes were able to segregate into distinct masses (Fig. 2.10B).

Using these assays, I found that both single and double inhibition/depletion of ZEN-4 and SPD-1 had little effect on anaphase microtubule bundling and chromosome segregation (Fig. 2.10A and 2.10B), consistent with a previous study[78]. Oocytes where both ZEN-4 and KLP-15/16 were inhibited/depleted appeared similar to *klp-15/16(RNAi)* alone, with most spindles containing bundled microtubules that were able to segregate chromosomes. However, I found that co-depletion of KLP-15/16 and SPD-1 largely abolished anaphase microtubule bundling and chromosome segregation (Fig. 2.10A and 2.10B) and resulted in spindles with shorter microtubule lengths (Fig. 2.10C). Furthermore, I observed an increase in the percentage of embryos with a single large polar body and no maternal pronucleus under these conditions, suggesting that the meiotic divisions lacked a functional spindle on which DNA could segregate (Fig. 2.11A, 2.11B, and 2.11C). Interestingly, my estimations of spindle microtubule lengths revealed that the microtubules in the *spd-1(RNAi)* condition were somewhat longer than microtubules in the control (Fig. 2.11C), suggesting that SPD-1 may perform a subtle role in regulating spindle length in anaphase. This observation is reminiscent of studies of mitotic anaphase in *C. elegans*, where an SPD-1 mutant displays larger distances between segregating chromosomes than wild-type embryos, suggesting that the microtubule crosslinking activity of SPD-1 can act to slow the rate of spindle midzone elongation[64]. Taken together, these data highlight a previously unknown role for SPD-1 on acentriolar anaphase spindles.

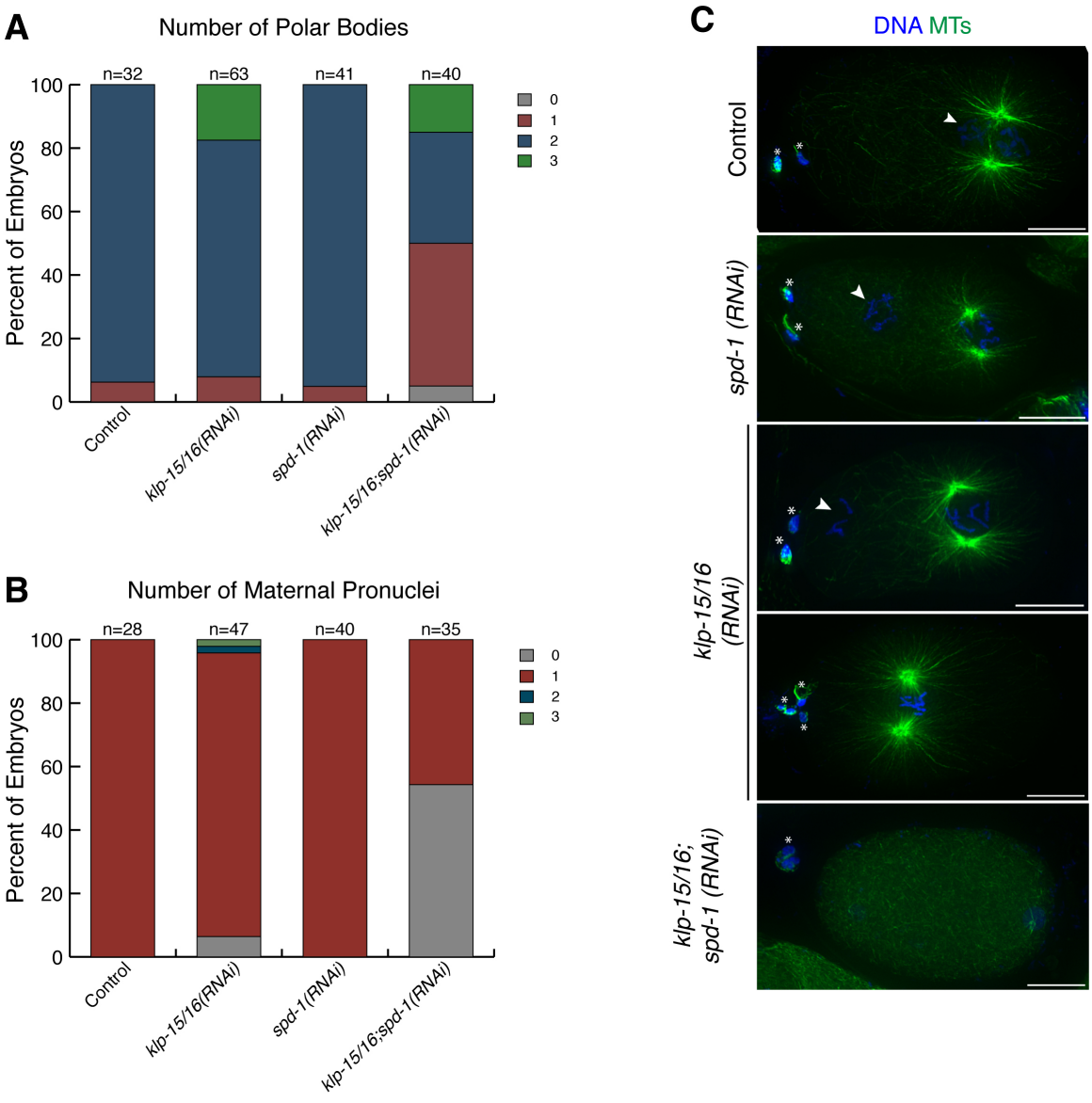
A
Number of Polar Bodies
n=32
n=63
n=41
n=40
Percent of Embryos
100
80
60
40
20
0
0
1
2
3
Control
klp-15/16(RNAi)
spd-1(RNAi)
klp-15/16;spd-1(RNAi)
B
Number of Maternal Pronuclei
n=28
n=47
n=40
n=35
Percent of Embryos
100
80
60
40
20
0
0
1
2
3
Control
klp-15/16(RNAi)
spd-1(RNAi)
klp-15/16;spd-1(RNAi)
C
DNA MTs
Control
spd-1 (RNAi)
klp-15/16 (RNAi)
klp-15/16; spd-1 (RNAi)

Figure 2.11

Figure 2.11. **Consequences of the anaphase defects observed in *klp-15/16(RNAi)* oocytes.** (A and B) Analyses of polar bodies and maternal pronuclei was done using live worms expressing GFP::tubulin, GFP::histone. (A) Quantification of the number of polar bodies per embryo for each condition listed. (B) Quantification of the number of maternal pronuclei per embryo for each condition listed. For A and B, embryos were only scored if the paternal pronucleus was decondensed to ensure that the meiotic divisions were complete. (C) Example mitotic embryos showing DNA (blue) and tubulin (green) to show some of the phenotypes observed in the quantification displayed in A and B. Asterisks denote polar bodies and arrowheads denote maternal pronuclei. I observe extra polar bodies and pronuclei following *klp-15/16(RNAi)*, indicative of meiotic defects. Co-depletion of KLP-15/16 and SPD-1 frequently resulted in ejection of all maternal chromosomes into a single polar body, resulting in no maternal pronucleus. Bars = 10 μm.

Given this finding, I more carefully assessed the dynamics of SPD-1 loading onto the spindle during anaphase. Live imaging of control oocytes expressing SPD-1::GFP and mCherry::histone revealed that SPD-1 begins to load onto the spindle between segregating chromosomes shortly after spindle rotation and then continues to accumulate as anaphase progresses (Fig. 2.9D, Movie 2-8), consistent with previous studies[123,124]. Similar to control oocytes, following depletion of KLP-15/16, SPD-1 loads onto microtubules in early anaphase, at the microtubule ball stage (Fig. 2.9D, Movie 2-8), Subsequently, as SPD-1 accumulates on the spindle, prominent bundles begin to form (Fig. 2.9D, Movie 2-8). This localization pattern, in combination with our functional analysis, is consistent with the interpretation that loading of SPD-1 in early anaphase provides a secondary bundling activity that provides spindle stability and allows for chromosome segregation.

2.6. KLP-18 potentially facilitates the reorganization of microtubule bundles during KLP-15/16-independent anaphase

My SPD-1::GFP live-imaging also revealed that when SPD-1 loads onto microtubules in *klp-15/16(RNAi)* oocytes, the forming bundles start out randomly oriented but are then restructured into a largely parallel array (Fig. 2.9D, Movie 2-8). Therefore, in addition to SPD-1 bundling microtubules, there is another mechanism working to reorganize these newly formed microtubule bundles into a functional orientation along which chromosomes are able to segregate. One candidate factor that could provide this function is KLP-18, since this motor sorts microtubule bundles during spindle assembly[84], and is present on anaphase spindles following KLP-15/16 depletion (Fig. 2.8C). It is currently unknown whether KLP-18 also functions during anaphase, because the requirement for this protein earlier during spindle assembly has made it difficult to assess an anaphase-specific role; in *klp-18* mutants or RNAi, chromosomes do not segregate into distinct groups in anaphase (Fig. 2.10D) because

the spindles are monopolar prior to anaphase onset[85,93]. However, the KLP-15/16 depletion phenotype offers a unique opportunity to address this question, since this condition has revealed a sorting activity that operates specifically during anaphase to generate parallel arrays of microtubule bundles. Notably, this activity does not require that the microtubules have been sorted previously; following *klp-15/16(RNAi)*, the microtubule bundles start out randomly oriented (Fig. 2.9D), yet they can still be organized into a parallel array. This feature allowed me to explore a potential role for KLP-18 during anaphase by co-depleting it with KLP-15/16.

To determine if KLP-18 could be required for this anaphase reorganization activity, I depleted KLP-15/16 in a KLP-18 mutant, *klp-18(tm2841)*, which results in a predicted early stop that is thought to eliminate KLP-18 function[84]. I then stained the spindles for SEP-1 and AIR-2 to stage them as before, to determine if microtubules were able to reorganize into spindles capable of mediating chromosome segregation in late anaphase, as they do following KLP-15/16 depletion in the wild type strain (Figs. 2.8A and 2.10A). Notably, I found that depletion of KLP-15/16 in the *klp-18(tm2841)* mutant results in a complete failure of microtubule reorganization and chromosome segregation in late anaphase (Fig. 2.10D), despite the fact that SPD-1 was still able to target to the microtubules (Fig. 2.10E) and that the early anaphase configuration appeared similar to KLP-15/16 depletion in the wild-type strain (Figs. 2.8A and 2.12). These results suggest that KLP-18 could provide the anaphase spindle reorganization activity that I observe in the *klp-15/16(RNAi)* condition. Although I cannot completely rule out the possibility that the metaphase defect in *klp-18* mutant oocytes prevents the microtubule reorganization that normally occurs following KLP-15/16 depletion, I think that my data are at least suggestive that KLP-18 provides this activity during anaphase and that it may therefore have an anaphase role in wild-type spindles.

Taken together, I propose that two complementary activities facilitate the reorganization of anaphase spindle microtubules following KLP-15/16 depletion: 1) SPD-1 loads in early anaphase to generate prominent microtubule bundles of mixed polarity, and 2) KLP-18 acts to orient these bundles into a parallel array that is capable of segregating chromosomes.

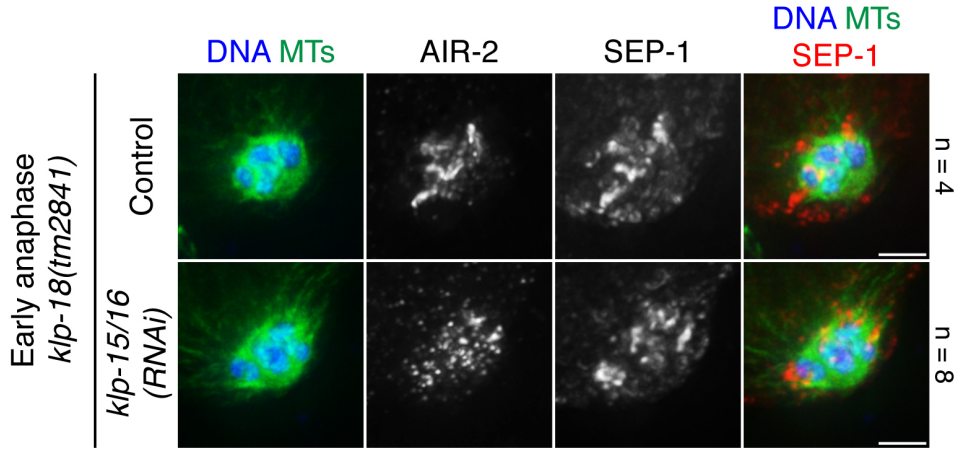

Figure 2.12. **Early anaphase in *klp-18(tm2841).*** DNA (blue), tubulin (green), AIR-2 (not in merge), and SEP-1 (red in merge). In the *klp-18(tm2841)* mutant strain, early anaphase spindles (where SEP-1 is colocalized with AIR-2) begin as a ball of microtubules surrounding the chromosomes, in both control and *klp-15/16(RNAi)* treated oocytes. n represents the number of spindles observed for each condition. Bars = 2.5 μm.

2.7. Lateral microtubule-chromosome contacts can be established during KLP-15/16-independent anaphase

Finally, I wanted to further investigate the mechanism of chromosome segregation during KLP-15/16-independent anaphase. During wild-type meiosis, microtubule bundles run along the sides of chromosomes prior to anaphase onset. These lateral associations remain in place during anaphase, creating channels that the chromosomes reside in as they move towards spindle poles[85], and then spindle elongation drives chromosomes further apart[78,88]. Given that microtubules are completely disorganized prior to anaphase onset following KLP-15/16

depletion and, unlike wild-type spindles, have no discernible lateral associations with chromosomes, I wanted to determine what types of microtubule-chromosome contacts were established during anaphase to facilitate segregation.

First, I asked if anaphase spindles in *klp-15/16(RNAi)* oocytes are able to form any channels that are analogous to those observed in wild-type oocytes. To this end, I stained spindles for SUMO, to mark the ring structures[80], and SPD-1, to mark anaphase microtubule bundles. In control spindles, each channel is comprised of a pair of separating chromosomes with a ring in between, and SPD-1 marks the microtubule bundles adjacent to the ring. Therefore, line scans of these components in control spindles show an alternating pattern of SUMO/SPD-1 and SUMO/microtubules across the channels (Fig. 2.13A). In *klp-15/16(RNAi)* oocytes, I found similar alternating patterns of these markers in a significant number of spindles (12/18 *klp-15/16(RNAi)* spindles examined; Fig. 2.13A); showing that the spindles are capable of forming microtubule channels during anaphase. Importantly, I also observed microtubules associating laterally with the segregating chromosomes (Fig. 2.13B, arrows and 2.13C; these associations were seen in 22/31 *klp-15/16(RNAi)* spindles) suggesting that this type of association can be established in anaphase, even if these associations are not in place at anaphase onset.

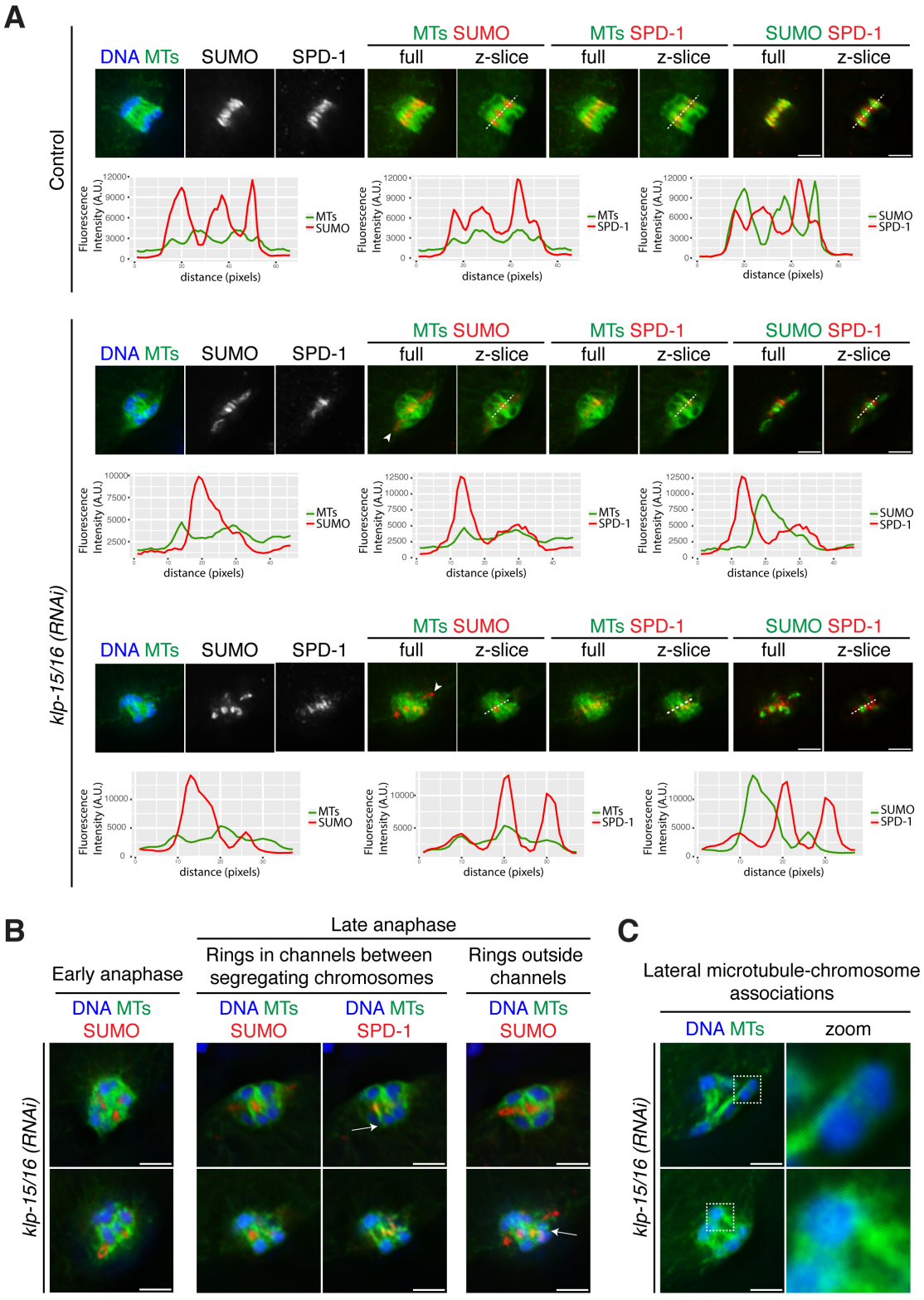
A
Control
klp-15/16 (RNAi)
DNA MTs
SUMO
SPD-1
MTs SUMO
MTs SPD-1
SUMO SPD-1
full
z-slice
Fluorescence Intensity (A.U.)
distance (pixels)
MTs
SUMO
SPD-1
B
Early anaphase
Late anaphase
Rings in channels between segregating chromosomes
Rings outside channels
C
Lateral microtubule-chromosome associations
zoom

Figure 2.13

Figure 2.13. **Anaphase spindle organization in *klp-15/16(RNAi)* oocytes.** (A) DNA (blue), tubulin (green in columns 1, 4, 5, 6, 7), SUMO (red in columns 4 and 5, green in columns 8 and 9), and SPD-1 (red, columns 6, 7, 8, 9); for each color combination, max projections of the full spindle are labeled "full" and the single z-slices used for the line scans are labeled "z-slice". In control and *klp-15/16(RNAi)* oocytes, chromosomes can be seen segregating through channels with SUMO in the middle of the channel flanked by SPD-1 on the microtubule bundles. Line scans across the channels in single z-slice images show colocalization of microtubules and SPD-1 and anti-correlation of SUMO/microtubules and SUMO/SPD-1; these oscillations were observed in 9/11 control anaphase spindles (82%) and 12/18 *klp-15/16(RNAi)* anaphase spindles (67%). However, following *klp-15/16(RNAi)*, some rings also appear to be on the periphery of the spindle (arrowheads). (B) Single z-slice images of DNA (blue), tubulin (green), SUMO (red, columns 1, 2, 4), and SPD-1 (red, column 3). In early anaphase following *klp-15/16(RNAi)*, rings are dissociated from chromosomes and are embedded within the microtubules of the spindle, or are excluded from the spindle. In late anaphase, the rings can be within channels between segregating chromosomes or outside of a channel not associated with a segregating chromosome pair. Arrows indicate examples of lateral microtubule-chromosome associations. Within each row, the late anaphase images are different z-slices from the same spindle, chosen to highlight different features. (C) DNA (blue) and tubulin (green); single z-slice images showing additional examples of lateral microtubule-chromosome associations in *klp-15/16(RNAi)* oocytes. I observed clear lateral associations in 31/35 control anaphase spindles (89%) and in 22/31 *klp-15/16(RNAi)* anaphase spindles (71%). Bars = 2.5 μm.

Despite the fact that channels can form during anaphase in *klp-15/16(RNAi)* oocytes, I also found that some rings appeared to be on the periphery of the spindle, demonstrating that not all separating chromosomes end up in a channel with a ring in the center (Fig. 2.13A, arrowheads). To gain insight into this variability, I looked earlier in anaphase before the microtubules were reorganized into bundles. In early anaphase spindles, at the "microtubule ball" stage when homologous chromosomes first begin to come apart, I observed some rings embedded in the microtubule ball close to the separating chromosomes, but also some rings towards the periphery of the structure (Fig. 2.13B). Subsequently, when the microtubules are bundled and aligned into parallel arrays, rings can be seen both in channels between segregating chromosomes and also completely outside of the reorganized spindle (Fig. 2.13B). This is likely due to the fact that microtubule bundling and reorganization are occurring as chromosomes begin to come apart. This results in some chromosomes and rings becoming organized within channels while others are not. This behavior may also contribute to the presence of lagging chromosomes in these spindles (Figs. 2.8B, 2.10A, and 2.13A). While it is unlikely that the complete formation of a ring-containing channel is essential for chromosome segregation, the fact that lateral associations are established suggests that they could contribute to segregation in this context. Furthermore, the preference for these initially disorganized spindles to establish lateral associations suggests that they are likely important for proper chromosome segregation in the context of wild-type spindles.

2.8. Expanded studies of lateral microtubule bundles during anaphase in wild-type *C. elegans* oocytes

Recently, two studies were published that used electron tomography to examine the microtubule architecture of the *C. elegans* oocyte meiotic spindle during anaphase in order to gain insights into the mechanisms of chromosome segregation[96,117]. These studies challenged my

hypothesis that the lateral microtubule bundles are an important feature of the chromosome segregation mechanism during anaphase and brought into question whether this type of interaction even exists in the later stages of anaphase. The first study by Laband et al.[96] makes no mention of microtubules interacting with the chromosomes laterally during anaphase and proposed that microtubule nucleation and/or polymerization between the segregating chromosomes is primarily responsible for driving the chromosome sets apart. In this model, chromosome segregation is driven exclusively by a combination of nucleation and sliding of microtubules in the spaces between the segregating chromosomes to "push" the chromosomes apart. It was proposed that these newly polymerized microtubules are crosslinked and acted upon by central spindle components such as SPD-1. However, the authors downplay the presence of microtubule deficient regions or channels between the segregating chromosomes that are visible in their reconstructions, making it difficult to understand their model. In the second study by Redemann et al.[117], the authors observed primarily lateral microtubule-chromosome attachments in metaphase and very early anaphase, but they did not observe lateral microtubule-chromosome attachments during Anaphase B (when the spindle elongates). Redemann et al.[117] clearly observed microtubule-free regions between the segregating chromosomes and termed these regions "inter-chromosomal spaces." Based on these observations, the authors proposed a model in which there is a switch from lateral to end-on microtubule-chromosome attachments as anaphase progresses. In this model, the chromosomes are initially moved apart by motor-generated forces on lateral microtubule bundles - as was previously proposed[85]. As anaphase progresses, the microtubules become oriented end-on in relation to a set of segregating chromosomes, which are then driven apart by sliding and polymerization of the microtubules in between the sets of chromosomes. It is important

to note that in these electron microscopy (EM) reconstructions a segregating set of chromosomes appears to merge into a single, electron-dense mass and the microtubules terminate at or just inside these masses. Therefore, in both of these models, the end-on microtubules generate force on these single, large masses of genetic material to move them apart. I question these models because by my high-resolution, fixed imaging, I can clearly observe individual chromosomes with laterally-associated microtubules during equivalent stages of anaphase as were analyzed by the electron tomography studies.

I wanted to know if the discrepancy in the organization of the anaphase spindles observed by light microscopy and electron tomography could be an artifact of the different fixation methods used to generate the samples for each study (see Chapter 5: Materials and methods and Woog et al.[133]). To eliminate artifacts generated by fixation, I imaged, at high-resolution, anaphase spindles *in utero* in live oocytes expressing GFP::tubulin and mCherry::histone. Using this method, I observed lateral microtubule bundles associating with the chromosomes during the later stages of anaphase when the chromosomes had segregated to similar distances as the spindles used in the EM reconstructions and where these studies primarily observed end-on associations (Fig. 2.14; arrowheads). Furthermore, I observed individual chromosomes within each segregating set (Fig 2.14; arrows) suggesting that the chromosomes do not merge into a single mass during anaphase.

I also set out to investigate the possible contribution of newly polymerized microtubules and their cross-linking by SPD-1 as it is this population of microtubules that was theorized to provide the pushing forces by Laband et al.[96]. To this end, I performed cold-stable assays of anaphase spindles and stained for SPD-1. It has been shown in other cell types that certain microtubule populations, such as K-fibers, are more resistant to cold treatment; that is, they are more stable[61,134]. Because K-fibers are the major way chromosomes attach to the spindle

during mitosis, I believed that the microtubule bundles that make lateral associations with the chromosomes in *C. elegans* oocytes could be a stable population of microtubules. In control oocytes, I find that SPD-1 localized to the lateral microtubule bundles (Fig. 2.15) and as shown in Figs. 2.9A and 2.13A. After cold treatment, the lateral microtubule bundles remained (Fig. 2.15), suggesting that the lateral bundles are the major stable population of microtubules within the spindle. Furthermore, I find SPD-1 primarily localizes to these lateral bundles (Fig. 2.15) and not to a population of microtubules between the segregating chromosomes that could be providing a pushing force. Collectively, these studies reinforce a model in which the lateral microtubules are an important feature of the anaphase mechanism in *C. elegans* oocytes.

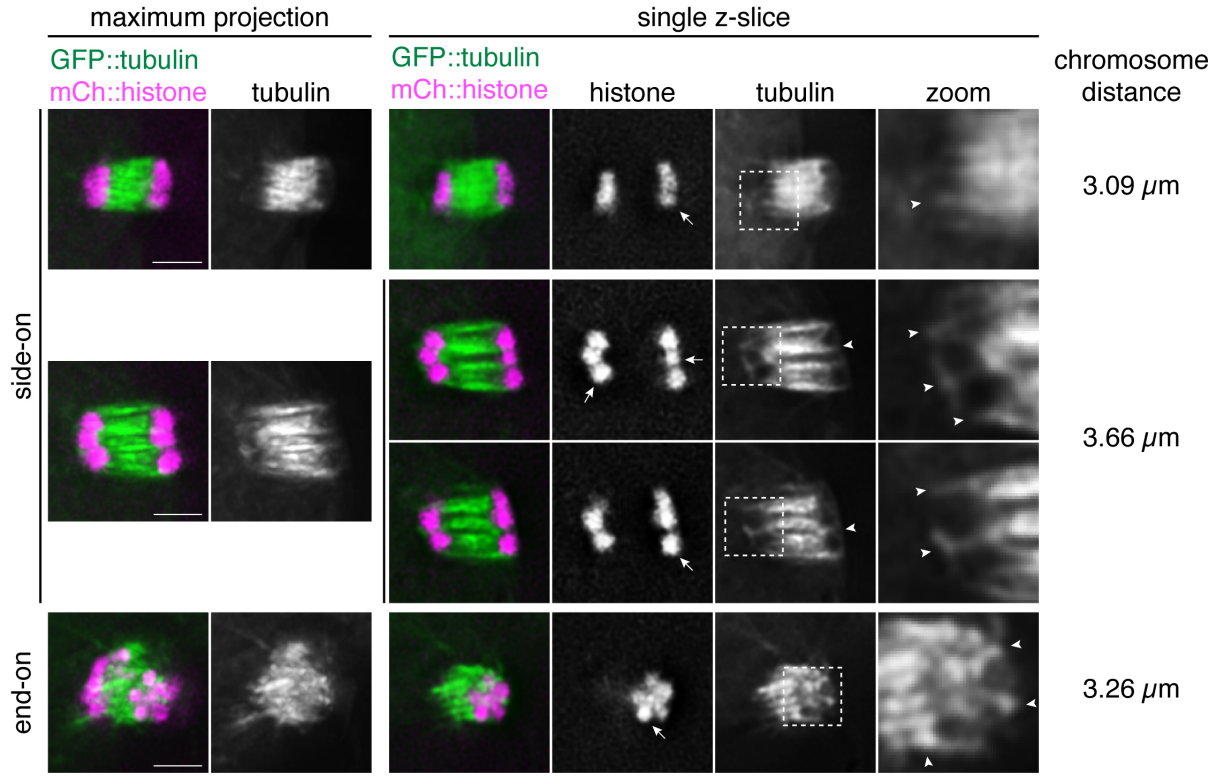

Figure 2.14. **Live imaging of anaphase spindles in *C. elegans* oocytes**. *Ex utero* live-imaging of oocytes expressing GFP::tubulin (green) and mCherry::histone (magenta). Maximum intensity projections are shown on the left and single z-slices are shown on the right. Examples of spindles viewed side-on (top two rows) and end-on (bottom row) show prominent microtubule bundles associating laterally with individual chromosomes of a segregating set. Chromosome segregation distances are indicated on the right. 87% (n = 15 spindles) of anaphase spindle analyzed contained lateral microtubule bundles associated with chromosomes. Arrows denote examples of individual chromosomes. Arrowheads denote examples of lateral microtubule-chromosome associations. Bars = 2.5 μm.

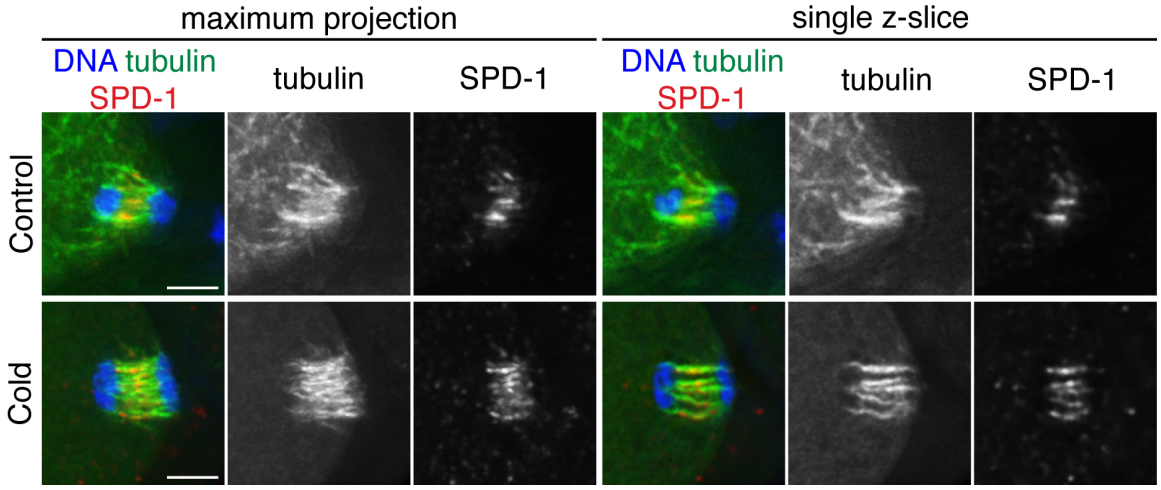

Figure 2.15. **Anaphase spindle organization and SPD-1 localization following cold-treatment.** Control and cold-treated anaphase spindles stained for DNA (blue), tubulin (green), and SPD-1 (red). Maximum intensity projections (left) and single z-slices (right) show that the lateral bundles are a stabilized population of microtubules in the anaphase spindle, and that SPD-1 localizes to these cold-stable microtubule bundles. Bars = 2.5 μm.

2.9. Discussion

Minus-end kinesins stabilize microtubule bundles in *C. elegans* acentriolar meiotic spindles

Taken together, my data suggest a mechanism in which KLP-15/16 act to bundle microtubules in acentriolar spindles. Prior to spindle assembly during MI, KLP-15/16 are excluded from the nucleus and localize diffusely throughout the cytoplasm, which is in contrast to kinesin-14s from other organisms that have been shown to be sequestered in the nucleus[102,135]. Then, as acentriolar spindles begin to form, KLP-15/16 load onto microtubule bundles during the cage stage, stabilizing them to facilitate spindle assembly (Fig. 2.16). This proposed function is consistent with previous studies of kinesin-14s in other organisms, which demonstrated that this family of kinesins is required for acentriolar spindle formation and localize uniformly to acentriolar spindle microtubules[40,42,43,54]. However, while depletion

of kinesin-14s in other organisms predominantly results in defects such as unfocused poles and splayed microtubules, depletion of KLP-15/16 in *C. elegans* oocytes completely prevents bipolar spindle formation and abolishes microtubule bundling prior to anaphase, implicating these proteins in the stabilization of microtubule bundles comprising the acentriolar meiotic spindle. Furthermore, unlike most other organisms where kinesin-14s perform essential roles in mitosis[40,136–138], KLP-15/16 are not required for mitotic spindle formation in *C. elegans*, suggesting a unique role for KLP-15/16 that is specific to acentriolar spindle assembly; this finding is also reminiscent of studies in *Drosophila*, where inhibition of the kinesin-14 Ncd has a much more severe phenotype in oocytes than it does in mitosis[102,136,139]. The presence of the "microtubule ball" comprised of short microtubules that ultimately forms prior to anaphase following *klp-15/16(RNAi)* raises the intriguing possibility that the function of KLP-15/16 could be to stitch together short microtubules into longer bundles that can then be sorted and organized into a bipolar spindle. Since kinesin-14s contain a motor domain in the C-terminus and a microtubule binding domain in the N-terminus[135,137,140], and it has been reported that this class of kinesins can stabilize and cross-link microtubules in a parallel configuration[41], it is possible that these motors could contribute to this stitching activity. This interpretation is consistent with a previous electron microscopy study, which reported the presence of many short microtubules in a partial reconstruction of a *C. elegans* oocyte spindle[51], and also with a study in Xenopus egg extracts that demonstrated that meiotic spindles are comprised of tiled arrays of short microtubules[141]; therefore a microtubule stitching activity might be something that is especially important in the context of acentriolar meiosis. My studies suggest that KLP-15/16 could be factors that organize these short microtubules into longer bundles capable of mediating chromosome congression and segregation.

New insights into chromosome segregation in acentriolar meiosis

In addition to revealing an important function for KLP-15/16, my studies have yielded insights into previously unknown mechanisms promoting accurate chromosome segregation during acentriolar meiosis. First, I found that the PRC1-family protein SPD-1 provides a secondary activity that stabilizes microtubule bundles during anaphase (Fig. 2.10A, 2.10B, and 2.10C). This activity was previously unidentified, as prior depletion of SPD-1[78], and confirmed by my own studies (Fig. 2.10A), failed to reveal an obvious anaphase defect. This is likely because KLP-15/16 are present on the anaphase spindle stabilizing the microtubule bundles (Fig. 2.6B), making SPD-1 non-essential until KLP-15/16 are depleted. This discovery is similar to findings in fission yeast, where the SPD-1 homolog Ase1 is not essential on its own but provides a backup mechanism for bipolar spindle assembly under conditions where the kinesin-5 motor Cut7 and the kinesin-14 motor Pkl1 are deleted[142].

During mitosis in other organisms, homologs of SPD-1 are known to crosslink antiparallel microtubules[55,143,144], and my data are consistent with SPD-1 performing a similar function in *C. elegans* oocytes. During wild-type meiotic anaphase, this protein loads onto the central region of the spindle (Fig. 2.9D) where this putative crosslinking activity could reinforce anaphase spindle structure. Under KLP-15/16 depletion conditions, SPD-1 begins to load at the microtubule ball stage (Fig. 2.9D), which contains many short microtubules that are likely randomly oriented (Fig. 2.1C); given this configuration, the ability to crosslink antiparallel microtubules would enable SPD-1 to bundle microtubules. Furthermore, because SPD-1 is a non-motor microtubule crosslinker and does not sort microtubules[55,143,144], this supports my interpretation that the diffuse ASPM-1 localization on KLP-15/16-depleted anaphase spindles is indicative of bundles that are comprised of microtubules of mixed polarity (Fig. 2.8B). These SPD-1-stabilized microtubule bundles could then be sorted and

aligned into a parallel array by the action of KLP-18. Therefore, my studies have uncovered a new function for SPD-1 on *C. elegans* acentriolar spindles, and also represent the first demonstration that PRC1-family proteins play a role during oocyte meiosis. My work also suggests that KLP-18 is likely functional during anaphase in these cells, since it appears to organize the microtubule bundles generated by SPD-1 (Fig. 2.10D and 2.10E) suggesting that this motor not only plays roles during bipolar spindle formation but may also be required to maintain spindle organization as chromosomes segregate.

Finally, my work has shed light on the mechanisms driving chromosome segregation in this unique form of anaphase. I found that anaphase spindles in KLP-15/16-depleted oocytes are sometimes able to form channels with lateral microtubule-chromosome associations (Fig. 2.13) despite the lack of microtubule bundles prior to anaphase onset. These data suggest that this form of microtubule-chromosome contact is preferred during anaphase and points to a role for the chromosomes providing significant structural cues for spindle organization as these associations can be established *de novo* following KLP-15/16 depletion. However, given that these laterally-associated bundles may be comprised of microtubules of mixed polarity (Fig. 2.8B and 2.8C), it is improbable that they would be able to efficiently facilitate directional chromosome movement (a mechanism I proposed to drive normal Anaphase A[85]). Therefore, I suggest that the primary force driving segregation in the absence of KLP-15/16 is the elongation of these laterally-associated bundles in an Anaphase-B type mechanism.

The discovery that lateral associations are established during anaphase is also interesting since two other types of chromosome-spindle contacts have been proposed to facilitate segregation during wild-type anaphase: 1) elongating and sliding of microtubules contacting the inside surfaces of separating chromosomes to provide a pushing force[78,96,117] and 2) chromosomes contacting and making attachments to the spindle poles, so that outward pole

separation can drive segregation in Anaphase B[88]. It is possible that the first type of association contributes to segregation during KLP-15/16-independent anaphase; since not every chromosome ends up in a normal microtubule channel (Fig. 2.13), some microtubules might randomly make contacts with chromosome surfaces and provide a pushing force, contributing to segregation alongside the bundles that are laterally-associated. Indeed, my data are consistent with this idea since I observe non-laterally-associated microtubules in the reorganized *klp-15/16(RNAi)* anaphase spindles (Fig. 2.13). In contrast, the second model proposed that spindle shrinkage enables the chromosomes to establish a physical tether to a cross-linked network of microtubules and pole proteins; outward sliding of interpolar microtubules would then drive the poles and the tethered chromosomes apart[88]. My observation that pole proteins KLP-18 and ASPM-1 are distributed throughout *klp-15/16(RNAi)* spindles both prior to and during anaphase (Figs. 2.1C, 2.1D, 2.8B, and 2.8C) makes it difficult to imagine how such a tether would efficiently form in this context. I speculate that pre-established spindle poles may not be absolutely required to segregate chromosomes in *C. elegans* oocytes (although I cannot rule out the possibility that other pole proteins exhibit a higher level of organization in these mutant spindles). My data also raise the possibility that spindle elongation could be capable of driving segregation even when the polarity of microtubules within the spindle is disrupted, potentially revealing an unusual mode of chromosome segregation that operates in this mutant context.

The case for lateral associations as being important for proper chromosome segregation is also strengthened by my live-imaging studies of wild-type anaphase spindles where I observe prominent, lateral microtubule-chromosome associations during the later stages of anaphase (Fig. 2.14). These laterally associated microtubule bundles are also the major stabilized

population of microtubules within the anaphase spindle (Fig. 2.15). These studies of wild-type and cold-treated anaphase spindles combined with my studies of anaphase spindles in *klp-15/16(RNAi)* oocytes have led me to favor a model in which lateral microtubule bundles are stably associated with the chromosomes, and it is primarily polymerization and sliding of the microtubules within these lateral bundles that drives spindle elongation and chromosome segregation during Anaphase B.

In summary, my studies have uncovered a crucial role for KLP-15 and KLP-16 in *C. elegans* acentriolar spindle assembly, revealed a second, anaphase-specific mechanism dependent on SPD-1 operating in parallel to these kinesins, and provided new insights into anaphase spindle organization and chromosome segregation mechanisms during acentriolar meiosis.

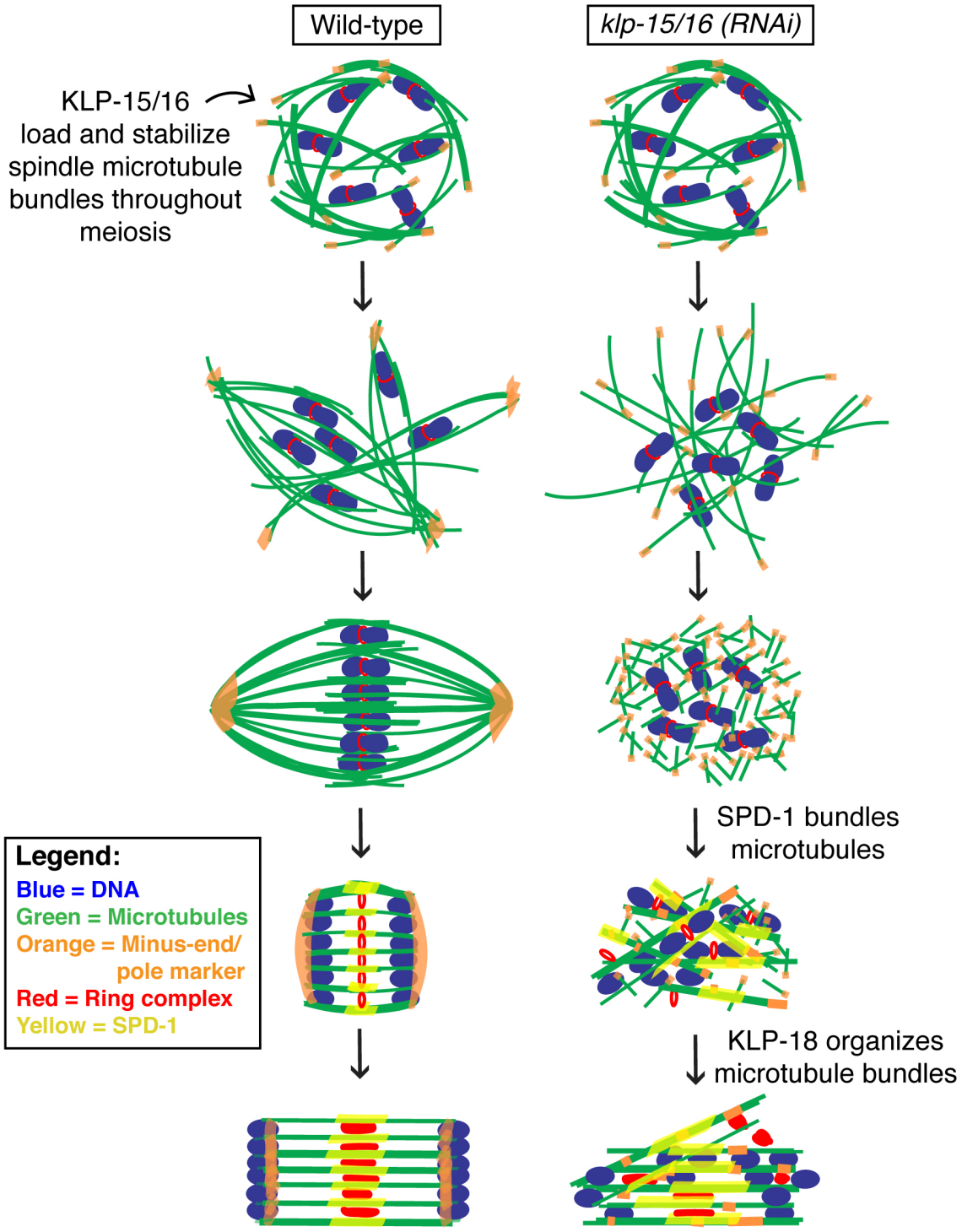
Wild-type
klp-15/16 (RNAi)
KLP-15/16
load and stabilize
spindle microtubule
bundles throughout
meiosis
SPD-1 bundles
microtubules
KLP-18 organizes
microtubule bundles
Legend:
Blue = DNA
Green = Microtubules
Orange = Minus-end/
pole marker
Red = Ring complex
Yellow = SPD-1

Figure 2.16

Figure 2.16. **Model: Interplay between microtubule-associated factors contributes to acentriolar spindle assembly and maintenance.** DNA (blue), microtubules (green), minus-end/pole marker (orange), ring complex (red), and SPD-1 (yellow). In wild-type spindles, KLP-15/16 load onto microtubules during the cage stage and remain associated through anaphase providing stability to microtubule bundles. At anaphase onset, SPD-1 loads onto the microtubules as the chromosomes begin to segregate towards the poles through microtubule channels (Anaphase A), and the ring complexes are left behind inside the channels. As anaphase progresses, the spindle microtubules elongate forcing the chromosomes further apart (Anaphase B), and the ring complexes disassemble. In *klp-15/16(RNAi)* oocytes, after the cage stage, microtubules form a disorganized array with ASPM-1 located throughout the structure. The array collapses into a microtubule ball around the chromosomes with ASPM-1 throughout. As anaphase begins, SPD-1 binds to the short, randomly oriented microtubules and bundles them, the ring complexes dissociate from the chromosomes, and KLP-18 sorts and aligns the bundles such that lateral microtubule-chromosome associations and channels can form. The spindle then elongates (Anaphase B) to facilitate chromosome segregation.

CHAPTER 3

ZYG-9$^{\mathbf{XMAP215}}$ is essential for acentriolar spindle formation and spindle pole integrity during *C. elegans* oocyte meiosis

The data presented in this chapter are part of a forthcoming manuscript in preparation. All of the data presented here was generated by me with the exception of the *zyg-9(RNAi)* fixed imaging experiments which were performed by Ian Wolff and the FRAP data fitting was done using a Python code made by Justin Finkle.

3.1. Introduction

When a cell divides, it must assemble a bipolar microtubule based spindle that attaches to and segregates the chromosomes. During mitosis centrosomes serve as the major microtubule organizing centers within the cell and provide structural cues that define and organize the spindle poles. The centrosome is a membraneless, phase-separated organelle comprised of a centriole pair surrounded by an amorphous collection of proteins called the pericentriolar material (PCM) from which microtubules are nucleated and the minus-end anchored[145,146]. In *C. elegans*, the PCM is made up of SPD-2 and SPD-5 which serve as the primary scaffold on which all other PCM components are recruited including the microtubule nucleating factor, γ-tubulin[60,61,104,106,147]. Also recruited to the PCM is the microtubule polymerase and XMAP215 family member ZYG-9[107,147,148]. During mitosis, ZYG-9 and its binding partner, TAC-1 (transforming acid coiled-coil) are mutually dependent on each other for their localization to the centrosome where they promote the assembly of long microtubules and are required for proper mitotic spindle formation[50,108,109,149,150]. Depletion of either ZYG-9 or TAC-1 from mitotic embryos results in identical phenotypes: failure of pronuclear migration, the mitotic spindle does not orient correctly, and the microtubules of the spindle are shorter[50,108,109,112,149]. Depletion of these proteins causes catastrophic errors during the first mitotic division and results in developmental arrest[50,108,109,112,151].

In the oocytes of many organisms, the meiotic divisions occur in the absence of these centriole-containing centrosomes (they are acentriolar). As a result the spindles are assembled and the poles are organized through unique, poorly-understood mechanisms. In *C. elegans*, oocyte meiotic spindle assembly proceeds through the following steps: 1) after nuclear envelope breakdown, the microtubules are nucleated, bundled and assembled into a

cage-like structure adjacent to the disassembling nuclear envelope, 2) the microtubule bundles are sorted and the minus-ends of the microtubules are forced to the periphery of the array away from the chromosomes where they form multiple nascent poles, and finally 3) the nascent poles coalesce into two poles and bipolarity is achieved[84]. Early on during this process, the microtubules make lateral contacts with the chromosomes, which are important for facilitating chromosome movement and alignment to the metaphase plate[37]. There have been many factors shown to be important for spindle assembly and spindle pole organization in this system. MEI-1/2 (katanin)[53,152,153], ASPM-1[53,95], KLP-7 (MCAK)[124,154], dynein[24], KLP-18(kinesin-12)[84], MESP-1[84] and KLP-15/16(kinesin-14)[120] are all required for proper acentriolar spindle assembly. Furthermore, many of these components are also present at the centrosome during mitosis[122]. However, unlike the mitotic spindle, assembly of the acentriolar spindle in *C. elegans* does not require the core PCM components SPD-2, SPD-5, or γ-tubulin, nor do these factors localize to the acentriolar spindle[86,87,104–106]. Therefore, how the poles of these specialized spindles are able to organize microtubules and maintain stability in the absence of a PCM scaffold to allow for the faithful segregation of genetic material is an important question. One mitotic spindle pole component that has not been studied in any careful detail during oocyte meiosis is ZYG-9. This protein localizes to the acentriolar spindle, where it is enriched at the poles, and is required for proper spindle assembly and chromosome segregation in oocytes[107,112], However, the function of this protein and how it promotes spindle assembly in oocytes is not understood. Furthermore, during mitosis, SPD-5 is required to recruit ZYG-9 to the centrosomes[104], yet in oocyte spindles without SPD-5, ZYG-9 is enriched at the spindle poles[107], suggesting that ZYG-9 may have different roles during mitosis and meiosis.

In the work described here, I have characterized the function of ZYG-9 during acentriolar spindle assembly in oocytes. I found that ZYG-9 is important for multiple stages of spindle assembly, including cage formation and spindle pole coalescence. Following ZYG-9 depletion, the cage does not properly form, and then as spindle assembly progresses, the poles of the spindle fragment before collapsing into a single mass. I then show that ZYG-9 is required for the maintenance of acentriolar spindle pole integrity, as acute ZYG-9 depletion using an auxin-inducible degron (AID) system caused the poles of bipolar spindles to fall apart. These observations suggest a role for ZYG-9 in meiosis where it acts to organize and stabilize the poles of the acentriolar spindle. Further, using FRAP experiments, I found that the dynamics of ZYG-9 at acentriolar spindle poles are distinct from its dynamics at centrosomes during mitosis. My data therefore point to a role for ZYG-9 in acentriolar spindle assembly and maintenance that is distinct from its role in mitosis when centrosomes are present. More broadly, understanding the molecular underpinnings of acentriolar spindle integrity has important implications for human health as it was shown that the acentriolar poles in human oocytes are very unstable and this instability can lead to errors in chromosome segregation[16]. Using the AID approach outlined here to identify other factors required for spindle pole integrity will be important future work.

3.2. ZYG-9 is required for acentriolar spindle assembly in oocytes

Previous studies from other groups had suggested that ZYG-9 is required for acentriolar spindle assembly and chromosome segregation during meiosis[107,112]. However, there has yet to be a detailed characterization of the role of ZYG-9 during the meiotic divisions. In order to better understand the function of ZYG-9 during meiosis, I performed a careful analysis of spindle assembly using fixed and live-cell imaging of oocytes following *zyg-9(RNAi)*. In control oocytes after nuclear envelope breakdown (NEBD), the microtubules organize into

prominent bundles that form a cage-like structure in the vicinity of the disassembling nuclear envelope (Figs. 2.1B and 3.2B, 3.2C, and 3.2D; Movie 3-1). The microtubule bundles are then stabilized and sorted by molecular motors such that the minus-ends of the microtubules (marked by ASPM-1) are forced to the periphery of the array where they form multiple nascent poles that coalesce until a bipolar structure is established[52,53,84,120] (Figs. 2.1B, 2.1C, 2.1D, 3.2B, and 3.2D; Movie 3-1). In *zyg-9(RNAi)* oocytes, there were defects early on during the spindle assembly process. After NEBD, I observed defects in the formation of the cage-like microtubule bundles associated with the disassembling nuclear envelope, and instead the microtubules appear to be nucleated in close proximity to the chromosomes (3/3 movies analyzed) (Figs. 3.1A, 3.2B, 3.2C, and 3.2D; Movie 3-1). In the example shown in Movie 3-1 and Figure 3.1A, following nucleation, the microtubules are then organized into a multipolar structure before establishing what appears to be a bipolar structure. This is a transient organization because the two poles of this spindle do not remain intact but fragment into multiple aster-like structures before collapsing into a single mass (Fig. 3.1A; Movie 3-1). Quantification of the phenotypes following *zyg-9(RNAi)* revealed a high incidence of multipolar spindles in the +1 position of the germline while the majority of spindles in wild-type animals had achieved bipolarity by this time, suggesting that the spindle poles in the *zyg-9(RNAi)* oocytes are unstable (Fig. 3.2B and 3.2C). When we performed fixed imaging and stained spindles from *zyg-9(RNAi)* oocytes for ASPM-1 to mark the spindle poles, we found that this protein localized to multiple foci within the spindle, suggesting that the multiple aster-like structures observed by live imaging are fragmented spindle poles (Figs. 3.1A, 3.1B, 3.1C). Surprisingly, there were examples of chromosome segregation in *zyg-9(RNAi)* oocytes despite the fact that the majority of the spindles were disorganized in this condition (Figs. 3.2B and 3.2C), suggesting that there may be other mechanisms to

organize the spindle into a structure capable of segregating chromosomes in the absence of ZYG-9. Together, these data point to a role for ZYG-9 during the early stages of acentriolar spindle assembly and spindle pole organization in oocytes.

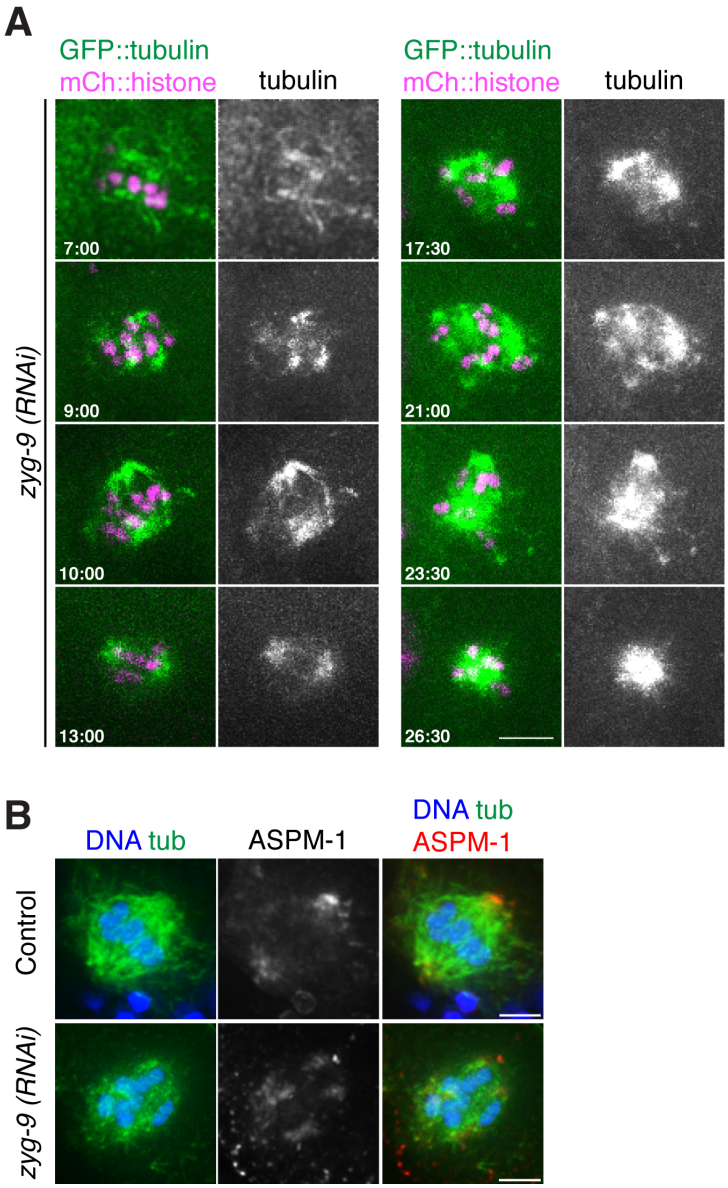

Figure 3.1. **ZYG-9 is required for spindle assembly in oocytes.** (A) Movie stills from *zyg-9(RNAi)* oocytes expressing GFP::tubulin (green) and mCherry::histone (magenta). Following *zyg-9(RNAi)*, the microtubules appear to nucleate in close proximity to the chromosomes (7:00). As spindle assembly progresses, a bipolar structure transiently forms (13:00) before the poles begin to fragment into multiple pole-like foci (21:00). This multipolar structure then collapses into a single mass of tubulin surrounding the chromosomes (26:30). (B) Control and *zyg-9(RNAi)* oocyte spindles stained for DNA (blue), tubulin (green), and ASPM-1 (red). In control spindles, ASPM-1 marks the two poles of the bipolar spindle. In *zyg-9(RNAi)* oocytes, ASPM-1 stains multiple, discrete structures within the spindle. Time stamp = mm:ss, Bars = (A) 5 μm; (B) 2.5 μm

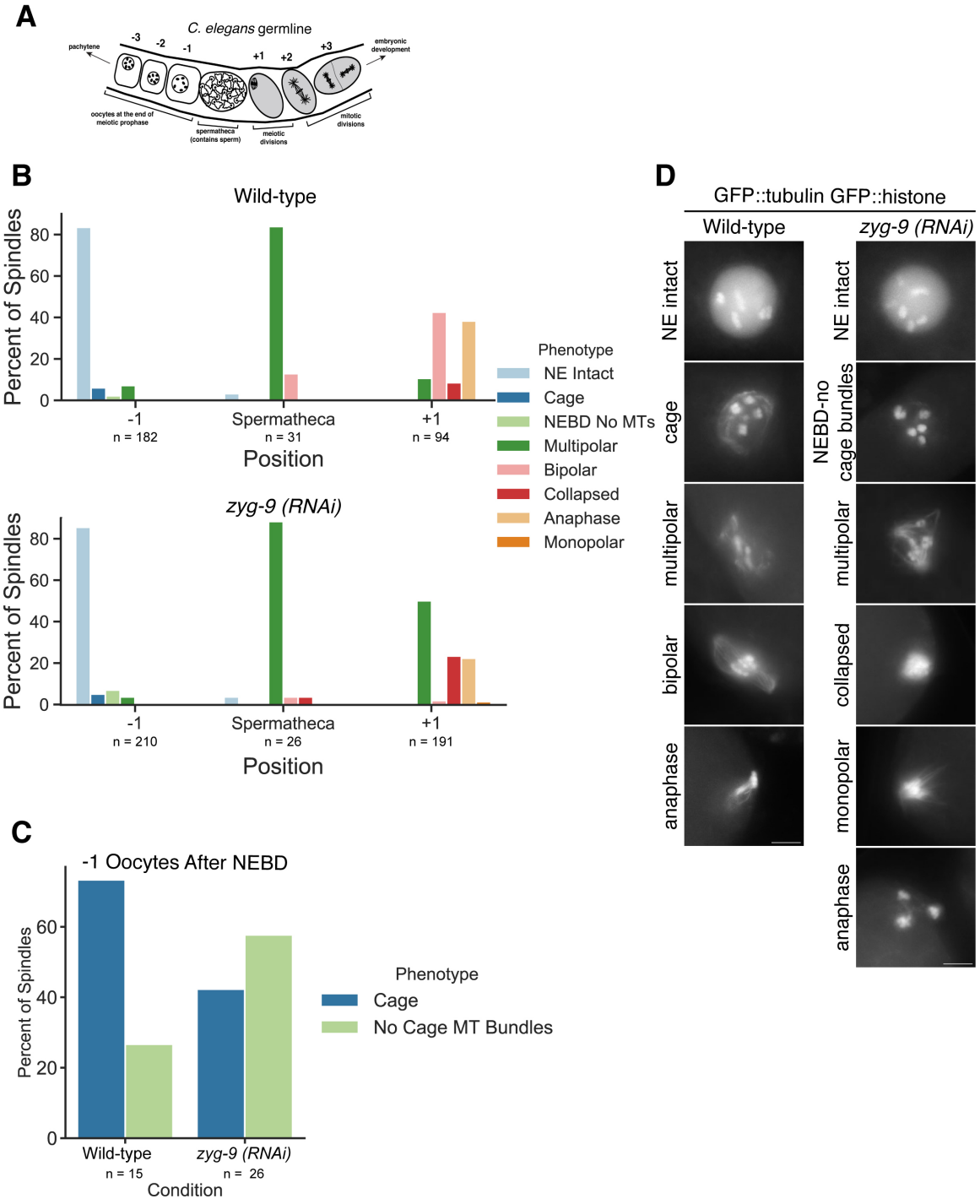
A
C. elegans germline
pachytene
-3
-2
-1
+1
+2
+3
embryonic development
oocytes at the end of meiotic prophase
spermatheca (contains sperm)
meiotic divisions
mitotic divisions
B
Wild-type
Percent of Spindles
80
60
40
20
0
-1
n = 182
Spermatheca
n = 31
+1
n = 94
Position
zyg-9 (RNAi)
Percent of Spindles
80
60
40
20
0
-1
n = 210
Spermatheca
n = 26
+1
n = 191
Position
Phenotype
NE Intact
Cage
NEBD No MTs
Multipolar
Bipolar
Collapsed
Anaphase
Monopolar
C
-1 Oocytes After NEBD
Percent of Spindles
60
40
20
0
Wild-type
n = 15
zyg-9 (RNAi)
n = 26
Condition
Phenotype
Cage
No Cage MT Bundles
D
GFP::tubulin GFP::histone
Wild-type
zyg-9 (RNAi)
NE intact
cage
multipolar
bipolar
anaphase
NE intact
NEBD-no cage bundles
multipolar
collapsed
monopolar
anaphase

Figure 3.2

Figure 3.2. **Quantification of *zyg-9(RNAi)* phenotypes.** (A) Schematic of the *C. elegans* germline. The germline is organized in a way that allows for temporal information about meiotic progression based on where the oocyte is located. Oocytes in the -1 position are ovulated into the spermatheca where they are fertilized and begin the meiotic divisions. The fertilized oocytes exit the spermatheca to the +1 position where they continue meiosis before beginning the mitotic divisions. (B) Quantification of the spindle phenotypes in wild-type (top) and *zyg-9(RNAi)* (bottom) animals. In *zyg-9(RNAi)* oocytes, there is an increase in the number of multipolar and collapsed spindles and a decrease in the number of bipolar spindles found in the +1 position. This analysis was done by viewing spindles in live worms expressing GFP::tubulin, GFP::histone. n represents the number of spindles analyzed at each position (C) Same data from the analysis in (B), but only showing spindles in the -1 position where the nuclear envelope has broken down. In *zyg-9(RNAi)* oocytes, there is an increase in the number of spindles that appear to have no cage microtubule bundles at this stage. n represents the number of spindles analyzed at each position. (D) Example images of the phenotypes quantified in (B) and (C) in control and *zyg-9(RNAi)* oocytes expressing GFP::tubulin, GFP::histone.

3.3. ZYG-9 is enriched at the acentriolar meiotic spindle poles and this localization is dependent on TAC-1

The striking phenotypes following ZYG-9 depletion prompted me to carefully determine the localization of ZYG-9 throughout spindle assembly. To this end, I generated a worm strain expressing GFP::ZYG-9 from the endogenous locus. When GFP::ZYG-9 expressing oocytes were stained with an antibody against GFP, I found that ZYG-9 is excluded from the nucleus prior to NEBD, becomes enriched at the spindle poles and is diffuse throughout the spindle at the multipolar stage, and remains enriched at the poles until late anaphase when it becomes diffuse along the spindle (Fig. 3.3A). Live imaging of bipolar metaphase spindles in oocytes expressing GFP::ZYG-9 and mCherry::histone, showed that ZYG-9 is enriched at the spindle poles, and that there is a significant population of ZYG-9 throughout the spindle as well (Fig. 3.3B), consistent with my fixed imaging and fixed imaging from a previous study[107]. This data suggests that ZYG-9 is in position where it could be functioning to organize the acentriolar spindle poles during meiosis.

Next I wanted to assess the requirement of TAC-1 on ZYG-9 localization during meiosis. During mitosis, TAC-1 and ZYG-9 form a complex[50,108], promote the stability of one another[108], and TAC-1 is responsible for the proper recruitment of ZYG-9 to the centrosome[149]. TAC-1, like ZYG-9, is enriched at the poles of the acentriolar metaphase spindle[108,109], however it is unknown whether these two proteins have a similar interplay during meiosis as they do during mitosis. Furthermore, the role of TAC-1 during meiosis is not well documented aside from observations of polar body defects following *tac-1* inhibition or depletion, suggesting that it has some meiotic functions[108,109]. To explore a possible functional relationship during meiosis, I depleted TAC-1 by RNAi and examined the localization of ZYG-9.

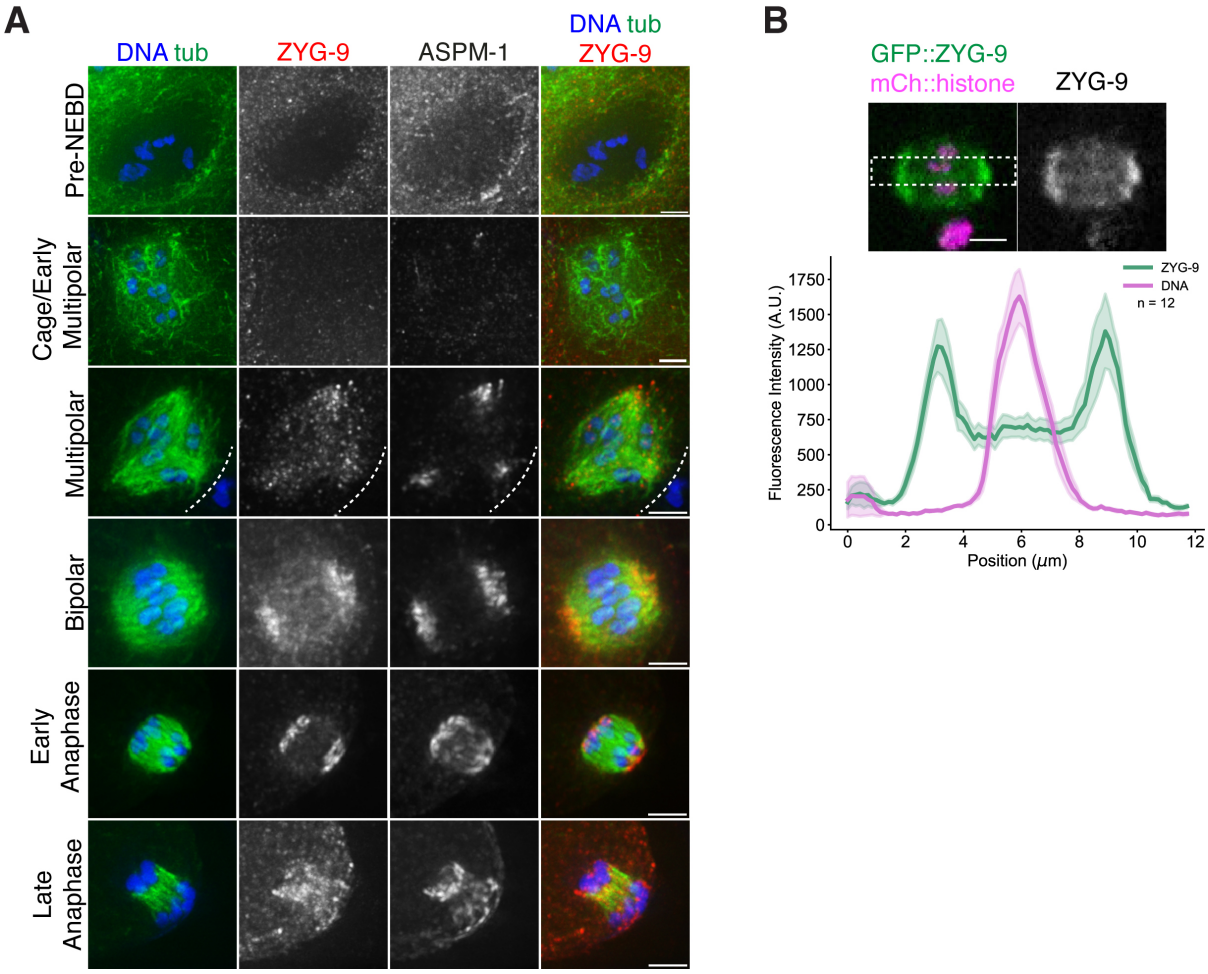

Figure 3.3. **ZYG-9 localization during acentriolar spindle assembly.** (A) Wild-type spindles stained for DNA (blue), tubulin (green), ZYG-9 (red in merge), and ASPM-1 (not in merge). ZYG-9 is excluded from the nucleus prior to NEBD, then it becomes enriched at the nascent poles (marked by ASPM-1) at the multipolar stage. ZYG-9 remains enriched at the spindle poles until late anaphase when it appears diffuse along the entire spindle. (B) Linescan profile of GFP::ZYG-9 (green) and mCherry::histone (magenta) fluorescence intensities from metaphase spindles in live oocytes. The plot shows ZYG-9 is enriched at the poles of the bipolar metaphase spindle, but there is a significant amount of ZYG-9 in the midspindle region as well; n = represents the number of spindles analyzed. Bars = 2.5 μm.

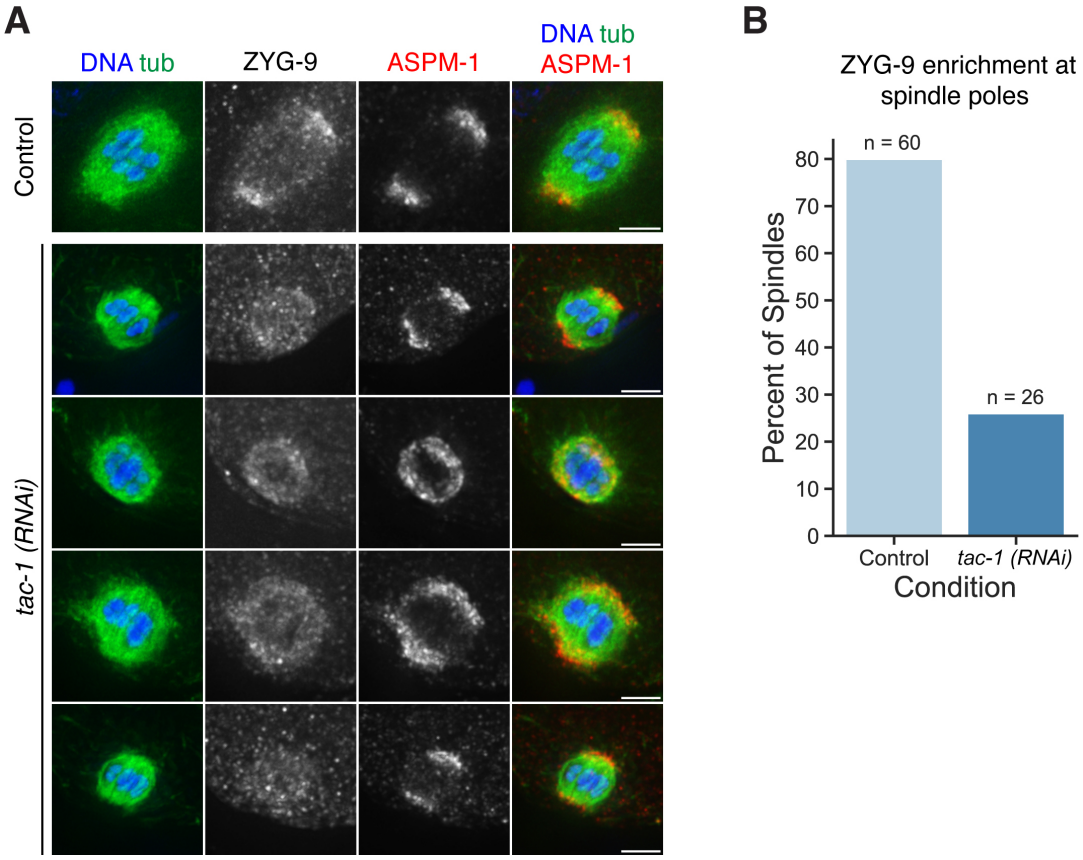

Figure 3.4. **TAC-1 is required for the enrichment of ZYG-9 to the acentriolar spindle poles.** (A) Control and *tac-1(RNAi)* spindles stained for DNA (blue), tubulin (green), ZYG-9 (not in merge), ASPM-1 (red in merge). In control spindles, ZYG-9 is enriched at the poles marked by ASPM-1, but there is also ZYG-9 signal throughout the spindle. In *tac-1 (RNAi)* oocytes, ZYG-9 enrichment at the poles is lost and appears uniform throughout the spindle. (B) Quantification of ZYG-9 enrichment at the spindle poles in (A). Only bipolar spindles (determined by ASPM-1 at two foci, or chromosome alignment) were used in the analysis. n represents the number of spindles analyzed. Bars = 2.5 μm.

Spindles from *tac-1(RNAi)* oocytes showed a loss of ZYG-9 enrichment at the spindle poles, and instead the signal appeared uniform across the entire spindle (Figs. 3.4A and 3.4B). This is an interesting finding because it suggests that ZYG-9 enrichment at acentriolar spindle poles is not absolutely necessary for spindle pole stability and spindle bipolarity in oocytes.

The depletion phenotype and localization pattern of ZYG-9 are consistent with a model in which ZYG-9 is functioning to promote acentriolar spindle pole organization and spindle

bipolarity. Although ZYG-9 enrichment at the spindle poles does not appear to required for spindle pole stability, it is possible that the amount of ZYG-9 that remains associated with the spindle in *tac-1(RNAi)* oocytes is enough to allow bipolar spindle formation (Figs. 3.4A and 3.4B). Finally, by fixed imaging, I do not observe ZYG-9 localization to the microtubule bundles at the cage stage even though ZYG-9 appears to important for the formation of cage microtubule bundles (Figs. 3.1A, 3.2B, 3.2C, and 3.2D). This could be a real finding, however, immunofluorescence staining of other components known to localize to the cage microtubule bundles has been challenging in the past (Figs. 2.6B and 2.6C), which means that this lack of staining could also be reflective of a technical issue. Live imaging of GFP::ZYG-9 throughout spindle assembly will be necessary to provide additional details of this protein's localization and to gain possible insights into its function.

3.4. ZYG-9 is required for acentriolar spindle pole integrity

The acentriolar spindle poles appear to be unstable in ZYG-9 depleted oocytes (Figs 3.1A, 3.2B and 3.2D). Therefore, I wanted to test directly if ZYG-9 is required for maintaining spindle pole integrity in oocytes. In order to answer this question, I needed a method to acutely deplete ZYG-9 in oocytes after the bipolar spindle has formed. To this end, I utilized an auxin-inducible-degron (AID) system that has been established for use in *C. elegans*[155]. Briefly, in this system, a protein is tagged with a 44-aa degron peptide that in the presence of the small molecule auxin mediates an interaction with TIR1 (a recognition component of the E3 ubiquitin ligase complex), ubiquitinates the degron-tagged protein and targets it for degradation via the proteasome. The construct used to make my GFP::ZYG-9 strain also contains this degron peptide fused to the N-terminus of GFP. Additionally, the degron::GFP::ZYG-9 was made in a worm strain that constitutively expresses TIR1 throughout the germline[155]. When adult worms expressing degron::GFP::ZYG-9 were transferred to

plates containing 1mM auxin for 18 hours, there was a complete loss of ZYG-9 signal from the spindle, and I observed spindle assembly defects that were identical to those observed in *zyg-9(RNAi)* oocytes (Figs. 3.5 and 3.1B). These data suggest that ZYG-9 is being degraded from oocytes in this worm strain upon treatment with auxin.

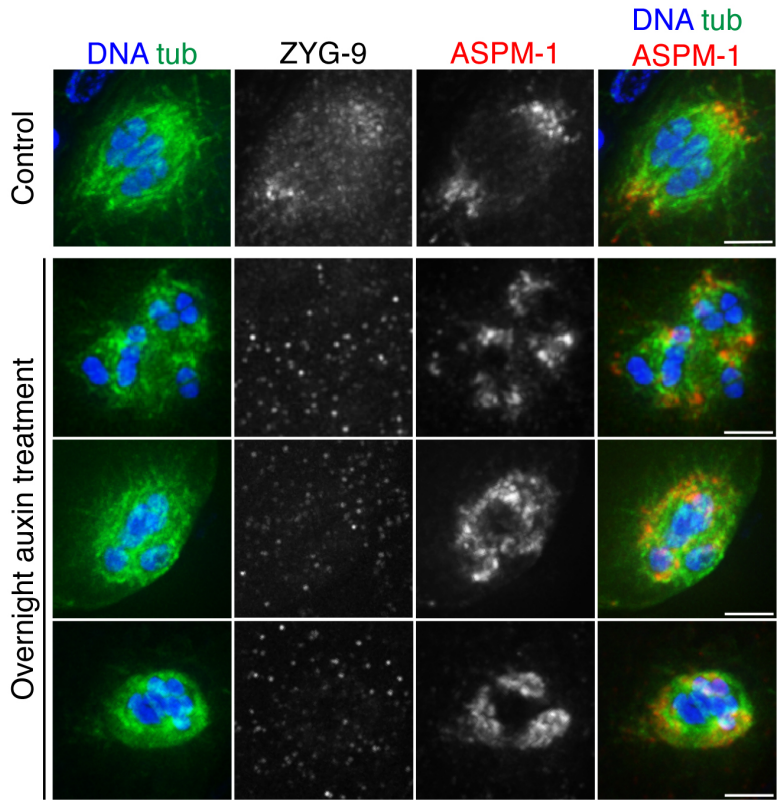

Figure 3.5. **Long-term auxin induced depletion of degron::ZYG-9 in oocytes.** Oocyte spindles from control animals and animals placed on 1mM auxin plates overnight stained for DNA (blue), tubulin (green), ZYG-9 (not in merge), and ASPM-1 (red in merge). Spindles from oocytes treated with auxin overnight show loss of ZYG-9 staining and spindle phenotypes identical to *zyg-9(RNAi)* spindles suggesting that ZYG-9 is being degraded. Bars = 2.5 μm.

To test the requirements of ZYG-9 for maintaining acentriolar spindle pole stability, I arrested oocytes at metaphase (when the bipolar spindle has formed) by depleting a component of the anaphase promoting complex (APC) via RNAi[156]. I then soaked the animals in either 1mM auxin or vehicle for 25-30 minutes before dissecting and fixing the oocytes.

Using this assay, I found that rapid depletion of ZYG-9 from oocytes resulted in a disruption of acentriolar spindle pole morphology (Figs. 3.6A and 3.6B). At the spindle poles in oocytes treated with auxin, I observed a range of spindle pole disruption phenotypes, including astral microtubules emanating from the poles away from the chromosomes and microtubules that appeared to be dissociated from the spindle pole marked by ASPM-1 staining at one end (Fig. 3.5A). In addition to defects at the spindle poles, I also observed a large proportion of spindles from auxin-treated oocytes that had defects in the organization of midspindle microtubules. While in control oocytes, microtubule bundles from each spindle pole run alongside chromosomes forming lateral associations, and therefore microtubule bundles in the overlap zone at the midspindle appear continuous. Following ZYG-9 depletion, the microtubules appeared to terminate near the chromosomes and splay away from the spindle (Figs. 3.6A, arrowheads and 3.6C). Finally, I observed that the spindles in the auxin treated oocytes were significantly shorter than the spindles from vehicle treated oocytes (Fig. 3.6D). Interestingly, I noticed these defects even in spindles where I could still detect some ZYG-9 signal (Fig. 3.6A, second row). This suggests that acentriolar spindles are hypersensitive to the levels of ZYG-9 in the cell, and that potentially small perturbations in the amount of ZYG-9 are sufficient to cause defects in spindle pole organization. Together, these data suggest that ZYG-9 is required to maintain the integrity of the acentriolar spindle poles during oocyte meiosis. Furthermore, ZYG-9 appears to important for maintaining correct spindle length and proper lateral microtubule-chromosome attachments at metaphase.

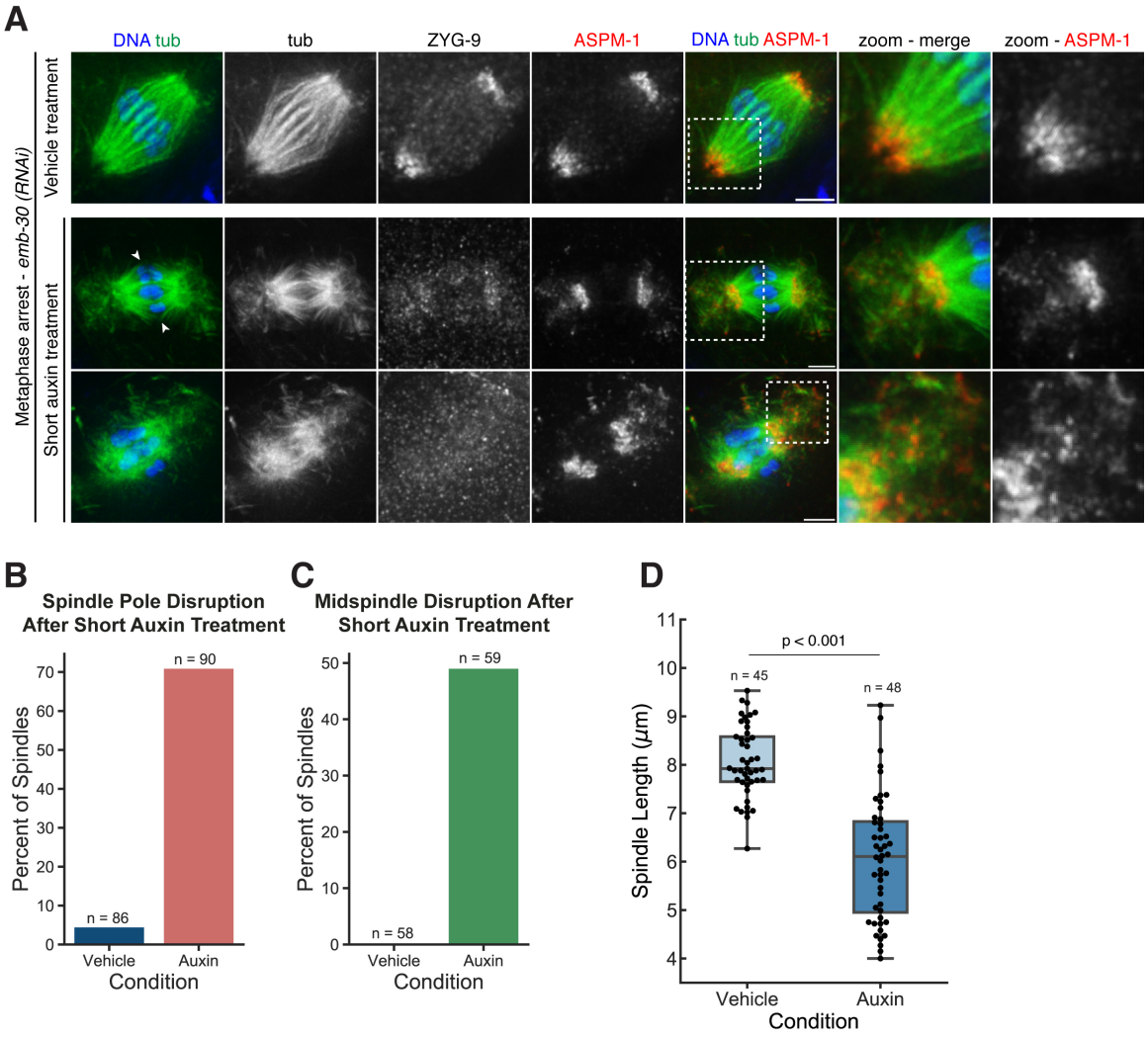
A
DNA tub
tub
ZYG-9
ASPM-1
DNA tub ASPM-1
zoom - merge
zoom - ASPM-1
Metaphase arrest - emb-30 (RNAi)
Vehicle treatment
Short auxin treatment
B
Spindle Pole Disruption
After Short Auxin Treatment
Percent of Spindles
n = 86
n = 90
Vehicle
Auxin
Condition
C
Midspindle Disruption After
Short Auxin Treatment
Percent of Spindles
n = 58
n = 59
Vehicle
Auxin
Condition
D
p < 0.001
n = 45
n = 48
Spindle Length (μm)
Vehicle
Auxin
Condition

Figure 3.6

Figure 3.6. **Acute ZYG-9 depletion causes acentriolar spindle pole disruption.** (A) Spindles from metaphase arrested (*emb-30(RNAi)*) oocytes treated with vehicle or 1mM auxin for 25-30 minutes stained for DNA (blue), tubulin (green), ZYG-9 (not in merge), and ASPM-1 (red in merge). In spindles from vehicle treated oocytes, the spindle poles are tightly organized, and the microtubule bundles appear to cross from one side of the spindle to the other without interruption. In spindles from auxin treated oocytes, the ZYG-9 signal is decreased and spindle pole integrity is compromised as shown by the ASPM-1 and tubulin staining coming off of the poles away from the spindle (zooms). Spindles from auxin-treated oocytes also showed defects in midspindle microtubules where they appeared to terminate near the chromosomes and splay away from the spindle. Finally, the spindles from auxin-treated oocytes appeared to have a shorter pole to pole distance compared to spindles from vehicle treated oocytes. (B) Quantification of spindle pole disruption in vehicle and auxin-treated oocytes. (C) Quantification of midspindle disruption in vehicle and auxin-treated oocytes. (D) Boxplots of spindle length (pole to pole) in vehicle and auxin-treated oocytes. Box represents the first quartile, median, and third quartile. Whiskers extend to maxima and minima. Significance determined using a two-tailed t-test. n represents the number of spindles analyzed. Bars = 2.5 μm.

3.5. ZYG-9 dynamics at the spindle pole are cell-type specific

My findings thus far point to model in which ZYG-9 functions to organize and stabilize the acentriolar spindle poles. This essential pole organization function in oocytes is in contrast to the requirements of ZYG-9 during mitotic spindle formation. In ZYG-9 depleted mitotic embryos, the spindle poles remain intact and a bipolar spindle forms (albeit mispositioned and comprised of shorter microtubules)[50,151]. Because of these differences, I reasoned that ZYG-9 may have cell-type specific roles at the acentriolar meiotic versus centrosomal mitotic spindle poles. To gain insight into this question, I performed fluorescence recovery after photobleaching (FRAP) experiments of ZYG-9 at acentriolar poles and at centrosomes of the mitotic spindle. My FRAP analysis revealed that ZYG-9 is much more dynamic at the metaphase acentriolar spindle pole ($t_{\frac{1}{2}} = 16.61$ s) compared to the prometaphase/metaphase centrosome ($t_{\frac{1}{2}} = 119.39$ s) (Figs. 3.7A and 3.8A; Movies 3-2 and 3-3). Furthermore, ZYG-9 fluorescence at the acentriolar pole recovers to pre-bleach levels whereas ZYG-9 fluorescence at the centrosome does not recover to pre-bleach levels before the cell enters anaphase. I wondered if the difference in ZYG-9 dynamics at the acentriolar versus centriolar spindle poles represents the behavior of all spindle pole components, and what I observed is a fundamental difference of pole components in these two contexts. To investigate this question, I performed this FRAP analysis on the spindle pole component ASPM-1. I found that ASPM-1 has relatively similar dynamics at the acentriolar and centrosomal spindle poles ($t_{\frac{1}{2}} = 49.48$ s and 38.70 s, respectively) and the fluorescence recovers to similar levels (Figs 3.7B and 3.8B; Movies 3-4 and 3-5). This suggests that not all spindle pole components have different dynamics at acentriolar versus centriolar spindle poles, and that a protein's association with the centrosome does not always causes a drastic change in its dynamics.

Finally, I found that tubulin fluorescence quickly recovers to pre-bleach levels at the acentriolar spindle poles (Figs. 3.7C and 3.8C; Movie 3-6). The differences in ZYG-9 dynamics at acentriolar and centrosomal spindle poles in conjunction with the phenotypic differences in oocytes and mitotic embryos depleted of ZYG-9 are consistent with a model in which ZYG-9 has distinct functions during spindle assembly in these two cell types.

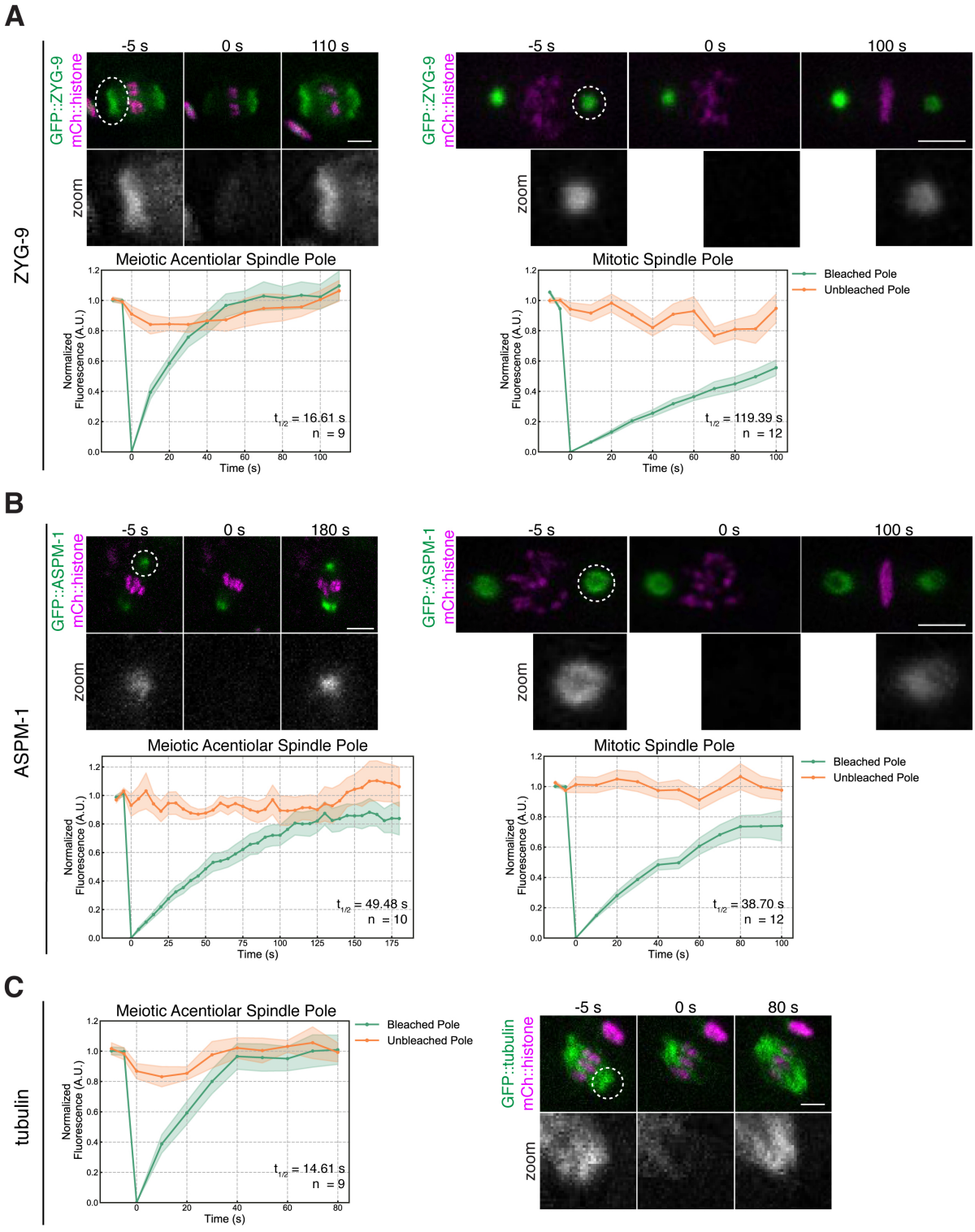
A
ZYG-9
-5 s
0 s
110 s
GFP::ZYG-9
mCh::histone
zoom
Meiotic Acentiolar Spindle Pole
Normalized Fluorescence (A.U.)
Time (s)
t1/2 = 16.61 s
n = 9
-5 s
0 s
100 s
Mitotic Spindle Pole
t1/2 = 119.39 s
n = 12
Bleached Pole
Unbleached Pole
B
ASPM-1
-5 s
0 s
180 s
GFP::ASPM-1
Meiotic Acentiolar Spindle Pole
t1/2 = 49.48 s
n = 10
-5 s
0 s
100 s
Mitotic Spindle Pole
t1/2 = 38.70 s
n = 12
C
tubulin
Meiotic Acentiolar Spindle Pole
t1/2 = 14.61 s
n = 9
-5 s
0 s
80 s
GFP::tubulin

Figure 3.7

Figure 3.7. **FRAP analysis of spindle pole components.** (A-C) FRAP recovery curves and stills from movies for ZYG-9 (A), ASPM-1 (B), and tubulin (C) at meiotic and mitotic spindle poles (except for tubulin - only recovery at meiotic spindle shown). In graphs, the bleached pole curve is green, the unbleached pole curve is orange, the solid lines are the average, and the standard error of the mean is shaded. For all images, the specified bleached protein is in green and the chromosomes are in magenta. Zooms show only the bleached protein. $t_{\frac{1}{2}}$'s were calculated from fitting the recovery curves to a single exponential function (see Chapter 5: Materials and methods) and Figure 3.8. n represents the number of spindles analyzed to generate each curve. Bars = 2.5 μm (meiosis) and 5 μm (mitosis).

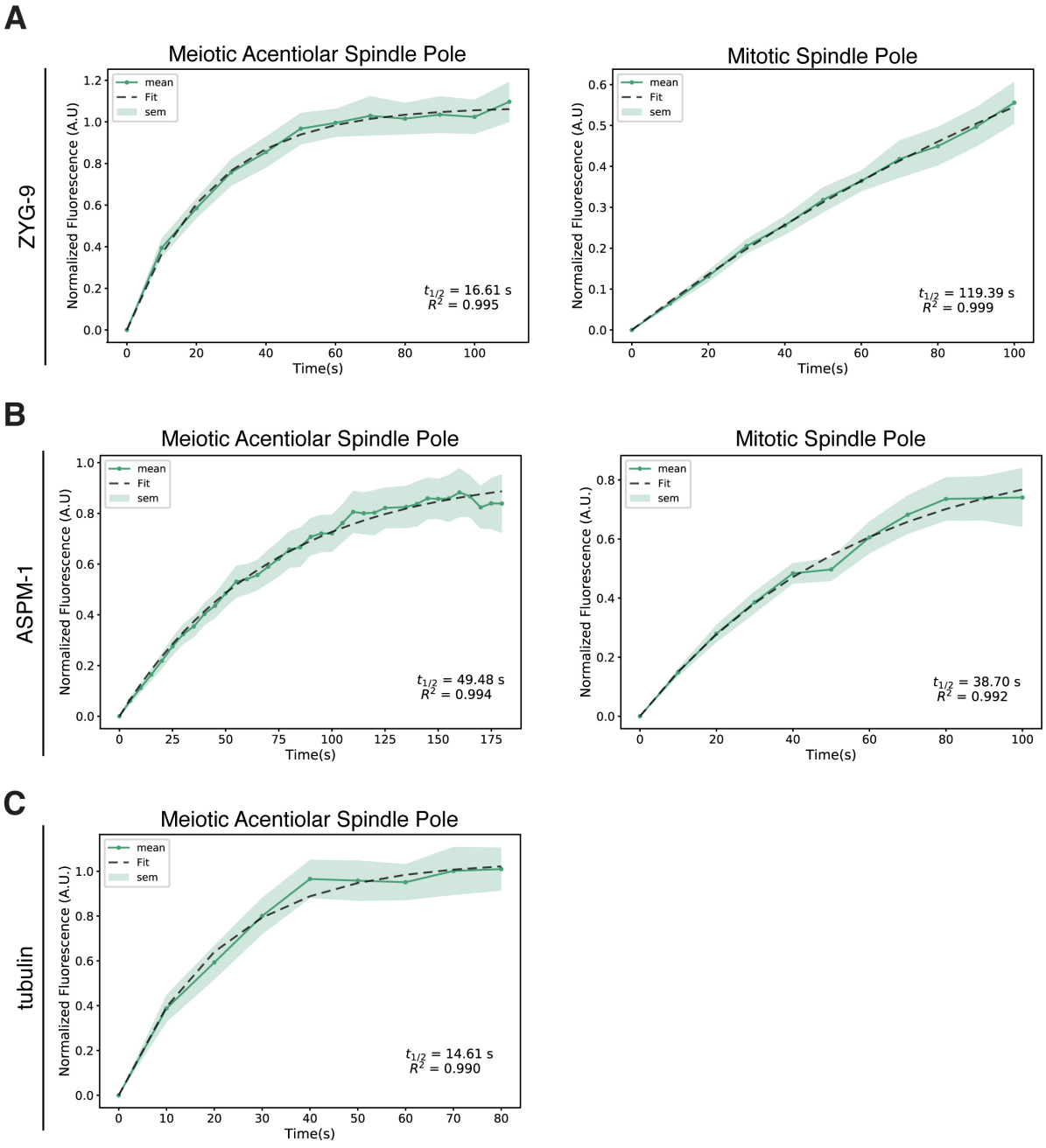

Figure 3.8. **FRAP analysis with fit curves.** (A-C) graphs of recovery curves and fit curves from the bleached poles of the FRAP experiments described in Fig. 3.7. The mean is a solid line, the standard error of the mean is the shaded region, and the single exponential function fit is a dashed line. $t_{\frac{1}{2}}$'s were calculated from these fit curves (see Chapter 5: Materials and methods).

3.6. ZYG-9 depletion causes ectopic aster formation in oocytes

One final observation that was made during the course of my studies was that ZYG-9 depletion resulted in the formation of astral microtubule clusters throughout the cytoplasm of the oocyte (Fig. 3.9). These structures have been documented in previous studies[112], but there has been no real analysis to determine their composition or the cause of their genesis. I found that these asters frequently colocalize with ASPM-1, a spindle pole component and a microtubule minus-end binding protein[41,52,53]. The formation of these asters in ZYG-9 depleted oocytes raises many interesting questions about the regulation of the entire microtubule network within the oocyte. More work will need to be done to further characterize these ectopic asters and to determine the cause of their formation in *zyg-9(RNAi)* oocytes.

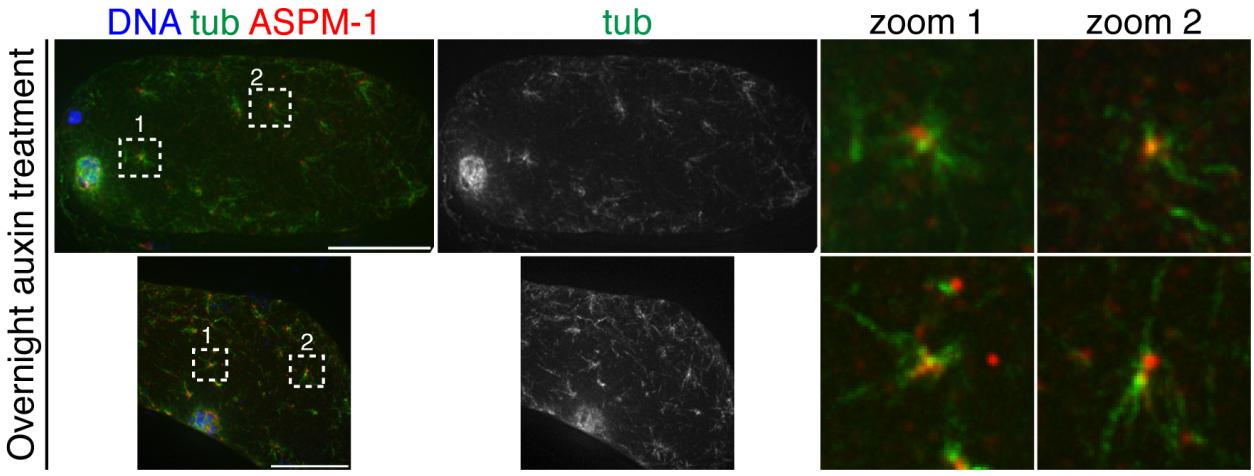

Figure 3.9. **ZYG-9 depletion causes ectopic microtubule aster formation.** Oocytes from worms placed on 1mM auxin plates overnight were stained for DNA (blue), tubulin (green), and ASPM-1 (red). Zooms show examples of ectopic asters denoted by dashed white boxes in the merge. Depletion of ZYG-9 results in the formation of microtubule asters throughout the cytoplasm, and these asters are frequently marked by an ASPM-1 focus. Bars = 10 μm.

3.7. Discussion

Taken together, my data suggest a novel role for ZYG-9 during acentriolar spindle assembly and for the maintenance of the acentriolar spindle poles during oocyte meiosis. During spindle assembly ZYG-9 becomes enriched at the spindle poles during the multipolar stage, and this localization is maintained through metaphase when bipolarity is established (Figs. 3.3A and 3.3B). The accumulation of ZYG-9 to the multiple nascent poles could be necessary to facilitate the focusing of these nascent poles into a bipolar structure. This interpretation is supported by the predominance of multipolar spindles observed by live and fixed imaging in *zyg-9(RNAi)* oocytes (Figs. 3.1B and 3.2B). This is also consistent with a study of acentriolar spindles in *Drosophila* oocytes where mutants of the ZYG-9 homolog Msps result in the formation of tripolar spindles[157]. Furthermore, I found that TAC-1 is required for the proper localization of ZYG-9 to the poles of the acentriolar spindle. This is similar to the role of TAC-1 during mitosis in *C. elegans* embryos[50,108,109] and in *Drosophila* oocytes[157] and embryos[158].

I also observed that depletion of ZYG-9 often prevented the formation of the cage microtubule bundles (Figs. 2.1B ,3.1A, 3.2B, 3.2C, and 3.2D; Movies 2-1 and 3-1). This finding suggests that ZYG-9 is an important factor for promoting the assembly of microtubules very early on during spindle assembly. It is tempting to speculate that ZYG-9 may possess microtubule nucleating capabilities as it was recently shown that XMAP215 can cooperate with the γ-tubulin ring complex (γ-TuRC) to promote microtubule nucleation in *Xenopus* extract[159]. In *C. elegans* oocytes, the γ-tubulin TBG-1 localizes around the disassembling nuclear envelope[86], which is in close proximity to where the cage microtubule bundles form[84]. However, TBG-1 does not localize to the meiotic spindle at metaphase[60,86,87], and depletion of TBG-1[86,87] and another γ-TuRC protein, GIP-1[86], have been reported to have no effect on

meiotic spindle morphology. It is possible, however, that there are more subtle microtubule nucleation or assembly defects that affect the earlier stages of spindle assembly. Further analysis including time-lapse imaging of ZYG-9 and γ-tubulin at the cage-stage as well as imaging of the cage microtubules in *tbg-1(RNAi)* oocytes will be necessary to determine if these factors could be promoting microtubule formation. Although the cage microtubule bundles fail to form in *zyg-9(RNAi)* oocytes, microtubules are still nucleated in the vicinity of the chromosomes (Fig. 3.1 and Movie 3-1). This suggests that there is another mechanism functioning to nucleate microtubules near the chromosomes at this stage. One possible alternative nucleation mechanism is through the Ran pathway of chromatin-mediated spindle assembly. The Ran pathway is important for microtubule formation and spindle assembly around chromatin in many other acentriolar systems[16,90,91,160]. Furthermore, Ran is important for aspects of mitotic spindle assembly in *C. elegans* embryos[161], but it has been reported to be non-essential for proper chromosome segregation in oocytes, suggesting that acentriolar spindle assembly does not require Ran[92]. However, the studies of Ran in *C.elegans* oocytes were limited and further analysis is needed to carefully assess the contribution of this pathway to spindle assembly in these cells. Because ZYG-9 appears to be required for the robust formation of cage microtubules, but does not completely prevent microtubule assembly, it is possible that ZYG-9 and Ran function in partially redundant pathways to stimulate microtubule assembly in *C. elegans* oocytes.

My results also confirmed a decades old observation that inhibition of *zyg-9* function results in the formation of microtubule asters throughout the cytoplasm of the oocyte (Fig. 3.9)[112]. This is an interesting result as it is hard to imagine how depleting a microtubule stabilizing protein could cause the formation of extra microtubule asters. One possible explanation is that ZYG-9 is important for regulating the levels of free tubulin in the cytoplasm

by binding tubulin dimers via its TOG domains[162,163]. Depletion of ZYG-9 would result in an increase in free tubulin which could promote the assembly of microtubules. Furthermore, it was recently shown that the microtubule depolymerase MCAK is required to prevent ectopic microtubule assembly in oocytes[124]. Together, these findings suggest that the balance of microtubule assembly and destruction and possibly the levels of free tubulin in the oocyte are tightly regulated to prevent ectopic microtubule structures from forming and restricts microtubule assembly to the spindle. A good test of this hypothesis would be to mutate the TOG domains in ZYG-9 such that they can no longer bind tubulin[147,163], and observe if asters form when only this mutant form of ZYG-9 is present. Alternatively, because the ectopic asters contain the microtubule minus-end binder and spindle pole protein ASPM-1[52–54,95] (Fig. 3.9), it is possible that ZYG-9 is responsible for recruiting and concentrating other spindle pole components to the spindle. Staining the asters for other factors that concentrate at the acentriolar spindle poles such as MEI-1/2(katanin)[86], KLP-18(kinesin-12)[84,93], and MCAK[124] will be necessary to understand if these structures are indeed ectopic poles.

Using the AID system to rapidly deplete ZYG-9 from bipolar metaphase spindles, I found that ZYG-9 is required for the maintenance of acentriolar spindle pole integrity (Figs. 3.6A, and 3.6B). My data suggests that ZYG-9 could be functioning as a molecular glue that is helping to maintain the structure of the pole. However, I cannot rule out the possibility that acute depletion of ZYG-9 is preventing the microtubules seen adjacent to the poles from being incorporated into the spindle as it has been shown that microtubules from the cytoplasm can be taken up into the spindle[124]. Time-lapse imaging of microtubules in metaphase arrested oocytes treated with auxin will allow me to determine the source of

the microtubules observed near the poles and to better understand ZYG-9's maintenance function.

The spindle pole assembly and maintenance function of ZYG-9 appears to be specific to acentriolar oocyte spindles, as bipolar (albeit mispositioned) mitotic spindles with intact centriole-containing centrosomes are able to form in *zyg-9(RNAi)* embryos[112]. This cell-type specific function of ZYG-9 may be unique to *C. elegans* as *Drosophila msps* mutants display multipolar acentriolar meiotic spindles in oocytes and multipolar mitotic spindles in embryos[164], and depletion of human ch-TOG results in multipolar mitotic spindles in HeLa cells[165,166]. Nevertheless, this proposed cell-type specific role of ZYG-9 is supported by my FRAP analysis where I found that the dynamics of ZYG-9 at the acentriolar and centrosome-containing spindle poles are vastly different (Figs 3.7A and 3.8A). The slow recovery of ZYG-9 at the mitotic spindle poles could be due to the compartmentalization and phase separated nature of the the mitotic centrosome in *C. elegans*[145,147]. However, FRAP analysis of ASPM-1 revealed similar dynamics at the poles of meiotic and mitotic spindles (Figs. 3.7B and 3.8B), suggesting that the localization of a pole protein to the centrosome does not necessarily cause a drastic change in dynamics. Further FRAP experiments of tubulin at the acentriolar spindle in *zyg-9(RNAi)* oocytes and in oocytes expressing the ZYG-9^{AA} TOG-mutant that is defective in tubulin binding[147,163] will be important for dissecting the function of ZYG-9 in these cells. A recent study used the ZYG-9^{AA} TOG mutant in reconstituted centrosomes *in vitro* to investigate how the PCM forms and nucleates microtubules. In this study, the authors incubated the PCM component SPD-5 with a crowding agent to produce spherical condensates of SPD-5. These SPD-5 condensates can selectively incorporate the centrosomal components TPXL-1 and ZYG-9, which together recruit tubulin into the condensate and promote microtubule nucleation[147]. Using the ZYG-9^{AA} TOG mutant,

the authors found that the ability of ZYG-9 to bind tubulin is necessary to recruit tubulin and promote microtubule nucleation from these reconstituted centrosomes[147]. During oocyte meiosis, there are no centrosomes or specialized structures that function to recruit tubulin to the spindle and promote microtubule nucleation that have been identified. Therefore, it is possible that ZYG-9 could be functioning to concentrate tubulin near the spindle in order to promote microtubule formation in this acentriolar system. FRAP experiments of tubulin at the acentriolar spindle in oocytes where ZYG-9's tubulin binding function is compromised would allow me to test this theory by analyzing changes in the rate of microtubule recruitment and turnover at the spindle poles.

The acute depletion of ZYG-9 also revealed a potential role for this protein in maintaining proper spindle length, possibly by stabilizing or promoting the assembly of microtubules in the midspindle region (Figs. 3.6A, 3.6C, and 3.6D). Furthermore, in my time-lapse imaging of *zyg-9(RNAi)* oocytes I observed nascent poles forming and then collapsing into a single mass suggesting that the microtubules mediating pole separation were unstable (Fig. 3.1A; Movie 3-1). In my fixed imaging of spindles acutely depleted of ZYG-9, there appear to be two half-spindles comprised of microtubules emanating from the poles that terminate near the chromosomes (Fig. 3.6A). Because ZYG-9 belongs to a family of microtubule polymerases[148] and localizes to the midspindle in *C. elegans* oocytes (Fig. 3.3B), it is possible that ZYG-9 could be promoting the elongation and/or stabilization of the microtubules emanating from the spindle poles to establish proper spindle length. As ZYG-9 is required for the formation of long microtubules during mitosis[50], it reasonable to suggest that this protein may have a similar function in meiosis where it promotes the formation of microtubules of the correct length. The observation that microtubules in the midspindle appear to splay away from the chromosomes also raises the possibility that ZYG-9 could be important for maintaining

the attachment of the lateral microtubule bundles to the chromosomes. A good test of this hypothesis will be to acutely deplete ZYG-9 from monopolar spindles. In this condition, the chromosomes are more spread out and the lateral microtubule-chromosome interactions can be easily assessed[37]. If ZYG-9 is important for the lateral microtubule-chromosome interactions, this finding would be important as it is not currently known how the lateral bundles are attached to the chromosomes in these cells.

The finding that ZYG-9 is an important factor for acentriolar spindle pole stability may be significant in regards to understanding spindle assembly in human oocytes. As spindles in human oocytes assemble, there is a significant amount of spindle instability marked by frequent transitions between bipolar, multipolar, and apolar structures[16]. Furthermore, it was found that the number of chromosome segregation errors during anaphase correlated with the amount of spindle instability during assembly[16]. *C. elegans* oocyte spindles share many characteristics with human oocyte spindles. For example, the acentriolar spindles in human oocytes assemble in the absence of multiple discrete MTOCs, they do not contain pericentrin, nor do they show an enrichment of γ-tubulin at the spindle poles[16], similar to *C. elegans* oocyte spindles[60,84,86,87,104–106]. It will be important to test if the human homolog of ZYG-9, ch-TOG[148], is required for promoting spindle pole stability in human oocytes. Of more broad importance, however, I believe that my studies have established the AID system in *C. elegans* oocytes as an excellent discovery tool to identify factors and probe the molecular requirements for acentriolar spindle stability. Together, these results deepen our understanding of the acentriolar spindle poles, and shed light on how the oocyte assembles and stabilizes a spindle in the absence of centriole-containing centrosomes.

CHAPTER 4

Summary of findings and future directions

4.1. Summary of findings

By studying the process of acentriolar spindle assembly and chromosome segregation in *C. elegans* oocytes, I have uncovered basic molecular mechanisms that allow cells to elegantly carry out incredibly complex tasks. I demonstrated that there are redundant mechanisms for organizing the microtubules of the oocyte spindle, and discovered factors that are essential for ensuring spindle stability. The work described here contributes to the overall knowledge of how cells are able to faithfully propagate their genetic material - a process at the core of all life.

In Chapter 2, I showed that there are multiple microtubule organizing mechanisms functioning to ensure accurate chromosome segregation in *C. elegans* oocytes. First, I found that during spindle assembly, the minus-end kinesins KLP-15/16 act to bundle the acentriolar spindle microtubules so they can be sorted and organized into a bipolar structure. Moreover, I was surprised to find that the severely aberrant spindles that form when KLP-15/16 are not present are able to assemble into a structure capable of supporting chromosome segregation. I then demonstrated that the rebundling of anaphase spindle reorganization is driven by the microtubule crosslinking protein SPD-1 and that KLP-18 arranges those bundles into a parallel array along which chromosomes can segregate. These anaphase specific roles for SPD-1 and KLP-18 were only revealed by first knocking down KLP-15/16. My findings touch upon a recurring theme in biology, which is that in order to promote robustness, evolution has endowed the cell with redundancies to ensure the faithful execution of complex processes.

In Chapter 3, I presented evidence for the role of a microtubule stabilizing protein during acentriolar spindle assembly. I found that depletion of this protein, ZYG-9, results in spindles that are often multipolar and collapsed. I then went on to show that ZYG-9 is specifically required to maintain spindle pole integrity during meiosis through the use of an

auxin-inducible-degron system (AID). The data suggest that ZYG-9 has specific functions during meiosis at acentriolar spindle poles that are distinct from its roles during mitosis at centrosomes. These distinct roles highlight how biology can co-opt a single protein and adapt it in order to accomplish different cellular tasks. In the case of ZYG-9, it is remarkable that this protein's role appears to change over the course of a single cell cycle in the same cytoplasm. These studies also established the AID system as a tool for probing the molecular requirements of spindle stability during oocyte meiosis.

In conclusion, the work described here has advanced our understanding of acentriolar spindle assembly and chromosome segregation in oocytes. I have answered important questions regarding how the spindle microtubules are organized and stabilized. Finally, the observations that I made and the approaches that I established throughout the course of this work will allow the lab and the field to answer exciting new questions.

4.2. Future directions

Moving forward, I think that there are two major questions that build directly on the work described here. First, what are the mechanisms for microtubule nucleation in the acentriolar spindle? Second, what factors are necessary to maintain spindle stability once the bipolar spindle has assembled?

4.2.1. How are microtubules of the acentriolar spindle nucleated in *C. elegans* oocytes?

During meiosis in *C. elegans*, there appear to be at least two different modes of microtubule nucleation acting at the earliest stages of MI and MII. During MI, the microtubules are nucleated away from the chromosomes and are initially localized adjacent to the disassembling nuclear envelope before ingressing inwards towards the chromosomes[84,124]. During MII, there is no disassembling nuclear envelope, and the microtubules appear to nucleate

in close proximity to the chromosomes[84]. Because of these observations, I hypothesize that oocyte meiosis in *C. elegans* employs multiple nucleation pathways to generate the spindle microtubules. Furthermore, in Chapter 3, I presented evidence that ZYG-9 may play a key role in nucleating and assembling the microtubules at the cage-stage of MI. When I depleted ZYG-9, I observed that after NEBD, the cage microtubule bundles either never form or are very weak compared to wild-type. However, by live, time-lapse imaging, I was able to watch microtubules eventually being nucleated near the chromosomes. These observations support a model in which there are multiple pathways acting to promote microtubule nucleation during oocyte meiosis.

There are four pathways of nucleation that have been shown to be important for generating spindle microtubules in various systems. I will only be discussing three of them as the fourth relies on the augmin complex which does not appear to be conserved in *C. elegans*[167]. The first relies on γ-tubulin and the γ-tubulin ring complex (γ-TuRC). In this complex, γ-tubulin is organized in a ring-like confirmation that is thought to serve as a template for microtubule nucleation[168,169]. During mitosis, the γ-TuRCs are recruited to the PCM of the centrosome where they promote microtubule nucleation and serve as an anchor for the microtubule minus-ends[58]. Interestingly, *C. elegans* mitotic spindles depleted of γ-tubulin are able to assemble extensive microtubule arrays, but are unable to complete mitosis[60,61]. These findings suggest that in mitosis, similar to meiosis, there are likely redundant mechanisms for nucleating spindle microtubules. The role of γ-tubulin during oocyte meiosis has not been studied in any careful detail. It has been published that there are no spindle assembly defects following *tbg-1(RNAi)*[60,86,87] or depletion of a component of the γ-TuRC[86]. It was also shown that TBG-1 does not localize to the acentriolar spindles at metaphase[86,87];

however, live imaging experiments showed that GFP::TBG-1 becomes enriched around the nuclear envelope about the time of NEBD and cage formation[86].

The Ran pathway of microtubule nucleation is a centrosome-independent mechanism that cells utilize to promote microtubule assembly around chromatin. In this pathway, the active, GTP-bound form of the small GTPase Ran binds to importins, which releases importin-bound spindle assembly factors (SAFs) that promote microtubule assembly and spindle formation[170–172]. A gradient of RanGTP is established at the chromatin by the activity of the chromatin bound RanGEF RCC-1[160,173]. In many systems, Ran likely functions in conjunction with other microtubule nucleation pathways. In mouse and *Xenopus* oocytes, Ran depletion causes only a delay in MI spindle assembly[174], and in *Drosophila*, spindles are able to form in the absence of Ran[90]. In *C. elegans*, Ran is necessary for the assembly of mitotic spindles[92,161]. It was reported that Ran is not required for the proper completion of meiosis[92], but this conclusion was based solely on the observation that there was not a detectable difference in the amount of chromatin in the maternal pronucleus following completion of MII in *ran-1(RNAi)* oocytes. A careful analysis of the role of Ran during acentriolar spindle assembly has not been conducted in *C. elegans*.

The third microtubule assembly pathway that could be contributing to spindle assembly in *C. elegans* oocytes is the CPC-mediated microtubule nucleation pathway. During mitotic spindle assembly, the CPC is required for microtubule assembly at chromosomes in the absence of active Ran[175]. In *C. elegans*, the CPC is required for acentriolar spindle assembly, but its role in microtubule nucleation has not been assessed[78].

I believe that the first step in establishing a role for these potential nucleation mechanisms is to deplete them by RNAi and film spindle assembly in oocytes expressing GFP::tubulin and mCherry::histone. Similar to the ZYG-9 depletion phenotype, there may be subtle

differences in microtubule nucleation during the early stages of spindle assembly. Because there are likely redundant mechanisms for nucleating microtubules, live imaging of oocytes co-depleted of these potential nucleators in different combinations will be important. Because ZYG-9 appears to have some role in microtubule assembly, it will also be worthwhile to deplete the components of the different nucleation pathways in a *zyg-9(RNAi)* background. Furthermore, in these different depletion experiments, it will be important to assess the timing of microtubule nucleation. Because there are likely redundant mechanisms, it is possible that they do not all function at the same time during spindle assembly. For example, in my ZYG-9 depletion experiment, the microtubule cage does not form, but microtubules are still nucleated near the chromosomes potentially through a Ran or CPC mediated mechanism. It will be important to know if the microtubule nucleation near the chromosomes occurs at the same time as the cage microtubules normally appear after NEBD. If it takes longer for the microtubules to appear around the chromosomes post NEBD than it normally takes for the cage microtubules to form, this delay would suggest that there is a sequence of microtubule nucleation events. Finally, both MI and MII spindle assembly should be examined under these various depletions. Qualitatively, the microtubules are nucleated in very different ways during MI and MII, and therefore it is likely that there are different nucleation pathways functioning in each case. Different nucleation pathways during MI and MII would not be unique to *C. elegans* oocytes. In mouse and *Xenopus* oocytes, spindle assembly during MI is not inhibited after altering Ran activity, but MII spindles fail form in the absence of Ran activity[174]. Additionally, the AID system will be a powerful tool for assessing the function of these potential nucleation factors. Because some of these factors are likely to have essential roles in other cellular processes, fully depleting them by RNAi may cause pleiotropic effects. The AID approach will allow for better control of the timing and amount of depletion.

Using the AID system, one could also examine the requirements of these different nucleation pathways on spindles that have already assembled, which will be essential to our understanding of microtubule nucleation in acentriolar spindles. In these experiments, one could use the AID system to tag potential nucleation components, arrest the spindles at metaphase when bipolarity is established by inhibiting the APC, treat with auxin, and observe any changes in spindle morphology. It would also be possible to perform the AID depletions in different RNAi backgrounds. In this way, one could assess potential redundancies in these pathways after the spindle has formed. This type of redundancy has been shown in mitotic spindles in HeLa cells[176]. In this study, injection of a dominant negative form of Ran did not have an effect on spindles that had already established bipolarity. Although the HeLa cells contain centrosomes, it is still possible that a hand off of nucleation mechanisms promotes spindle assembly in acentriolar systems as well.

Similarly, it will also be important to investigate how microtubules are continuously nucleated within the spindle. An excellent method for assessing the effects of these potential nucleation pathways would be to deplete them by RNAi, alone and in different combinations, in a worm strain expressing a fluorescently tagged tubulin and perform FRAP experiments. It is possible, however, that depletion of some of these potential nucleation factors may cause spindle assembly defects, which would make performing FRAP experiments difficult. This is true for at least the CPC, which does not assemble a functional spindle after RNAi depletion[78]. If there are spindle assembly defects following RNAi depletion, one could use an AID approach similar to the one described above where one could tag these factors with a degron peptide, arrest the spindles at metaphase after the spindle has formed, treat with auxin to degrade the protein, and then FRAP spindle tubulin. By measuring the rates of recovery of tubulin associated with the acentriolar spindle in these different conditions, it

will be possible to quantitatively assess any differences in the dynamics of tubulin. The depletion of factors that are necessary for efficient microtubule nucleation should result in a slowing of the rate of recovery of tubulin fluorescence on the spindle.

Another phenomenon that requires continuous microtubule nucleation is microtubule flux. Classically, microtubule flux is the behavior in which tubulin subunits are added to the plus-end of a microtubule, near the chromosomes, while simultaneously, there are tubulin subunits being removed from that same microtubule near the poles[177,178]. In acentriolar systems, such as *Xenopus* egg extracts, microtubule flux has also been reported. Here, microtubules are continuously nucleated near the chromosomes and are then transported poleward by microtubule motors with their minus-ends leading. This is also accompanied by microtubule depolymerization near the poles to achieve a steady state of microtubule mass in the spindle[179]. Furthermore, in bipolar acentriolar spindles in *Xenopus* egg extracts, Ran is required for the nucleation of microtubules near the chromosomes and subsequently for microtubule flux[180]. It is also possible that the CPC plays a role in microtubule flux, but to my knowledge that function has not been shown definitively in any system. Therefore, I think testing a role for Ran and the CPC on microtubule flux in *C. elegans* acentriolar spindles is an important question. First, however, it will be necessary to show that there is microtubule flux occurring in the acentriolar spindles in *C. elegans* oocytes. Using a worm strain expressing GFP::tubulin, I have done preliminary experiments where I bleached a line down the center of the spindle perpendicular to the long axis, and found that the microtubules do indeed appear to flux towards the poles (Fig. 4.1). One could deplete components of the Ran pathway and the CPC, either by RNAi or by tagging these components with a degron peptide, as described above, and use this type of assay to measure the rate of flux. In order to test the contribution of the Ran pathway on microtubule flux, I believe the

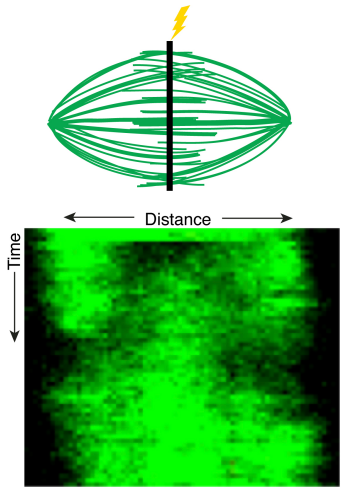

Figure 4.1. **Microtubule flux in *C. elegans* acentriolar spindles.** Example kymograph of microtubule flux in an metaphase spindle in an oocyte expressing GFP::tubulin. A line down the center of the spindle along the short axis was photobleached. Kymograph shows the bleached microtubules moving away from the center of the spindle near the chromosomes and towards the poles with new microtubules being incorporated at the center of the spindle.

best experiment would be to deplete the chromatin bound RanGEF, RCC-1, (*ran-3* in *C. elegans*) to show that it is indeed the active Ran near the chromosomes that is promoting microtubule nucleation and flux. It may be worthwhile perform these flux experiments on monopolar spindles as this spindle configuration would make it easier to visualize the fluxing microtubules. I have also generated a photoconvertible mMaple3::tba-1 strain that could be used in these experiments to make visualizing and tracking the microtubules easier. If active Ran or the CPC is mediating microtubule nucleation at the chromosomes, I would expect to see a decrease in the rate of flux in the absence of RCC-1, Ran, or the CPC.

4.2.2. What factors promote acentriolar spindle stability in *C. elegans* oocytes?

The establishment of the AID system as a tool to study the molecular requirements of spindle stability has opened the doors to many new and exciting avenues of research in the lab. I believe that this approach can be used to answer several important questions regarding how the bipolar spindle maintains its structure. These types of studies are very pertinent to

human oocyte biology as it was found that the acentriolar spindles in these cells are very unstable, and the instability leads to chromosome segregation errors during anaphase[16]. Therefore, using *C. elegans* as model to begin to interrogate spindle stability is essential to inform the next big questions in human oocyte spindle assembly and stability, in addition to understanding the fundamental mechanisms important for maintaining spindle architecture.

This system should be used to continue investigating what factors are important for acentriolar spindle pole stability. Using the AID system and metaphase arrested spindles, I have already shown that ZYG-9 plays an important role in promoting the integrity of the spindle poles. These types of studies should be extended to all of the other known pole proteins as well. These include the proteins ASPM-1[95], LIN-5[95], dynein[97], MEI-1/2[152,181], TAC-1[108], KLP-18[93], MESP-1[84] and MCAK[53]. Some of these factors have well characterized roles during spindle assembly, but it is unknown if their continued activity is required for pole integrity after the bipolar spindle has formed. Furthermore, these studies relied on temperature sensitive alleles, small molecule inhibitors, and RNAi to assess function. These approaches often do not allow for an accurate assessment of the level depletion or inhibition. The AID system overcomes most of those obstacles. Because it is possible to use the degron in conjunction with a GFP tag, one can get a quantitative measurement of the amount of depletion. I believe an important next step for all of the AID/spindle stability experiments is to do them in live oocytes. By tagging the protein of interest with a degron::GFP tag in a worm strain that expresses mCherry::tubulin, it will be possible to watch the protein being degraded (through a decrease in GFP signal) and view, in real time, what happens to spindle morphology. In this way, one can also assess the amounts of protein that are required for pole stability as well. It would be interesting to see if the spindle poles and the spindle in general are more sensitive to the amounts of one protein versus another.

Next, the requirements of the motor proteins KLP-15/16 (kinesin-14) and KLP-18 (kinesin-12)/MESP-1 on spindle stability should also be examined. While it appears that KLP-15/16 are essential for bundling the microtubules of the acentriolar spindle, it will be important to know if this bundling activity is continually necessary for spindle stability. A potential role for KLP-18 and MESP-1 in stabilizing the acentriolar spindle could be very interesting. Right now we know that KLP-18 and MESP-1 are interdependent for their localization to the spindle and depletion of either factor results in a monopolar spindle[84]. Using the AID approach on metaphase arrested spindles, one could ask if the outward directed force generated by KLP-18 is needed after the bipolar spindle has formed. It will also be important to know if MESP-1 is necessary for the activity of KLP-18, or if MESP-1 is only needed to target KLP-18 to the spindle initially. Moreover, if KLP-18 or MESP-1 are depleted from the bipolar spindle and it maintains its structure, it will be necessary to re-examine the role of BMK-1 (kinesin-5). BMK-1 localizes to the acentriolar oocyte spindle during metaphase and anaphase, but, unlike other systems, is not required for spindle assembly or chromosome segregation in *C. elegans*[65]. It is possible that BMK-1 could compensate for the activity of KLP-18 but only after the bipolar spindle has formed. In mammalian cells, kinesin-12 can compensate for the loss of Eg5 activity to establish a bipolar spindle, and therefore, kinesin-12 is the back up mechanism in this system[31,182]. In *C. elegans*, the opposite may be true since the kinesin-12 (KLP-18) is the dominant motor required for generating bipolarity. Therefore, in *C. elegans* BMK-1 could be the backup mechanism. If the spindles remain bipolar after KLP-18 depletion, the same experiment should be performed in a *bmk-1(RNAi)* background.

Finally, the AID system should be used to ask questions about the signalling mechanisms required for continued maintenance of the spindle. Specifically, the roles of the Aurora A

kinase AIR-1 and the polo-like kinase PLK-1 should be investigated as both of these kinases localize to the acentriolar spindle[111,183]. AIR-1 is proposed to be required for the maintenance of microtubules that can be incorporated into the spindle, but these studies were done at low resolution and are worth revisiting using better imaging in conjunction with the degron approach. The function of PLK-1 during oocyte spindle assembly has not been studied in any detail other than its localization. In mitosis, PLK-1 is necessary to phosphorylate the PCM component SPD-5, which promotes its incorporation into the centrosome[184]. SPD-5 is not present on the acentriolar spindle, but it is possible that PLK-1 phosphorylates other substrates that are necessary for spindle assembly in oocytes.

Applying the AID system to study questions regarding acentriolar spindle stability will provide important insights into understanding how these unique spindles are able to maintain their structure in order to accurately segregate chromosomes.

4.3. Final remarks

The field of cell biology has come a long way since Flemming's illustrations of mitosis[2], and today, we know many of the factors that contribute to the vital process of cell division. However, now that we have a decent parts list, the challenge going forward is understanding how all of those parts fit together. The spindle, in particular, is a great example of just one aspect of the cell division apparatus of which we know many of the components, but we have only begun to scratch the surface of understanding how the individual behaviors of these components collectively contribute to the assembly of an amazingly complex cellular machine. Fully understanding this complex self-assembling structure remains an incredibly daunting undertaking. I am confident, however, that as the lines between disciplines blur and cell biologists adopt approaches and ideas pioneered by other scientific fields, we will begin to see a deeper, more complete picture of spindle assembly emerge.

It is important to remember that the thread of evolution permeates through all we do as biologists. Evolution has fine-tuned the chemistry of all of the molecules involved every cellular process, including spindle assembly, to ensure their precise execution. Therefore, studying these cellular processes in different organisms and contexts across evolutionary time will be essential to fully understand the fundamental biology at their core. The work described in this dissertation would not have been possible without key insights gleaned from the work of other researchers carried out in organisms other then *C. elegans*. In turn, it is now my hope that the discoveries I have made and described in this dissertation will provide others with the insights they need to move their science forward.

As cell biologists strive to adopt more quantitative approaches to answer fundamental questions, I think it is also important to remember that an image is worth a thousand words. Looking through a microscope and being able to see a phenomenon with one's own eyes will always inspire and be a strength of cell biology.

CHAPTER 5

Materials and methods

Strains

In this study, 'wild-type' refers to N2 (Bristol) or EU1067 worms grown on NGM/OP50 plates, and 'control' refers to the RNAi vector control (L4440).

Strain	**Description**
N2	Bristol
ANA065	*adeIs1[pMD191, mex-5::spd-1::GFP]* II (gift from Marie Delattre)
ANA072	*adeIs1[pMD191, mex-5::spd-1::GFP]* II; *ltIs37[pAA64; pie-1::mCherry::his-58; unc-119(+)]* IV (gift from Marie Delattre)
EU716	*zen-4(or153)* IV (from the CGC). For experiments using *zen-4(or153)*, plates were shifted to 25^{o}C 16–18 hours before dissection and fixation.
EU1067	*unc-119(ed3) ruIs32[unc-119(+) pie-1::GFP::H2B]* III; *ruIs57[unc-119(+) pie-1::GFP::tubulin]* (gift from Bruce Bowerman)
OD56	*ltIs37 [(pAA64) pie-1::mCherry::his-58 + unc-119(+)]* IV
OD57	*unc-119(ed3)* III; *ltIs37[pAA64; pie-1::mCherry::his-58; unc-119(+)]* IV; *ltIs25[pAZ132; pie-1::GFP::tba-2; unc-119 (+)]* (gift from Arshad Desai)[78]
RB1593	*klp-15(ok1958)* I. *ok1958* is a deletion allele of the last 391 amino acids of KLP-15 (from the CGC)
SMW15	*klp-16(wig1)* I. This strain was generated using a CRISPR approach detailed below.
SMW16	*Pklp-16::klp-16::GFP (C1971->A–PAM site mutation)* I. This strain was generated using a CRISPR approach detailed below.
SMW18	(SMW16 x OD56) *Pklp-16::klp-16::GFP (C1971->A–PAM site mutation)* I; *ltIs37 [(pAA64) pie-1::mCherry::his-58 + unc-119(+)]* IV

Table 5.1. **Worm strains used in Chapter 2.**

Strain	Description
EU1067	*unc-119(ed3) ruIs32 [unc-119(+) pie-1::GFP::H2B]* III; *ruIs57 [unc-119(+) pie-1::GFP::tubulin]* (gift from Bruce Bowerman)
OD56	*ltIs37 [(pAA64) pie-1::mCherry::his-58 + unc-119(+)]* IV
OD57	*unc-119(ed3)* III; *ltIs37 [pAA64; pie-1::mCherry::his-58; unc-119(+)]* IV; *ltIs25 [pAZ132; pie-1::GFP::tba-2; unc-119 (+)]* (gift from Arshad Desai)
EU2876	*or1935[GFP::aspm-1]* I; *ltIs37 [pAA64; pie-1::mCherry::his-58; unc-119(+)]* IV
CA1199	*unc-119(ed3)*; *ieSi38 [Psun-1::TIR1::mRuby::sun-1 3'UTR, cb-unc-119(+)]* IV (gift from Abby Dernburg)
SMW21	CA1199 x OD56; *unc-119(ed3)*; *ieSi38 [Psun-1::TIR1::mRuby::sun-1 3'UTR, cb-unc-119(+)]* IV; *ltIs37 [(pAA64) pie-1::mCherry::his-58 + unc-119(+)]* IV
SMW24	*Pzyg-9::degron::EmGFP::zyg-9* II; *unc-119(ed3)*; *ieSi38 [Psun-1::TIR1::mRuby::sun-1 3'UTR, cb-unc-119(+)]* IV
SMW26	SMW24 x SMW21; *Pzyg-9::degron::EmGFP::zyg-9* II; *unc-119(ed3)*; *ieSi38 [Psun-1::TIR1::mRuby::sun-1 3'UTR, cb-unc-119(+)]* IV; *ltIs37 [(pAA64) pie-1::mCherry::his-58 + unc-119(+)]* IV

Table 5.2. **Worm strains used in Chapter 3.**

Generation of KLP-16::GFP strain

A CRISPR-based approach[22,23] was used to generate an endogenously tagged KLP-16::GFP strain (SMW16). Briefly, 27μM recombinant Alt-R *S. pyogenes* Cas9 protein (IDT) was co-injected with 13.6μM tracrRNA (IDT), 4μM *dpy-10* crRNA, 1.34μM *dpy-10* repair oligo, 9.6μM *klp-16* crRNA, and 136ng/μL ssDNA *klp-16* repair template into N2 worms, that were then allowed to produce progeny (See Table 5.3 for list of tracrRNA, crRNA, and primers used). Worms from plates containing rollers and dumpys were screened for GFP expression, and homozygous KLP-16::GFP worms were identified by PCR screening. To make the *klp-16* repair template, I generated a C-terminal LAP tag using a GBlock (IDT) and Gibson Assembly to create an S-TEV-GFP construct (pTM6). The tag was then amplified using PCR with primers that contained homology to the *klp-16* locus with the final product

containing 68 bp of homology upstream of the *klp-16* stop codon and 100 bp of homology downstream of the stop codon. ssDNA was generated by asymmetric PCR. SMW16 (KLP-16::GFP) was also crossed with OD56 (mCherry::histone) to generate SMW18: *Pklp-16::klp-16::GFP (C1971->A—PAM site mutation)* I; *ltIs37 [(pAA64) pie-1::mCherry::his-58 + unc-119(+)]* IV.

Name	**Sequence**
Alt-R CRISPR-Cas9 tracrRNA	Proprietary from IDT
dpy-10 crRNA	5'-GCUACCAUAGGCACCACGAG-3'
dpy-10 repair oligo (Ultramer from IDT)	5'-CACTTGAACTTCAATACGGCAAGATGAGAAT GACTGGAAACCGTACCGCATGCGGTGCCTATG GTAGCGGAGCTTCACATGGCTTCAGACCAACAG CCTAT-3'
klp-16 crRNA	5'-UGUCUAGUUCAUAGACAUCU-3'
klp-16 repair-F1	5'-GGACTCTCCTGGGTGACGTGTCACAGATGTCTAT GAACGGAGGTGGAGGTAAAGAAACCG-3'
klp-16 repair-R1	5'-GAAGTTATTTTACATGAAATGTTAAAATATAATTA AATGTCTATTTGTATAGTTCATCCATGCCATG-3'
klp-16 repair-F2	5'-GTACTCACATCGGATCGGCCGTGCAGCAACGGACT CTCCTGGG-3'
klp-16 repair-R2	5'-GATTTGCACAAGGCAATAAATATGAAGTTATTTT ACATGAAATGTTA-3'
klp-16 insertion check-F	5'-AGTACTCACATCGGATCGG-3'
klp-16 insertion check-R	5'-AAATAAATCAATTGACTCCTGAAAACAG-3'
pTM6	linker-S peptide-TEV-GFP plasmid template for PCR reactions to generate *klp-16* repair template. Derived from pEZ13.

Table 5.3. **Primer and CRISPR sequences for KLP-16::GFP strain (SMW16) generation.**

Generation of *klp-16(wig1)* strain (SMW15)

A CRISPR-based approach similar to the one above was used to generate a worm strain with a 600 bp deletion in the *klp-16* locus beginning 100 bp upstream of the start codon. Essentially the same approach was used as above; the differences being two crRNAs (4.8μM each) (one upstream and one downstream of the klp-16 start codon, respectively), and a ssDNA oligo (4μM) (Ultramer from IDT) were used in the injection mix (see Table 5.4 for list of reagents). The repair Ultramer sequence is homologous to the sequence just upstream and downstream to the two CRISPR cut sites thereby deleting the 600 base pairs. Worms from plates containing rollers and dumpys were screened by PCR and homozygous mutants were isolated.

crRNA upstream of start codon	5'-AGGCGGAGUUUAAGUUUGAG-3'
crRNA downstream of start codon	5'- CUCCUCAAGAAGCGUCACUU-3'
klp-16 KO Ultramer (IDT)	5'-CAGCCATCTCACGCTCCAATTGCGCATTTCTCTC CTCAAGAAGCGTCACTTCTCAAACTTAAACTCCGC CTCTGAAAATTCCCGCCAAATCGGATGGATTAC-3'

Table 5.4. **CRISPR sequences for *klp-16(wig1)* strain (SMW15) generation.**

Generation of degron::EmGFP::ZYG-9 strain

A CRISPR-based approach[22,23] was used to generate an endogenously tagged degron::EmGFP::ZYG-9 (SMW24). Briefly, 27μM recombinant Alt-R *S. pyogenes* Cas9 protein (IDT) was co-injected with 13.6μM tracrRNA (IDT), 4μM *dpy-10* crRNA, 1.34μM *dpy-10* repair oligo, 9.6μM *zyg-9* crRNA, and 136ng/μL ssDNA *zyg-9* repair template into CA1199 (*Psun-1::TIR1::mRuby*) worms, that were then allowed to produce progeny (See Table 5.5 for list of tracrRNA, crRNA, and primers used). Worms from plates containing rollers and dumpys were screened for degron::GFP insertions by PCR screening. To make the

zyg-9 repair template, we generated an N-terminal degron::EmGFP::linker (pADR28) using site directed mutagenesis and pLZ29 (gift from Abby Dernburg). The linker we inserted is from pIC26. The tag was then amplified using PCR with primers that contained homology to the *zyg-9* locus with the final product containing 57 bp of homology upstream of the *zyg-9* start codon and 61 bp of homology downstream of the start codon. ssDNA was generated by asymmetric PCR. SMW24 (degron::EmGFP::ZYG-9) was also crossed with SMW21 (mCherry::histone; TIR1::mRuby) to generate SMW26: *Pzyg-9-16::degron::EmGFP::ZYG-9 (C6->T—PAM site mutation)* II; *ieSi38 [Psun-1::TIR1::mRuby::sun-1 3'UTR, cb-unc-119(+)]* IV*ltIs37 [(pAA64) pie-1::mCherry::his-58 + unc-119(+)]* IV.

Name	**Sequence**
Alt-R CRISPR-Cas9 tracrRNA	Proprietary from IDT
dpy-10 crRNA	5'-GCUACCAUAGGCACCACGAG-3'
dpy-10 repair oligo (Ultramer from IDT)	5'-CACTTGAACTTCAATACGGCAAGATGAGAAT GACTGGAAACCGTACCGCATGCGGTGCCTATG GTAGCGGAGCTTCACATGGCTTCAGACCAACAG CCTAT-3'
zyg-9 crRNA	5'-CUCGUCCAGAUAAUCCCAAU-3'
zyg-9 repair-F1	5'-ACGTAGTAAACTGTCATTTTTCAGATAATGCCTAAA GATCCAGCCAAACC-3'
zyg-9 repair-R1	5'-CCACCTCGTCCAGATAATCCCAATTAGACATTCTAG AGCGGCCGCCA-3'
zyg-9 repair-F2	5'-TTCGTTCGCTTTCTTTGTTTATTGCAAGGCACGTA GTAAACTGTCATTTTTCAG-3'
zyg-9 repair-R2	5'-CGAAGTTCGGTGGAAGTTTGGGAAGGATATCCACC TCGTCCAGATAATC-3'
zyg-9 insertion check-F	5'-CGGAAATCTATTGTTGAAATCTCCTTTC-3'
zyg-9 insertion check-R	5'-CTTTCATTTTTTCGAAAATGACGGG-3'
pADR28	degron::EmGFP::linker plasmid template for PCR reactions to generate *zyg-9* repair template. Derived from pLZ29.

Table 5.5. **Primer and CRISPR sequences for degron::EmGFP::ZYG-9 strain (SMW24) generation.**

Generation of mMaple3::TBA-1 strain

A CRISPR-based approach[22,23] similar to the one described above was used to generate an endogenously tagged mMaple3::TBA-1 (SMW28) strain. Briefly, 27μM recombinant Alt-R *S. pyogenes* Cas9 protein (IDT) was co-injected with 13.6μM tracrRNA (IDT), 4μM *dpy-10* crRNA, 1.34μM *dpy-10* repair oligo, 9.6μM *zyg-9* crRNA, and 136ng/μL ssDNA *zyg-9* repair template into CA1199 (*Psun-1::TIR1::mRuby*) worms, that were then allowed

to produce progeny (See Table 5.6 for list of tracrRNA, crRNA, and primers used). Worms from plates containing rollers and dumpys were screened for mMaple3 insertions by PCR screening. To make the *tba-1* repair template, I used an mMaple3 construct (pSK52 - gift from the Dernburg Lab) that was codon optimized for *C. elegans* and contains introns to help expression. The tag was then amplified using PCR with primers that contained homology to the *tba-1* locus with the final product containing 66 bp of homology upstream of the *tba-1* start codon and 69 bp of homology downstream of the start codon. Silent mutations in the PAM site and proximal to the PAM site were introduced to prevent cutting of the repair template. ssDNA was generated by asymmetric PCR.

Name	**Sequence**
Alt-R CRISPR-Cas9 tracrRNA	Proprietary from IDT
dpy-10 crRNA	5'-GCUACCAUAGGCACCACGAG-3'
dpy-10 repair oligo (Ultramer from IDT)	5'-CACTTGAACTTCAATACGGCAAGATGAGAAT GACTGGAAACCGTACCGCATGCGGTGCCTATG GTAGCGGAGCTTCACATGGCTTCAGACCAACAG CCTAT-3'
tba-1 crRNA	5'-GUUCGUUUUCAACAUGCGUG-3'
tba-1 repair-F1	5'-CCGTTAATTTTCAGGTTCGTTTTCAACATGATCTC CAAGGGAGAGG-3'
tba-1 repair-R1	5'-GTCCGACGTGGATGGAGATGACTTCGCGCATAGAT CCTCCTCCTCCC-3'
tba-1 repair-F2	5'-GTTATCCGCGTTCATTTATGATTTCATTTCTTCTAA TTTCCGTTAATTTTCAGGTTCG-3'
tba-1 repair-R2	5'-GAGCTCCCAGCAAGCATTACCGATTTGGACTCCGG CTTGTCCGACGTGGATGG-3'
tba-1 AMP-F	5'-GTTATCCGCGTTCATTTATGATTTC-3'
tba-1 AMP-R	5'-GAGCTCCCAGCAAGC-3'
tba-1 insertion check-F	5'-CGCCATATGTTATCCGCG-3'
tba-1 insertion check-R	5'-CCTTGAAGACCACTGCAG-3'
pSK52	mMaple3 plasmid template for PCR reactions to generate *tba-1* repair template.

Table 5.6. **Primer and CRISPR sequences for mMaple3::TBA-1 strain (SMW28) generation.**

RNAi

From a feeding library[21,185], individual RNAi clones were picked and grown overnight at 37°C in LB with 100μg/ml ampicillin. Overnight cultures were spun down and plated on NGM (nematode growth media) plates containing 100μg/ml ampicillin and 1mM IPTG.

Plates were dried overnight. Worm strains were synchronized by bleaching gravid adults and letting the eggs hatch overnight without food. L1s were then plated on RNAi plates and grown to adulthood at 15°C for 5–6 days.

KLP-15/16 domain analysis

Protein domains were determined using PsiPred[186] and Paircoil2[153]. Protein sequences were analyzed using Clustal Omega[187]. Proline-rich regions of proteins have been shown to bind microtubules[140]. The proline content of amino acids 1–149 is 14% for KLP-15 and 13% for KLP-16.

Embryonic lethality

Young adult worms grown on control plates or plates containing RNAi-expressing bacteria were transferred to new plates containing either control or RNAi-expressing bacteria and allowed to lay eggs for 24 hours at 15°C before being moved to another fresh plate of either control or RNAi-expressing bacteria. The eggs were allowed to hatch for 24 hours and then the progeny (eggs and hatched worms) were counted. For each parent worm this process was repeated twice, resulting in three days of progeny being counted. For each condition, the progeny of at least 15 worms were scored.

Immunofluorescence and antibodies

Immunofluorescence was performed by dissecting worms into M9 or L-15 blastomere media (0.5 mg/mL Inulin from dahlia tubers (CAS Number 9005-80-5), 25 mM HEPES, pH 7.5, 60% Leibovitz's L-15 Media (Gibco 11415-049), 20% Heat-inactivated Fetal Bovine Serum), freeze cracking embryos, and plunging into -20°C methanol as described[24]. Embryos were fixed for 35–45 minutes, rehydrated in PBS, and blocked in AbDil (PBS plus 4% BSA, 0.1% Triton X-100, 0.02% Na-Azide) for 30 minutes. Primary antibodies were incubated overnight at 4^{o}C. The next day, embryos were washed 3x with PBST (PBS plus

0.1% Triton X-100), incubated in secondary antibody for 1 hour and 15 minutes, washed again as before, incubated in mouse anti-α-tubulin-FITC for 1.5 hours, washed again, and incubated in Hoechst (1:1000 in PBST) for 15 minutes. Embryos were then washed 2x with PBST, mounted in 0.5% p-phenylenediamine, 20mM Tris-Cl, pH 8.8, 90% glycerol, and sealed with nail polish; except for the overnight primary, the entire procedure was performed at room temperature. For experiments using the rabbit anti-KLP-16 antibody and staining of SPD-1::GFP (ANA065), KLP-16::GFP (SMW16), and GFP::ZYG-9 (SMW24) with mouse anti-GFP, embryos were blocked in AbDil overnight at 4^{o}C and incubated in primary antibody for 2 hours at room temperature. Primary antibodies used in this study: rabbit anti-ASPM-1 (1:5000, gift from Arshad Desai), rabbit anti-SEP-1 (1:400; gift from Andy Golden), rabbit anti-KLP-18 (1:10,000, gift from O. Bossinger), rabbit anti-ZEN-4 (1:500; gift from Michael Glotzer), mouse anti-SUMO (1:500; gift from Federico Pelisch), mouse anti-GFP (1:200; Invitrogen). Rat anti-AIR-2 was generated by Covance using the C-terminal peptide sequence N-KIRAEKQQKIEKEASLRNH-C (synthesized by the Peptide Synthesis Core Facility at Northwestern University), then affinity purified and used at 1:1000. Rabbit anti-KLP-16 was generated by Covance using the N-terminal peptide sequence N-CMNVARRRSGLFRSTIGAPPK-C (synthesized by the Peptide Synthesis Core Facility at Northwestern University), then affinity purified and used at 1:2000. Rabbit anti-SPD-1 was generated by Proteintech using the C-terminal peptide sequence N-CIASSTPSSAKKVLTRRNQFL-C, then affinity purified and used at 1:1000. Directly conjugated mouse anti-α-tubulin-FITC (DM1α, Sigma) and Alexa-fluor directly conjugated secondary antibodies (Invitrogen) were used at 1:500. All antibodies were diluted in AbDil.

Microscopy

All fixed imaging and high resolution imaging of KLP-16::GFP (SMW16), KLP-16::GFP; mCherry::histone (SMW18), and GFP::tubulin; mCherry::histone (OD57) was performed on a DeltaVision Core deconvolution microscope with a 100x objective (NA = 1.4) (Applied Precision). This microscope is housed in the Northwestern University Biological Imaging Facility supported by the NU Office for Research. Image stacks were obtained at 0.2μm z-steps and deconvolved using SoftWoRx (Applied Precision). All images in this study were deconvolved and displayed as full maximum intensity projections of data stacks encompassing the entire spindle structure, unless stated otherwise. For live KLP-16::GFP and KLP-16::GFP; mCherry::histone imaging, live worms were mounted in anesthetic (0.2% tricaine, 0.02% levamisole in M9). For *ex utero* live imaging of GFP::tubulin; mCherry::histone, oocytes were dissected into a drop of L-15 blastomere media (0.5 mg/mL Inulin from dahlia tubers (CAS Number 9005-80-5), 25 mM HEPES, pH 7.5, 60% Leibovitz's L-15 Media (Gibco 11415-049), 20% Heat-inactivated Fetal Bovine Serum) and mounted in a home-made slide mount[188].

Cold stable assays

N2 worms were picked into a drop of either 15^{o}C (control) or ice cold (cold treatment) L-15 blastomere media[188] on Poly-L-lysine slides and then cut to release oocytes. Slides were then incubated at either 15^{o}C (control) in a humidity chamber or directly on ice (cold treatment) for 10 minutes. Slides were then prepared as described above for immunofluorescence.

Time-lapse imaging

Two-color live imaging was performed using a spinning disk confocal microscope with a 63x HC PL APO 1.40 NA objective lens. A spinning disk confocal unit (CSU-X1; Yokogawa Electric Corporation) attached to an inverted microscope (Leica DMI6000 SD) and a Spectral Applied Imaging laser merge ILE3030 and a back-thinned electron-multiplying

charge-coupled device (EMCCD) camera (Photometrics Evolve 521 Delta) were used for image acquisition. The microscope and attached devices were controlled using Metamorph Image Series Environment software (Molecular Devices). For the acquisitions in Chapter 2, typically, ten to twelve z-stacks at 1μm increments were taken every 20–45 seconds at room temperature. Image deconvolution was done using AutoQuant X3 (Media Cybernetics Inc.). For the acquisitions in Chapter 3, 7 z-stacks at 2μm increments were taken every 30 seconds at room temperature. Images were processed using ImageJ. Images are shown as maximum intensity projections of entire spindle structure. For time-lapse imaging in Chapter 2, live, intact worms were mounted on 3-5% agarose, M9 pads in 50% live imaging solution (modified S-basal [50mM KH2PO4,10mM K-citrate, 0.1M NaCl, 0.025mg/ml cholesterol, 3mM MgSO4, 3mM CaCl2, 40mM serotonin creatinine sulfate monohydrate]), 50% 0.1 micron polystyrene Microspheres (Polysciences Inc.), and covered with a coverslip. For time-lapse imaging in Chapter 3, live, intact worms were mounted on a homemade slide holder on 4% agarose in M9 pads that were made on Bob Dylan's "A Shot of Love" vinyl, LP (CBS) to make grooves for immobilizing worms. The worms were picked into a drop of M9, 20μM serotonin creatinine sulfate monohydrate (Sigma), 2% tricaine, and 0.4% tetramisole and covered with a coverslip. The spinning disk microscope is housed in the Northwestern University Biological Imaging Facility supported by the NU Office for Research.

For Movie 2-6, EU1067 worms were picked into a solution of tricaine (2%) and tetramisole (0.4%), and incubated for 30 min. Worms were then pipetted onto a 3% agarose pad, covered with a coverslip, and imaged immediately on a DeltaVision Core deconvolution microscope (same as above). Image stacks were obtained at 1μm z-steps at 10 second intervals using 2x2 binning, and then deconvolved. Video images are full projections of data stacks.

FRAP

FRAP experiments were performed on the same spinning disk confocal microscope mentioned above using a 63x HC PL APO 1.40 NA oil immersion objective. Photo-bleaching was performed with a 405 nm laser (5.5 mW-11.0 mW output). Poles were bleached for and images were taken at 5-10 s intervals. Analysis of the recovery curves and the half-time recovery were carried out with the FIJI to obtain raw fluorescence data and the curves we fit using Equation 5.1 and a custom Python script (https://github.com/justinfinkle/mullen-frap). For all FRAP acquisitions except ASPM-1 meiotic spindles, oocytes and embryos were mounted as previously described[188]. Briefly, oocytes and embryos were dissected into a drop of L-15 blastomere media (0.5 mg/mL Inulin from dahlia tubers (CAS Number 9005-80-5), 25 mM HEPES, pH 7.5, 60% Leibovitz's L-15 Media (Gibco 11415-049), 20% Heat-inactivated Fetal Bovine Serum) and mounted in a home-made slide mount. Bleaching of the mitotic centrosomes was done in the EMS cell in the 4-cell stage embryo, and MI and MII meiotic spindles were bleached for the acentriolar spindle pole FRAP experiments. For ASPM-1 meiotic spindle FRAP experiments live, intact worms were mounted on 3-5% agarose, M9 pads in 50% live imaging solution (modified S-basal [50mM KH2PO4,10mM K-citrate, 0.1M NaCl, 0.025mg/ml cholesterol, 3mM MgSO4, 3mM CaCl2, 40mM serotonin creatinine sulfate monohydrate]), 50% 0.1 micron polystyrene Microspheres (Polysciences Inc.), and covered with a coverslip.

$$f(t) = A(1 - e^{-\tau t}) \tag{5.1}$$

Auxin Treatment

For overnight auxin treatment, worms were transferred onto NGM plates containing 1mM auxin (indol-3-acetic acid, Alfa Aesar) seeded with OP-50, and processed for immunofluorescence as described above.

For short auxin treatment, worms were picked into a drop of L-15 blastomere media (0.5 mg/mL Inulin from dahlia tubers (CAS Number 9005-80-5), 25 mM HEPES, pH 7.5, 60% Leibovitz's L-15 Media (Gibco 11415-049), 20% Heat-inactivated Fetal Bovine Serum) with 1mM auxin (indol-3-acetic acid, Alfa Aesar) and incubated for 25-30 minutes in a humidity chamber before dissection and freeze cracked. For vehicle treatment, 0.25% ethanol in L-15 blastomere media was used. The rest of the protocol is the same as the immunofluorescence procedure described above.

Western blotting

Seventy-five EU1067, RB1593, or SMW15 worms were picked off of control, *klp-16(RNAi)* (EU1067 and SMW15), or *klp-15(RNAi)* (RB1593) plates onto new, empty (no bacteria) plates. The worms were washed off the plates with cold M9 and transferred to a 1.5ml microcentrifuge tube. Worms were pelleted by spinning at 2000 rpm for 1 minute, and the tube was put on ice for 2 minutes to allow worms to slow down and form a tight pellet. The M9 was removed and the tube was filled with fresh, cold M9 and mixed. The worms were washed a total of 3 times. After the final wash, as much M9 was removed as possible and 2X SDS sample buffer was added to the remaining worm/M9 mixture and boiled for 10 minutes. Samples were run on a 10% SDS-PAGE gel and blotted. For western analysis, rabbit anti-KLP-16 antibody (1:10,000) and mouse anti-tubulin (1:5000) (Sigma, DM1α) were used.

Quantification of *zyg-9(RNAi)* phenotypes in live worms

Live, intact worms expressing GFP::tubulin, GFP::histone (EU1067) fed either wild-type or *zyg-9(RNAi)*-expressing bacteria were anesthetized in 0.2% tricaine, 0.02% levamisole in M9 and viewed on a Leica DM5500B widefield fluorescence microscope. Spindles in embryos in the -1, spermatheca, and +1 positions within the gonad were scored for microtubule organization by eye. A spindle was scored as: "cage" if microtubule bundles could be clearly seen after the haze of histone::GFP in the nucleus had disappeared, which indicates that the nuclear envelope had broken down; "multipolar" if it had prominent microtubule bundles that formed more than two organized poles; "collapsed" if the microtubule structure had collapsed around the chromosomes and lacked prominent bundles and organized poles; "bipolar" if there were two organized spindle poles; "monopolar" if there was a radially array of microtubules emanating from a single point; "anaphase" if there were two or more sets of segregated chromosomes.

Line scans of ZYG-9 localization in live oocytes

Oocytes were imaged using the same set-up as described for the FRAP analysis. A 10 pixel wide x 12 μm line profile analysis was performed on max projected images of 12 different metaphase spindles after background subtraction.

Spindle length and chromosome segregation distance measurements

Imaris 3D Imaging Software (Bitplane) was used for spindle length measurements. To calculate spindle length, the "Surfaces" tool was first used to determine the volume of each pole stained with ASPM-1 and then to assign the center of the volume for each pole. The distance between these two center points was then measured as the spindle length. To calculate chromosome segregation distance, the "Surfaces" tool was first used to determine the volume of each segregated chromosome mass, stained with Hoechst, and then to assign the

center of the volume for each mass. The distance between these two center points was then measured as the chromosome segregation distance.

Statistical methods

For spindle length measurements, the mean spindle lengths for auxin treatment were compared with the control spindle widths using a two-tailed t test, resulting in a p-value of <0.001. Data distribution was assumed to be normal, but this was not formally tested.

Image analysis and quantification

Fig. 2.1D: Slides made on the same day were imaged within an 8 hour window on a DeltaVision Core deconvolution microscope (see Microscopy section) using the same exposure conditions and times for all slides. In ImageJ, linescans of 154 x 75 pixels (L x W) were performed on 6 z-slice sum projections of representative spindles from control (n = 8) and *klp-15/16(RNAi)* (n = 9) embryos. In control spindles, the linescans were done along the pole-to-pole axis. In spindles from *klp-15/16(RNAi)* embryos, linescans were done straight along the x-axis of the image, since these spindles lack a discernible orientation. The average fluorescence intensity for each channel was graphed (solid line) along with the SEM (standard error of the mean) (shaded area) using the ggplot package in R Studio. The y-axes of the graphs are the same between control and experiment for a given channel.

Fig. 2.6B: anti-KLP-16 staining for each stage of spindle assembly in wild-type oocytes/ embryos. Oocytes in prophase with the nuclear envelope intact were scored as "localized" if the KLP-15/16 signal was primarily cytoplasmic. During all other stages, oocytes were scored as "localized" if the KLP-15/16 signal was colocalized with spindle microtubules. The quantification is as follows: diakinesis 81.8% (n = 22), cage 0% (n = 13), multipolar 31.3% (n = 67), bipolar 64% (n = 114), anaphase 51.9% (n = 79), mitotic spindles 3.7% (n = 27). Although not every spindle is stained, I think that this represents variability with

the immunofluorescence procedure and with the antibody (since I see 100% localization of KLP-16::GFP to oocyte spindle microtubules and to mitotic spindles; see Fig. 2.7A).

Fig. 2.6C: anti-KLP-16 staining was scored in *klp-15/16(RNAi)* oocytes. The number of oocytes in which I could discern any spindle staining is as follows: microtubule ball stage 8% (n = 75), anaphase 2.9% (n = 35). anti-KLP-16 staining was scored in *klp-15(ok1958)* oocytes. Oocytes in prophase with the nuclear envelope intact were scored as "localized" if the KLP-15/16 signal was primarily cytoplasmic. During all other stages, oocytes were scored as "localized" if the KLP-15/16 signal was colocalized with spindle microtubules. The quantification is as follows: diakinesis 100% (n = 3), cage 14% (n = 7), multipolar 44% (n = 25), bipolar 72.2% (n = 18), anaphase 38% (n = 21). anti-KLP-16 staining was scored in *klp-16(wig1)* oocytes as above. The quantification is as follows: diakinesis 100% (n = 10), cage 42.9% (n = 7), multipolar 89% (n = 19), bipolar 81.8% (n = 11), anaphase 79.2% (n = 24). As with the control strain (see Fig. 2.6B quantification above), I think that the incomplete staining I observe is due to variability with the procedure and antibody.

Fig. 2.4B: Live, intact worms expressing GFP::tubulin, GFP::histone (EU1067) fed either control or *klp-16(RNAi)*-expressing bacteria were anesthetized in 0.2% tricaine, 0.02% levamisole in M9 and viewed on a Leica DM5500B widefield fluorescence microscope. Spindles in embryos in the -1, spermatheca, and +1 positions within the gonad were scored for microtubule organization by eye. A spindle was scored as "multipolar" if it had prominent microtubule bundles that formed more than two organized poles. A spindle was scored as an "array" if the microtubule structure lacked prominent bundles and organized poles. A spindle was scored as "MT ball" if the microtubule structure had collapsed around the chromosomes and lacked prominent bundles and organized poles.

Fig. 2.5B: Spindle volumes were measured using the surfaces tool in Imaris (Bitplane). Using the full 3D image stack, this tool renders a 3D surface based on fluorescence signal (for my analysis, I used the tubulin signal). The volume of this 3D surface is then measured. The volumes of metaphase and early anaphase spindles (staged by SEP-1/AIR-2 localization) from *klp-15/16(RNAi)* oocytes were measured and compared to the volumes of the spindles used for the linescan measurements in Fig. 2.1D. This analysis allowed me to conclude that the spindles used in my linescans for Fig. 2.1D are within the range of metaphase spindles based on spindle volume.

Fig, 2.7A: Live, intact worms expressing KLP-16::GFP, mCherry::histone (SMW18) were anesthetized in 0.2% tricaine, 0.02% levamisole in M9 and viewed on a Leica DM5500B wide-field fluorescence microscope. The localization of KLP-16::GFP was scored in oocytes/embryos in the -1, spermatheca, and +1 positions within the gonad. KLP-16::GFP signal was scored as cytoplasmic if it was absent/reduced in the nucleus. Because the localization of KLP-16::GFP on the spindle looks identical to the organization of GFP::tubulin, I scored localization for the following categories: cage, multipolar, bipolar, and anaphase. The organization of the chromosomes visualized by mCherry::histone was used to identify and better stage the spindles.

2.7D, E: anti-GFP staining for each stage of spindle assembly in SMW16 (KLP-16::GFP). Oocytes in prophase with the nuclear envelope intact were scored as "localized" if the anti-GFP signal was primarily cytoplasmic. During all other stages, oocytes were scored as "localized" if the anti-GFP signal was colocalized with spindle microtubules. The quantification is as follows: diakinesis 100% (n = 2), cage 0% (n = 4), multipolar 76.5% (n = 17), bipolar 96.2% (n = 26), anaphase 83.3% (n = 24), mitotic spindles 100% (n = 5). As with

the KLP-15/16 antibody, I think that the lack of staining in all embryos represents variability with the immunofluorescence procedure, since I see robust localization of KLP-16::GFP to microtubules when I visualize this strain live.

Fig. 2.8B: Linescans of control anaphase spindles and anaphase spindles from *klp-15/16 (RNAi)* oocytes stained for ASPM-1 were performed using the arbitrary profile tool in SoftWoRx (Applied Precision). A spindle was scored as having staining at poles if the ASPM-1 signal was enriched at two ends of the spindle near the segregating chromosomes. ASPM-1 was enriched at the poles of 21/24 control spindles, but was largely diffuse along spindle microtubules in anaphase of *klp-15/16(RNAi)* oocytes (only 9/26 spindles could be classified as having any type of ASPM-1 enrichment, and this enrichment was not as strong as in the control spindles).

Fig. 2.8C: Linescans of control anaphase spindles and anaphase spindles from *klp-15/16 (RNAi)* oocytes stained for KLP-18 were performed using the arbitrary profile tool in SoftWoRx (Applied Precision). A spindle was scored as having staining at poles if the KLP-18 signal was enriched at two ends of the spindle near the segregating chromosomes. KLP-18 was enriched at poles in 11/12 control spindles but was diffuse in *klp-15/16(RNAi)* spindles (0/6 had KLP-18 concentrated into poles).

Fig. 2.8D: Aneuploidy in MII embryos was quantified by counting the number of chromosomes in MII in immunofluorescence images of control and *klp-15/16(RNAi)* embryos. An embryo was scored as 'aneuploid' if the number of chromosomes was not 6.

Fig. 2.9A and 2.9B: ZEN-4 and SPD-1 staining was scored in control spindles and spindles from *klp-15/16(RNAi)* oocytes. Staining of metaphase and anaphase spindles (staged by AIR-2 localization) was scored for each condition. ZEN-4: Control metaphase 1.6% (n

= 63), Control anaphase 90% (n = 20); *klp-15/16(RNAi)* metaphase 2.9% (n = 134), *klp-15/16(RNAi)* anaphase 80.3% (n = 66). SPD-1: Control metaphase 9.5% (n = 42), Control anaphase 97% (n = 66); *klp-15/16(RNAi)* metaphase 1% (n = 100), *klp-15/16(RNAi)* anaphase 88.2% (n = 85).

Fig. 2.10A and 2.10B: Quantification of microtubule bundling and chromosome segregation was done using immunofluorescence images of anaphase spindles with SEP-1 gone and AIR-2 relocalized to the microtubules (mid/late anaphase) for the conditions shown. I scored microtubule bundling by eye, looking through the entire z-stack in SoftWoRx (Applied Precision). An anaphase spindle was scored as "bundled" if one or more microtubule bundles were discernible. Chromosomes were scored as "segregated" if two or more distinct masses of chromosomes were observed. The simple matching coefficient (SMC) for microtubule bundling and chromosome segregation = 0.82 (n = 251); in other words, 82% of the spindles were scored as microtubules bundled and chromosomes segregated or as no microtubule bundles and no chromosome segregation.

Fig. 2.10C: To approximate anaphase microtubule lengths, I used the measure distances tool in SoftWoRx (Applied Precision). Using this tool, a line was manually drawn (point by point) along the most prominent spindle microtubule bundle through the 3D stack of an image to measure its full length.

Fig. 2.11A and 2.11B: Polar body number and maternal pronuclei number were quantified by scoring live EU1067 worms mounted in anesthetic (0.2% tricaine, 0.02% levamisole in M9) on a Leica DM5500B fluorescent microscope.

Fig. 2.13A: Linescans of control anaphase spindles and anaphase spindles from *klp-15/16(RNAi)* oocytes stained for tubulin, SUMO, and SPD-1 were performed using the arbitrary profile tool in SoftWoRx (Applied Precision). A spindle was scored as having

oscillations if one or more instances of alternating MTs/SUMO and SUMO/SPD-1 signal was observed. This analysis was done by examining both single z-slices and max projections of spindles. Oscillations were observed in 9/11 control anaphase spindles and 12/18 *klp-15/16(RNAi)* anaphase spindles.

Fig. 2.13C: Lateral microtubule associations to chromosomes were scored in control anaphase spindles and anaphase spindles from *klp-15/16(RNAi)* oocytes. A spindle was scored as having lateral microtubule/chromosome associations if a microtubule appeared to contact and run along the side of a chromosome. This analysis was done by examining both single z-slices and max projections of spindles. I observed clear lateral associations in 31/35 control anaphase spindles and in 22/31 *klp-15/16(RNAi)* anaphase spindles.

References

1. Skibbens, R. V. Chapter 5 Mechanisms of sister chromatid pairing. vol. 269 of *International Review of Cell and Molecular Biology*, 283–339 (Academic Press, 2008).

2. Flemming, W. CONTRIBUTIONS TO THE KNOWLEDGE OF THE CELL AND ITS VITAL PROCESSES. *The Journal of Cell Biology* **25**, 3–69 (1965).

3. Allen, C. & Borisy, G. G. Structural polarity and directional growth of microtubules of *Chlamydomonas* flagella. *Journal of Molecular Biology* **90**, 381–402 (1974).

4. Mitchison, T. & Kirschner, M. Dynamic instability of microtubule growth. *Nature* **312**, 237–242 (1984).

5. Goodson, H. V. & Jonasson, E. M. Microtubules and microtubule-associated proteins. *Cold Spring Harbor Perspectives in Biology* **10** (2018).

6. Oriola, D., Needleman, D. J. & Brugués, J. The physics of the metaphase spindle. *Annual Review of Biophysics* **47**, 655–673 (2018).

7. Gordon, D. J., Resio, B. & Pellman, D. Causes and consequences of aneuploidy in cancer. *Nature Reviews Genetics* **13**, 189–203 (2012).

8. MacLennan, M., Crichton, J. H., Playfoot, C. J. & Adams, I. R. Oocyte development, meiosis and aneuploidy. *Seminars in Cell & Developmental Biology* **45**, 68–76 (2015).

9. Marston, A. L. & Amon, A. Meiosis: cell-cycle controls shuffle and deal. *Nature Reviews Molecular Cell Biology* **6**, 818–818 (2005).

10. Szollosi, D., Calarco, P. & Donahue, R. P. Absence of centrioles in the first and second meiotic spindles of mouse oocytes. *Journal of Cell Science* **11**, 521–541 (1972).

11. Tsou, M.-F. B. & Stearns, T. Mechanism limiting centrosome duplication to once per cell cycle. *Nature* **442**, 947–951 (2006).

12. Washitani-Nemoto, S., Saitoh, C. & Nemoto, S. Artificial parthenogenesis in starfish eggs: behavior of nuclei and chromosomes resulting in tetraploidy of parthenogenotes produced by the suppression of polar body extrusion. *Developmental Biology* **163**, 293–301 (1994).

13. Munro, E. & Bowerman, B. Cellular symmetry breaking during *Caenorhabditis elegans* development. *Cold Spring Harbor Perspectives in Biology* **1** (2009).

14. Nagaoka, S. I., Hassold, T. J. & Hunt, P. A. Human aneuploidy: mechanisms and new insights into an age-old problem. *Nature Reviews Genetics* **13**, 493–504 (2012).

15. Hassold, T. & Hunt, P. To err (meiotically) is human: the genesis of human aneuploidy. *Nature Reviews Genetics* **2**, 280–291 (2001).

16. Holubcova, Z., Blayney, M., Elder, K. & Schuh, M. Error-prone chromosome-mediated spindle assembly favors chromosome segregation defects in human oocytes. *Science* **348**, 1143–1147 (2015).

17. Crittenden, S. L., Leonhard, K. A., Byrd, D. T., Kimble, J. & Schwarzbauer, J. Cellular analyses of the mitotic region in the *Caenorhabditis elegans* adult germ line. *Molecular Biology of the Cell* **17**, 3051–3061 (2006).

18. Dernburg, A. F., Zalevsky, J., Colaiacovo, M. P. & Villeneuve, A. M. Transgene-mediated cosuppression in the *C. elegans* germ line. *Genes & Development* **14**, 1578–1583 (2000).

19. McCarter, J., Bartlett, B., Dang, T. & Schedl, T. On the control of oocyte meiotic maturation and ovulation in *Caenorhabditis elegans*. *Developmental Biology* **205**, 111–128 (1999).

20. Timmons, L. & Fire, A. Specific interference by ingested dsRNA. *Nature* **395**, 854–854 (1998).

21. Fraser, A. G. *et al.* Functional genomic analysis of *C. elegans* chromosome I by systematic RNA interference. *Nature* **408**, 325–330 (2000).

22. Paix, A., Folkmann, A., Rasoloson, D. & Seydoux, G. High efficiency, homology-directed genome editing in *Caenorhabditis elegans* using CRISPR-Cas9 ribonucleoprotein complexes. *Genetics* **201**, 47–54 (2015).

23. Arribere, J. A. *et al.* Efficient marker-free recovery of custom genetic modifications with CRISPR/Cas9 in *Caenorhabditis elegans*. *Genetics* **198**, 837–846 (2014).

24. Gönczy, P., Pichler, S., Kirkham, M. & Hyman, A. A. Cytoplasmic dynein is required for distinct aspects of MTOC positioning, including centrosome separation, in the one cell stage *Caenorhabditis elegans* embryo. *The Journal of Cell Biology* **147**, 135–150 (1999).

25. Cross, R. A. & Mcainsh, A. Prime movers: the mechanochemistry of mitotic kinesins. *Nature Reviews Molecular Cell Biology* **15**, 257–271 (2014).

26. Roberts, A. J., Kon, T., Knight, P. J., Sutoh, K. & Burgess, S. A. Functions and mechanics of dynein motor proteins. *Nature Reviews Molecular Cell Biology* **14**, 713–726 (2013).

27. Verhey, K. J. & Hammond, J. W. Traffic control: regulation of kinesin motors. *Nature Reviews Molecular Cell Biology* **10**, 765–777 (2009).

28. Kashlna, A. S. *et al.* A bipolar kinesin. *Nature* **379**, 270–272 (1996).

29. Sawin, K. E., Leguellec, K., Philippe, M. & Mitchison, T. J. Mitotic spindle organization by a plus-end-directed microtubule motor. *Nature* **359**, 540–543 (1992).

30. Kapitein, L. C. *et al.* The bipolar mitotic kinesin Eg5 moves on both microtubules that it crosslinks. *Nature* **435**, 114–118 (2005).

31. Tanenbaum, M. E. *et al.* Kif15 cooperates with Eg5 to promote bipolar spindle assembly. *Current Biology* **19**, 1703–1711 (2009).

32. Sturgill, E. & Ohi, R. Kinesin-12 differentially affects spindle assembly depending on its microtubule substrate. *Current Biology* **23**, 1280–1290 (2013).

33. Drechsler, H., McHugh, T., Singleton, M. R., Carter, N. J. & McAinsh, A. D. The kinesin-12 Kif15 is a processive track-switching tetramer. *eLife* **3**, e01724 (2014).

34. Sturgill, E. *et al.* Kinesin-12 Kif15 targets kinetochore fibers through an intrinsic two-step mechanism. *Current Biology* **24**, 2307 – 2313 (2014).

35. Drechsler, H. & McAinsh, A. D. Kinesin-12 motors cooperate to suppress microtubule catastrophes and drive the formation of parallel microtubule bundles. *Proceedings of the National Academy of Sciences* **113**, E1635–E1644 (2016).

36. Mann, B. J., Balchand, S. K., Wadsworth, P. & Zheng, Y. Regulation of Kif15 localization and motility by the C-terminus of TPX2 and microtubule dynamics. *Molecular Biology of the Cell* **28**, 65–75 (2017).

37. Wignall, S. M. & Villeneuve, A. M. Lateral microtubule bundles promote chromosome alignment during acentrosomal oocyte meiosis. *Nature Cell Biology* **11**, 839–844 (2009).

38. Subramanian, R., Ti, S.-C., Tan, L., Darst, S. & Kapoor, T. Marking and measuring single microtubules by PRC1 and kinesin-4. *Cell* **154**, 377–390 (2013).

39. Wickstead, B. & Gull, K. A "holistic" kinesin phylogeny reveals new kinesin families and predicts protein functions. *Molecular Biology of the Cell* **17**, 1734–1743 (2006).

40. Walczak, C. E., Vernos, I., Mitchison, T. J., Karsenti, E. & Heald, R. A model for the proposed roles of different microtubule-based motor proteins in establishing spindle

bipolarity. *Current Biology* **8**, 903–913 (1998).

41. Fink, G. *et al.* The mitotic kinesin-14 Ncd drives directional microtubule–microtubule sliding. *Nature Cell Biology* **11**, 717–723 (2009).

42. Matthies, H. J., McDonald, H. B., Goldstein, L. S. & Theurkauf, W. E. Anastral meiotic spindle morphogenesis: role of the non-claret disjunctional kinesin-like protein. *The Journal of Cell Biology* **134**, 455–464 (1996).

43. Mountain, V. *et al.* The kinesin-related protein, HSET, opposes the activity of Eg5 and cross-links microtubules in the mammalian mitotic spindle. *The Journal of Cell Biology* **147**, 351–366 (1999).

44. Mishima, M., Kaitna, S. & Glotzer, M. Central spindle assembly and cytokinesis require a kinesin-like protein/RhoGAP complex with microtubule bundling activity. *Developmental Cell* **2**, 41–54 (2002).

45. Ogawa, T., Nitta, R., Okada, Y. & Hirokawa, N. A common mechanism for microtubule destabilizers—M type kinesins stabilize curling of the protofilament using the class-specific neck and loops. *Cell* **116**, 591–602 (2004).

46. Hunter, A. W. *et al.* The kinesin-related protein MCAK is a microtubule depolymerase that forms an ATP-hydrolyzing complex at microtubule ends. *Molecular Cell* **11**, 445–457 (2003).

47. Kline-Smith, S. L., Khodjakov, A., Hergert, P. & Walczak, C. E. Depletion of centromeric MCAK leads to chromosome congression and segregation defects due to improper kinetochore attachments. *Molecular Biology of the Cell* **15**, 1146–1159 (2004).

48. Billington, N. & Sellers, J. R. Dynein struts its stuff. *Nature Structural & Molecular Biology* **18**, 635–636 (2011).

49. Heald, R. *et al.* Self-organization of microtubules into bipolar spindles around artificial chromosomes in *Xenopus* egg extracts. *Nature* **382**, 420–425 (1996).

50. Srayko, M., Quintin, S., Schwager, A. & Hyman, A. A. *Caenorhabditis elegans* TAC-1 and ZYG-9 form a complex that is essential for long astral and spindle microtubules. *Current Biology* **13**, 1506–1511 (2003).

51. Srayko, M., Otoole, E. T., Hyman, A. A. & Müller-Reichert, T. Katanin disrupts the microtubule lattice and increases polymer number in *C. elegans* meiosis. *Current Biology* **16**, 1944–1949 (2006).

52. Jiang, K. *et al.* Microtubule minus-end regulation at spindle poles by an ASPM–katanin complex. *Nature Cell Biology* **19**, 480–492 (2017).

53. Connolly, A. A. *et al.* *Caenorhabditis elegans* oocyte meiotic spindle pole assembly requires microtubule severing and the calponin homology domain protein ASPM-1. *Molecular Biology of the Cell* **25**, 1298–1311 (2014).

54. Ito, A. & Goshima, G. Microcephaly protein Asp focuses the minus ends of spindle microtubules at the pole and within the spindle. *The Journal of Cell Biology* **211**, 999–1009 (2015).

55. Subramanian, R. *et al.* Insights into antiparallel microtubule crosslinking by PRC1, a conserved nonmotor microtubule binding protein. *Cell* **142**, 433–443 (2010).

56. Verbrugghe, K. J. & White, J. G. SPD-1 is required for the formation of the spindle midzone but is not essential for the completion of cytokinesis in *C. elegans* embryos. *Current Biology* **14**, 1755–1760 (2004).

57. Petry, S. Mechanisms of mitotic spindle assembly. *Annual Review of Biochemistry* **85**, 659–683 (2016).

58. Bornens, M. Centrosome composition and microtubule anchoring mechanisms. *Current Opinion in Cell Biology* **14**, 25–34 (2002).

59. Zheng, Y., Wong, M. L., Alberts, B. & Mitchison, T. Nucleation of microtubule assembly by a γ-tubulin-containing ring complex. *Nature* **378**, 578–583 (1995).

60. Strome, S. *et al.* Spindle dynamics and the role of γ-tubulin in early *Caenorhabditis elegans* embryos. *Molecular Biology of the Cell* **12**, 1751–1764 (2001).

61. Hannak, E. *et al.* The kinetically dominant assembly pathway for centrosomal asters in *Caenorhabditis elegans* is γ-tubulin dependent. *The Journal of Cell Biology* **157**, 591–602 (2002).

62. Mayer, T. U. *et al.* Small molecule inhibitor of mitotic spindle bipolarity identified in a phenotype-based screen. *Science* **286**, 971–974 (1999).

63. Burbank, K. S., Mitchison, T. J. & Fisher, D. S. Slide-and-cluster models for spindle assembly. *Current Biology* **17**, 1373–1383 (2007).

64. Nahaboo, W., Zouak, M., Askjaer, P., Delattre, M. & Zheng, Y. Chromatids segregate without centrosomes during *Caenorhabditis elegans* mitosis in a Ran- and CLASP-dependent manner. *Molecular Biology of the Cell* **26**, 2020–2029 (2015).

65. Bishop, J. D., Han, Z. & Schumacher, J. M. The *Caenorhabditis elegans* Aurora B kinase AIR-2 phosphorylates and is required for the localization of a BimC kinesin to meiotic and mitotic spindles. *Molecular Biology of the Cell* **16**, 742–756 (2005).

66. Rieder, C. L. & Alexander, S. P. Kinetochores are transported poleward along a single astral microtubule during chromosome attachment to the spindle in newt lung cells. *The Journal of Cell Biology* **110**, 81–95 (1990).

67. Rieder, C. L. Kinetochore fiber formation in animal somatic cells: dueling mechanisms come to a draw. *Chromosoma* **114**, 310–318 (2005).

68. Cheerambathur, D. K. & Desai, A. Linked in: formation and regulation of microtubule attachments during chromosome segregation. *Current Opinion in Cell Biology* **26**, 113–122 (2014). Cell architecture.

69. Musacchio, A. The molecular biology of spindle assembly checkpoint signaling dynamics. *Current Biology* **25**, R1002–R1018 (2015).

70. Ganem, N. J., Upton, K. & Compton, D. A. Efficient mitosis in human cells lacking poleward microtubule flux. *Current Biology* **15**, 1827–1832 (2005).

71. Oegema, K., Desai, A., Rybina, S., Kirkham, M. & Hyman, A. A. Functional analysis of kinetochore assembly in *Caenorhabditis elegans*. *The Journal of Cell Biology* **153**, 1209–1226 (2001).

72. Mollinari, C. *et al.* Ablation of PRC1 by small interfering RNA demonstrates that cytokinetic abscission requires a central spindle bundle in mammalian cells, whereas completion of furrowing does not. *Molecular Biology of the Cell* **16**, 1043–1055 (2005).

73. Maton, G. *et al.* Kinetochore components are required for central spindle assembly. *Nature Cell Biology* **17**, 697–705 (2015).

74. Nguyen-Ngoc, T., Afshar, K. & Gönczy, P. Coupling of cortical dynein and Gα proteins mediates spindle positioning in *Caenorhabditis elegans*. *Nature Cell Biology* **9**, 1294–1302 (2007).

75. Monen, J., Maddox, P. S., Hyndman, F., Oegema, K. & Desai, A. Differential role of CENP-A in the segregation of holocentric *C. elegans* chromosomes during meiosis and mitosis. *Nature Cell Biology* **7**, 1248–1255 (2005).

76. Kaitna, S., Pasierbek, P., Jantsch, M., Loidl, J. & Glotzer, M. The Aurora B kinase AIR-2 regulates kinetochores during mitosis and is required for separation of homologous chromosomes during meiosis. *Current Biology* **12**, 798–812 (2002).

77. Rogers, E., Bishop, J. D., Waddle, J. A., Schumacher, J. M. & Lin, R. The Aurora kinase AIR-2 functions in the release of chromosome cohesion in *Caenorhabditis elegans* meiosis. *The Journal of Cell Biology* **157**, 219–229 (2002).

78. Dumont, J., Oegema, K. & Desai, A. A kinetochore-independent mechanism drives anaphase chromosome separation during acentrosomal meiosis. *Nature Cell Biology* **12**, 894–901 (2010).

79. Davis-Roca, A. C., Muscat, C. C. & Wignall, S. M. *Caenorhabditis elegans* oocytes detect meiotic errors in the absence of canonical end-on kinetochore attachments. *The Journal of Cell Biology* 10.1083/jcb.201608042 (2017).

80. Pelisch, F. *et al.* A SUMO-dependent protein network regulates chromosome congression during oocyte meiosis. *Molecular Cell* **65**, 66–77 (2017).

81. Davis-Roca, A. C., Divekar, N. S., Ng, R. K. & Wignall, S. M. Dynamic SUMO remodeling drives a series of critical events during the meiotic divisions in *Caenorhabditis elegans*. *PLOS Genetics* **14**, 1–27 (2018).

82. Mikeladze-Dvali, T. *et al.* Analysis of centriole elimination during *C. elegans* oogenesis. *Development* **139**, 1670–1679 (2012).

83. Miller, M. A. *et al.* A sperm cytoskeletal protein that signals oocyte meiotic maturation and ovulation. *Science* **291**, 2144–2147 (2001).

84. Wolff, I. D., Tran, M. V., Mullen, T. J., Villeneuve, A. M. & Wignall, S. M. Assembly of *Caenorhabditis elegans* acentrosomal spindles occurs without evident microtubule-organizing centers and requires microtubule sorting by KLP-18/kinesin-12 and MESP-1. *Molecular Biology of the Cell* **27**, 3122–3131 (2016).

85. Muscat, C. C., Torre-Santiago, K. M., Tran, M. V., Powers, J. A. & Wignall, S. M. Kinetochore-independent chromosome segregation driven by lateral microtubule bundles. *eLife* **4**, e06462 (2015).

86. McNally, K., Audhya, A., Oegema, K. & McNally, F. J. Katanin controls mitotic and meiotic spindle length. *The Journal of Cell Biology* **175**, 881–891 (2006).

87. Bobinnec, Y., Fukuda, M. & Nishida, E. Identification and characterization of *Caenorhabditis elegans* gamma-tubulin in dividing cells and differentiated tissues. *Journal of Cell Science* **113**, 3747–3759 (2000).

88. McNally, K. P. *et al.* A novel chromosome segregation mechanism during female meiosis. *Molecular Biology of the Cell* **27**, 2576–2589 (2016).

89. Wilde, A. & Zheng, Y. Stimulation of microtubule aster formation and spindle assembly by the small GTPase Ran. *Science* **284**, 1359–1362 (1999).

90. Cesario, J. & Mckim, K. S. RanGTP is required for meiotic spindle organization and the initiation of embryonic development in *Drosophila*. *Journal of Cell Science* (2011).

91. Schuh, M. & Ellenberg, J. Self-organization of MTOCs replaces centrosome function during acentrosomal spindle assembly in live mouse oocytes. *Cell* **130**, 484–498 (2007).

92. Askjaer, P., Galy, V., Hannak, E., Mattaj, I. W. & McIntosh, J. R. Ran GTPase cycle and importins α and β are essential for spindle formation and nuclear envelope assembly in living *Caenorhabditis elegans* embryos. *Molecular Biology of the Cell* **13**, 4355–4370 (2002).

93. Segbert, C. *et al.* Klp-18, a Klp2 kinesin, is required for assembly of acentrosomal meiotic spindles in *Caenorhabditis elegans*. *Molecular Biology of the Cell* **14**, 4458–4469 (2003).

94. McNally, K. *et al.* Katanin maintains meiotic metaphase chromosome alignment and spindle structure in vivo and has multiple effects on microtubules in vitro. *Molecular Biology of the Cell* **25**, 1037–1049 (2014).

95. Voet, M. V. D. *et al.* NuMA-related LIN-5, ASPM-1, calmodulin and dynein promote meiotic spindle rotation independently of cortical LIN-5/GPR/Gα. *Nature Cell Biology* **11**, 269–277 (2009).

96. Laband, K. *et al.* Chromosome segregation occurs by microtubule pushing in oocytes. *Nature Communications* **8** (2017).

97. Ellefson, M. L., McNally, F. J. & Stearns, T. Kinesin-1 and cytoplasmic dynein act sequentially to move the meiotic spindle to the oocyte cortex in *Caenorhabditis elegans*. *Molecular Biology of the Cell* **20**, 2722–2730 (2009).

98. Cheeseman, I. M., Chappie, J. S., Wilson-Kubalek, E. M. & Desai, A. The conserved KMN network constitutes the core microtubule-binding site of the kinetochore. *Cell* **127**, 983–997 (2006).

99. Yang, H. Y., McNally, K. & McNally, F. J. MEI-1/katanin is required for translocation of the meiosis I spindle to the oocyte cortex in *C. elegans*. *Developmental Biology* **260**, 245–259 (2003).

100. Burbank, K. S., Groen, A. C., Perlman, Z. E., Fisher, D. S. & Mitchison, T. J. A new method reveals microtubule minus ends throughout the meiotic spindle. *The Journal of Cell Biology* **175**, 369–375 (2006).

101. Brugués, J., Nuzzo, V., Mazur, E. & Needleman, D. Nucleation and transport organize microtubules in metaphase spindles. *Cell* **149**, 554–564 (2012).

102. Sköld, H. N., Komma, D. J. & Endow, S. A. Assembly pathway of the anastral *Drosophila* oocyte meiosis I spindle. *Journal of Cell Science* **118**, 1745–1755 (2005).

103. Liang, Z.-Y., Hallen, M. A. & Endow, S. A. Mature *Drosophila* meiosis I spindles comprise microtubules of mixed polarity. *Current Biology* **19**, 163–168 (2009).

104. Hamill, D. R., Severson, A. F., Carter, J. & Bowerman, B. Centrosome maturation and mitotic spindle assembly in *C. elegans* require SPD-5, a protein with multiple coiled-coil domains. *Developmental Cell* **3**, 673–684 (2002).

105. Pelletier, L. *et al.* The *Caenorhabditis elegans* centrosomal protein SPD-2 is required for both pericentriolar material recruitment and centriole duplication. *Current Biology* **14**, 863–873 (2004).

106. Kemp, C. A., Kopish, K. R., Zipperlen, P., Ahringer, J. & O'Connell, K. F. Centrosome maturation and duplication in *C. elegans* require the coiled-coil protein SPD-2. *Developmental Cell* **6**, 511–523 (2004).

107. Matthews, L. R., Carter, P., Thierry-Mieg, D. & Kemphues, K. ZYG-9, a *Caenorhabditis elegans* protein required for microtubule organization and function, is a component of meiotic and mitotic spindle poles. *The Journal of Cell Biology* **141**, 1159–1168 (1998).

108. Bellanger, J.-M. & Gönczy, P. TAC-1 and ZYG-9 form a complex that promotes microtubule assembly in *C. elegans* embryos. *Current Biology* **13**, 1488–1498 (2003).

109. Bot, N. L., Tsai, M.-C., Andrews, R. K. & Ahringer, J. TAC-1, a regulator of microtubule length in the *C. elegans* embryo. *Current Biology* **13**, 1499–1505 (2003).

110. Hannak, E., Kirkham, M., Hyman, A. A. & Oegema, K. Aurora-A kinase is required for centrosome maturation in *Caenorhabditis elegans*. *The Journal of Cell Biology* **155**, 1109–1116 (2001).

111. Sumiyoshi, E., Fukata, Y., Namai, S. & Sugimoto, A. *Caenorhabditis elegans* Aurora A kinase is required for the formation of spindle microtubules in female meiosis. *Molecular Biology of the Cell* **26**, 4187–4196 (2015).

112. Kemphues, K. J., Wolf, N., Wood, W. B. & Hirsh, D. Two loci required for cytoplasmic organization in early embryos of *Caenorhabditis elegans*. *Developmental Biology* **113**, 449–460 (1986).

113. Ellefson, M. L. & McNally, F. J. CDK-1 inhibits meiotic spindle shortening and dynein-dependent spindle rotation in *C. elegans*. *The Journal of Cell Biology* **193**, 1229–1244 (2011).

114. Nasmyth, K. Segregating sister genomes: the molecular biology of chromosome separation. *Science* **297**, 559–565 (2002).

115. Albertson, D. G. & Thomson, J. N. Segregation of holocentric chromosomes at meiosis in the nematode, *Caenorhabditis elegans*. *Chromosome Research* **1**, 15–26 (1993).

116. Crowder, M. E. *et al.* Dynactin-dependent cortical dynein and spherical spindle shape correlate temporally with meiotic spindle rotation in *Caenorhabditis elegans*. *Molecular Biology of the Cell* **26**, 3030–3046 (2015).

117. Redemann, S. *et al.* A switch in microtubule orientation during *C. elegans* meiosis. *Current Biology* (2018).

118. Fabritius, A. S., Flynn, J. R. & McNally, F. J. Initial diameter of the polar body contractile ring is minimized by the centralspindlin complex. *Developmental Biology* **359**, 137–148 (2011).

119. Shelton, C. A., Carter, J. C., Ellis, G. C. & Bowerman, B. The nonmuscle myosin regulatory light chain gene mlc-4 is required for cytokinesis, anterior-posterior polarity, and body morphology during *Caenorhabditis elegans* embryogenesis. *The Journal of Cell Biology* **146**, 439–451 (1999).

120. Mullen, T. J. & Wignall, S. M. Interplay between microtubule bundling and sorting factors ensures acentriolar spindle stability during *C. elegans* oocyte meiosis. *PLOS Genetics* **13**, 1–31 (2017).

121. Dumont, J. & Desai, A. Acentrosomal spindle assembly and chromosome segregation during oocyte meiosis. *Trends in Cell Biology* **22**, 241–249 (2012).

122. Severson, A. F., von Dassow, G. & Bowerman, B. Chapter Five - oocyte meiotic spindle assembly and function. In *Essays on Developmental Biology, Part A*, vol. 116 of *Current Topics in Developmental Biology*, 65–98 (Academic Press, 2016).

123. Hattersley, N. *et al.* A nucleoporin docks protein phosphatase 1 to direct meiotic chromosome segregation and nuclear assembly. *Developmental Cell* **38**, 463–477 (2016).

124. Gigant, E. *et al.* Inhibition of ectopic microtubule assembly by the kinesin-13 KLP-7 prevents chromosome segregation and cytokinesis defects in oocytes. *Development* **144**, 1674–1686 (2017).

125. Ali, M., Siddiqui, Z., Malik, A. & Siddiqui, S. S. A novel C-terminal kinesin subfamily may be involved in chromosomal movement in *Caenorhabditis elegans*. *FEBS Letters* **470**, 70–76 (2000).

126. Robin, G. *et al.* Essential kinesins; characterization of *Caenorhabditis elegans* KLP-15. *Biochemistry* **44**, 6526–6536 (2005).

127. Zipperlen, P., Fraser, A. G., Kamath, R. S., Martinez-Campos, M. & Ahringer, J. Roles for 147 embryonic lethal genes on *C.elegans* chromosome I identified by RNA interference and video microscopy. *The EMBO Journal* **20**, 3984–3992 (2001).

128. Sonnichsen, B. *et al.* Full-genome RNAi profiling of early embryogenesis in *Caenorhabditis elegans*. *Nature* **434**, 462–469 (2005).

129. Piano, F., Schetter, A. J., Mangone, M., Stein, L. & Kemphues, K. J. RNAi analysis of genes expressed in the ovary of *Caenorhabditis elegans*. *Current Biology* **10**, 1619–1622 (2000).

130. Colaiacovo, M. P. *et al.* A targeted RNAi screen for genes involved in chromosome morphogenesis and nuclear organization in the *Caenorhabditis elegans* germline. *Genetics* **162**, 113–128 (2002).

131. Schumacher, J. M., Golden, A. & Donovan, P. J. AIR-2: An Aurora/Ipl1-related protein kinase associated with chromosomes and midbody microtubules is required for polar body extrusion and cytokinesis in *Caenorhabditis elegans* embryos. *The Journal of Cell Biology* **143**, 1635–1646 (1998).

132. Lee, K.-Y., Esmaeili, B., Zealley, B. & Mishima, M. Direct interaction between centralspindlin and PRC1 reinforces mechanical resilience of the central spindle. *Nature Communications* **6** (2015).

133. Woog, I., White, S., Büchner, M., Srayko, M. & Müller-Reichert, T. Chapter 12 - correlative light and electron microscopy of intermediate stages of meiotic spindle assembly in the early *Caenorhabditis elegans* embryo. In *Correlative Light and Electron Microscopy*, vol. 111 of *Methods in Cell Biology*, 223–234 (Academic Press, 2012).

134. Brinkley, B. R. & Cartwright, J. Cold-labile and cold-stable microtubules in the mitotic spindle of mammalian cells. *Annals of the New York Academy of Sciences* **253**, 428–439 (1975).

135. Ems-McClung, S. C., Zheng, Y. & Walczak, C. E. Importin α/β and Ran-GTP regulate XCTK2 microtubule binding through a bipartite nuclear localization signal. *Molecular Biology of the Cell* **15**, 46–57 (2004).

136. Goshima, G., Nédélec, F. & Vale, R. D. Mechanisms for focusing mitotic spindle poles by minus end–directed motor proteins. *The Journal of Cell Biology* **171**, 229–240 (2005).

137. Cai, S., Oconnell, C. B., Khodjakov, A. & Walczak, C. E. Chromosome congression in the absence of kinetochore fibres. *Nature Cell Biology* **11**, 832–838 (2009).

138. Hallen, M. A., Liang, Z.-Y. & Endow, S. A. Ncd motor binding and transport in the spindle. *Journal of Cell Science* **121**, 3834–3841 (2008).

139. Hatsumi, M. & Endow, S. Mutants of the microtubule motor protein, nonclaret disjunctional, affect spindle structure and chromosome movement in meiosis and mitosis. *Journal of Cell Science* **101**, 547–559 (1992).

140. Karabay, A. & Walker, R. A. Identification of microtubule binding sites in the Ncd tail domain. *Biochemistry* **38**, 1838–1849 (1999). PMID: 10026264.

141. Yang, G. *et al.* Architectural dynamics of the meiotic spindle revealed by single-fluorophore imaging. *Nature Cell Biology* **9**, 1233–1242 (2007).

142. Rincon, S. A. *et al.* Kinesin-5-independent mitotic spindle assembly requires the antiparallel microtubule crosslinker Ase1 in fission yeast. *Nature Communications* **8**, 15286 (2017).

143. Gaillard, J. *et al.* Two microtubule-associated proteins of Arabidopsis MAP65s promote antiparallel microtubule bundling. *Molecular Biology of the Cell* **19**, 4534–4544 (2008).

144. Loïodice, I. *et al.* Ase1p organizes antiparallel microtubule arrays during interphase and mitosis in fission yeast. *Molecular Biology of the Cell* **16**, 1756–1768 (2005).

145. Woodruff, J. B., Wueseke, O. & Hyman, A. A. Pericentriolar material structure and dynamics. *Philosophical Transactions of the Royal Society of London B: Biological Sciences* **369** (2014).

146. Conduit, P. T., Wainman, A. & Raff, J. W. Centrosome function and assembly in animal cells. *Nature Reviews Molecular Cell Biology* **16**, 611–624 (2015).

147. Woodruff, J. B. *et al.* The centrosome is a selective condensate that nucleates microtubules by concentrating tubulin. *Cell* **169**, 1066–1077.e10 (2017).

148. Ohkura, H., Garcia, M. A. & Toda, T. Dis1/TOG universal microtubule adaptors - one MAP for all? *Journal of Cell Science* **114**, 3805–3812 (2001).

149. Bellanger, J.-M. *et al.* ZYG-9, TAC-1 and ZYG-8 together ensure correct microtubule function throughout the cell cycle of *C. elegans* embryos. *Journal of Cell Science* **120**, 2963–2973 (2007).

150. Gergely, F. Centrosomal TACCtics. *BioEssays* **24**, 915–925 (2002).

151. Albertson, D. G. Formation of the first cleavage spindle in nematode embryos. *Developmental Biology* **101**, 61–72 (1984).

152. Srayko, M., Buster, D. W., Bazirgan, O. A., McNally, F. J. & Mains, P. E. MEI-1/MEI-2 katanin-like microtubule severing activity is required for *Caenorhabditis elegans* meiosis. *Genes & Development* **14**, 1072–1084 (2000).

153. McDonnell, A. V., Jiang, T., Keating, A. E. & Berger, B. Paircoil2: improved prediction of coiled coils from sequence. *Bioinformatics* **22**, 356–358 (2006).

154. Connolly, A. A., Sugioka, K., Chuang, C.-H., Lowry, J. B. & Bowerman, B. KLP-7 acts through the Ndc80 complex to limit pole number in *C. elegans* oocyte meiotic spindle assembly. *The Journal of Cell Biology* **210**, 917–932 (2015).

155. Zhang, L., Ward, J. D., Cheng, Z. & Dernburg, A. F. The auxin-inducible degradation (AID) system enables versatile conditional protein depletion in *C. elegans*. *Development* **142**, 4374–4384 (2015).

156. Davis, E. S. *et al.* Multiple subunits of the *Caenorhabditis elegans* anaphase-promoting complex are required for chromosome segregation during meiosis I. *Genetics* **160**, 805–813 (2002).

157. Cullen, C. F. & Ohkura, H. Msps protein is localized to acentrosomal poles to ensure bipolarity of *Drosophila* meiotic spindles. *Nature Cell Biology* **3**, 637–642 (2001).

158. Lee, M. J., Gergely, F., Jeffers, K., Peak-Chew, S. Y. & Raff, J. W. Msps/XMAP215 interacts with the centrosomal protein D-TACC to regulate microtubule behaviour. *Nature Cell Biology* **3**, 643–649 (2001).

159. Thawani, A., Kadzik, R. S. & Petry, S. XMAP215 is a microtubule nucleation factor that functions synergistically with the γ-tubulin ring complex. *Nature Cell Biology* **20**, 575–585 (2018).

160. Carazo-Salas, R. E. *et al.* Generation of GTP-bound Ran by RCC1 is required for chromatin-induced mitotic spindle formation. *Nature* **400**, 178–181 (1999).

161. Bamba, C., Bobinnec, Y., Fukuda, M. & Nishida, E. The GTPase Ran regulates chromosome positioning and nuclear envelope assembly in vivo. *Current Biology* **12**, 503–507 (2002).

162. Al-Bassam, J., Larsen, N. A., Hyman, A. A. & Harrison, S. C. Crystal structure of a TOG domain: Conserved features of XMAP215/Dis1-Family TOG domains and implications for tubulin binding. *Structure* **15**, 355–362 (2007).

163. Widlund, P. O. *et al.* XMAP215 polymerase activity is built by combining multiple tubulin-binding TOG domains and a basic lattice-binding region. *Proceedings of the National Academy of Sciences* **108**, 2741–2746 (2011).

164. Cullen, C. F., Deák, P., Glover, D. M. & Ohkura, H. *Mini spindles*: A gene encoding a conserved microtubule-associated protein required for the integrity of the mitotic spindle in *Drosophila*. *The Journal of Cell Biology* **146**, 1005–1018 (1999).

165. Gergely, F., Draviam, V. M. & Raff, J. W. The ch-TOG/XMAP215 protein is essential for spindle pole organization in human somatic cells. *Genes Development* **17**, 336–341 (2003).

166. Cassimeris, L. & Morabito, J. TOGp, the human homolog of XMAP215/Dis1, is required for centrosome integrity, spindle pole organization, and bipolar spindle assembly. *Molecular Biology of the Cell* **15**, 1580–1590 (2004).

167. Edzuka, T., Yamada, L., Kanamaru, K., Sawada, H. & Goshima, G. Identification of the augmin complex in the filamentous fungus *Aspergillus nidulans*. *PLOS ONE* **9**, 1–11 (2014).

168. Moritz, M., Braunfeld, M. B., Guénebaut, V., Heuser, J. & Agard, D. A. Structure of the γ-tubulin ring complex: a template for microtubule nucleation. *Nature Cell Biology* **2**, 365–370 (2000).

169. Keating, T. J. & Borisy, G. G. Immunostructural evidence for the template mechanism of microtubule nucleation. *Nature Cell Biology* **2**, 352–357 (2000).

170. Gruss, O. J. *et al.* Ran induces spindle assembly by reversing the inhibitory effect of Importin α on TPX2 activity. *Cell* **104**, 83–93 (2001).

171. Nachury, M. V. *et al.* Importin β is a mitotic target of the small GTPase Ran in spindle assembly. *Cell* **104**, 95–106 (2001).

172. Wiese, C. *et al.* Role of importin-β in coupling Ran to downstream targets in microtubule assembly. *Science* **291**, 653–656 (2001).

173. Caudron, M., Bunt, G., Bastiaens, P. & Karsenti, E. Spatial coordination of spindle assembly by chromosome-mediated signaling gradients. *Science* **309**, 1373–1376 (2005).

174. Dumont, J. *et al.* A centriole- and RanGTP-independent spindle assembly pathway in meiosis I of vertebrate oocytes. *The Journal of Cell Biology* **176**, 295–305 (2007).

175. Maresca, T. J. *et al.* Spindle assembly in the absence of a RanGTP gradient requires localized CPC activity. *Current Biology* **19**, 1210–1215 (2009).

176. Kaláb, P., Pralle, A., Isacoff, E. Y., Heald, R. & Weis, K. Analysis of a RanGTP-regulated gradient in mitotic somatic cells. *Nature* **440**, 697–701 (2006).

177. Mitchison, T., Evans, L., Schulze, E. & Kirschner, M. Sites of microtubule assembly and disassembly in the mitotic spindle. *Cell* **45**, 515–527 (1986).

178. Mitchison, T. J. Polewards microtubule flux in the mitotic spindle: evidence from photoactivation of fluorescence. *The Journal of Cell Biology* **109**, 637–652 (1989).

179. Mitchison, T. Mechanism and function of poleward flux in *Xenopus* extract meiotic spindles. *Philosophical Transactions of the Royal Society of London B: Biological Sciences* **360**, 623–629 (2005).

180. Mitchison, T. *et al.* Bipolarization and poleward flux correlate during *Xenopus* extract spindle assembly. *Molecular Biology of the Cell* **15**, 5603–5615 (2004).

181. Clark-Maguire, S. & Mains, P. E. Localization of the *mei-1* gene product of *Caenorhaditis elegans*, a meiotic-specific spindle component. *The Journal of Cell Biology* **126**, 199–209 (1994).

182. Vanneste, D., Takagi, M., Imamoto, N. & Vernos, I. The role of Hklp2 in the stabilization and maintenance of spindle bipolarity. *Current Biology* **19**, 1712–1717 (2009).

183. Chase, D. *et al.* The polo-like kinase PLK-1 is required for nuclear envelope breakdown and the completion of meiosis in *Caenorhabditis elegans*. *genesis* **26**, 26–41 (2000).

184. Wueseke, O. *et al.* Polo-like kinase phosphorylation determines *Caenorhabditis elegans* centrosome size and density by biasing SPD-5 toward an assembly-competent conformation. *Biology Open* **5**, 1431–1440 (2016).

185. Kamath, R. S. *et al.* Systematic functional analysis of the *Caenorhabditis elegans* genome using RNAi. *Nature* **421**, 231–237 (2003).

186. Jones, D. T., Tress, M., Bryson, K. & Hadley, C. Successful recognition of protein folds using threading methods biased by sequence similarity and predicted secondary structure. *Proteins: Structure, Function, and Bioinformatics* **37**, 104–111 (1999).

187. Sievers, F. *et al.* Fast, scalable generation of high-quality protein multiple sequence alignments using clustal omega. *Molecular Systems Biology* **7** (2011).

188. Laband, K., Lacroix, B., Edwards, F., Canman, J. C. & Dumont, J. Chapter 11 - Live imaging of *C. elegans* oocytes and early embryos. In *Mitosis and Meiosis Part B*, vol. 145 of *Methods in Cell Biology*, 217–236 (Academic Press, 2018).

APPENDIX A

Chapter 2 and Chapter 3 movie descriptions

Movie 2-1. Movie shows spindle assembly in control (left) and *klp-15/16(RNAi)* (right) oocytes expressing mCherry::histone; GFP::tubulin and corresponds to Fig. 2.1B. Bar = 10 μm.

Movie 2-2. Movie shows another example of spindle assembly in a *klp-15/16(RNAi)* embryo expressing mCherry::histone; GFP::tubulin. Bar = 10 μm.

Movie 2-3. Movie stepping through and rotating around a control spindle stained for DNA (blue), microtubules (green), and ASPM-1 (red). Bar = 2 μm.

Movie 2-4. Movie stepping through and rotating around an oocyte spindle stained for DNA (blue), microtubules (green), and ASPM-1 (red) following *klp-15/16(RNAi)*. Bar = 2 μm.

Movie 2-5. Movie shows MII spindle assembly in a wild-type oocyte expressing mCherry::histone; GFP::tubulin and corresponds to Fig. 2.3A. Bar = 5 μm.

Movie 2-6. Movie shows mitosis in a GFP::histone; GFP::tubulin, *klp-15/16(RNAi)* embryo. Mitotically dividing cell is marked with an asterisk. Bar = 10 μm.

Movie 2-7. Movie shows anaphase in wild-type (left) and *klp-15/16(RNAi)* (right) oocytes expressing mCherry::histone; GFP::tubulin. Bar = 5 μm (wild-type); 10 μm (*klp-15/16(RNAi)*.

Movie 2-8. Movie shows anaphase in control (left) and *klp-15/16(RNAi)* (right) oocytes expressing mCherry::histone; SPD-1::GFP and corresponds to Fig. 2.9D. Bar = 5 μm.

Movie 3-1. Movie shows spindle assembly in a *zyg-9(RNAi)* oocyte expressing mCherry::histone (magenta in merge); GFP::tubulin (green in merge and in grayscale) and corresponds to

Fig. 3.1A.

Movie 3-2. Movie shows an example of a FRAP experiment from an oocyte expressing mCherry::histone (magenta); GFP::ZYG-9 (green).

Movie 3-3. Movie shows an example of a FRAP experiment from a mitotic embryo expressing mCherry::histone (magenta); GFP::ZYG-9 (green).

Movie 3-4. Movie shows an example of a FRAP experiment from an oocyte expressing mCherry::histone (magenta); GFP::ASPM-1 (green).

Movie 3-5. Movie shows an example of a FRAP experiment from a mitotic embryo expressing mCherry::histone (magenta); GFP::ASPM-1 (green).

Movie 3-6. Movie shows an example of a FRAP experiment from an oocyte expressing mCherry::histone (magenta); GFP::tubulin (green).

APPENDIX B

klp-15/16(RNAi) and metaphase arrest

KLP-15/16 depletion and metaphase arrest resulted in spindles with fragmented poles that appear to associate with the cortex of the oocyte. I do not understand why the metaphase arrest causes this phenotype in the *klp-15/16(RNAi)* background. Unarrested spindles depleted of KLP-15/16 show in the MT ball phenotype described in Chapter 2.

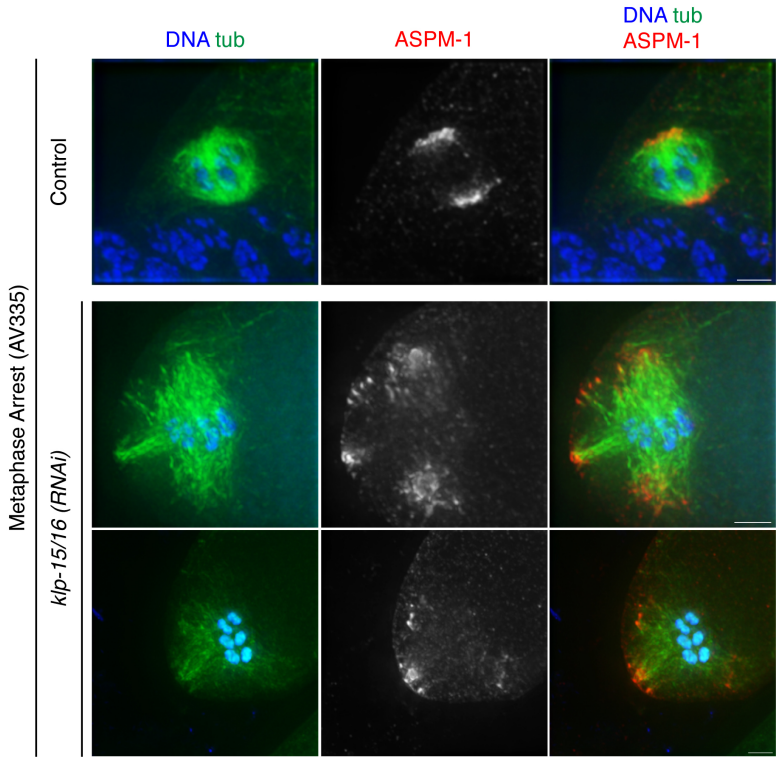

Figure B.1. ***klp-15/16(RNAi)* and metaphase arrest.** Metaphase arrested spindles stained for DNA (blue), tubulin (green), and ASPM-1 (red). Using a worm strain (AV335) with a temperature sensitive allele of *emb-27*, a component of the APC, at the restrictive temperature in a *klp-15/16(RNAi)* background, the spindle poles appear splayed and make associations with the cortex of the oocyte. Bars = 2.5μm.

APPENDIX C

Photoconvertible tubulin strain (mMaple3::TBA-1)

Using CRISPR, I generated a worm strain that expresses TBA-1 (an α-tubulin) tagged with mMaple3 (a photoconvertible green-to-red fluorescent protein) from the endogenous locus. The reagents used to make this strain are described in the Materials and methods chapter.

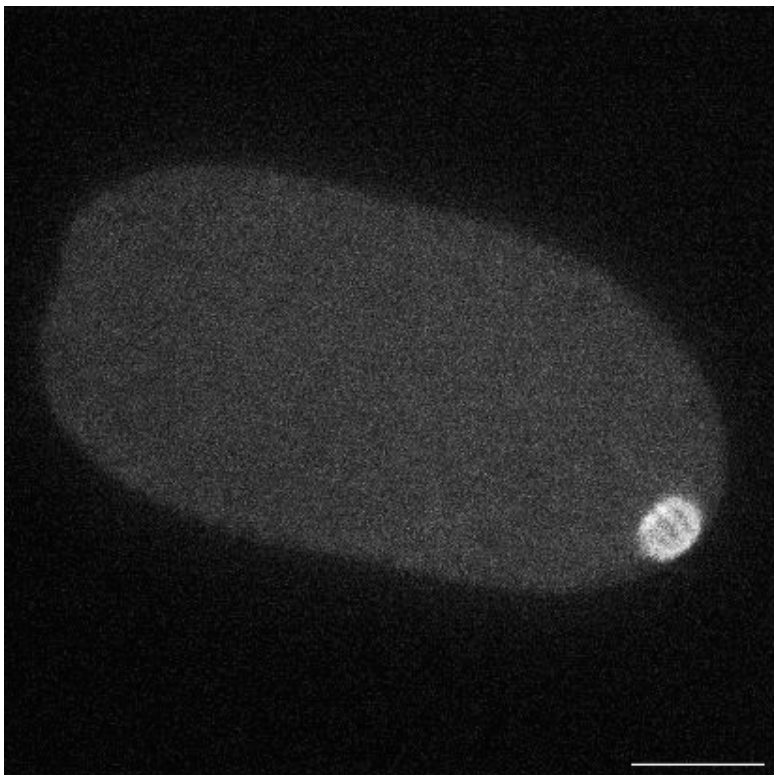

Figure C.1. **Oocyte expressing mMaple::TBA-1.** Example of a late metaphase spindle in a live oocyte expressing mMaple::TBA-1. Bar = 10μm.